



AARHUS
UNIVERSITY



UNIVERSITY OF BERGEN

Master thesis

Monitoring of the aqueous phase from
hydrothermal liquefaction using GC-MS
and qNMR

Tina Hemmingsen

Department of Chemistry, University of Bergen

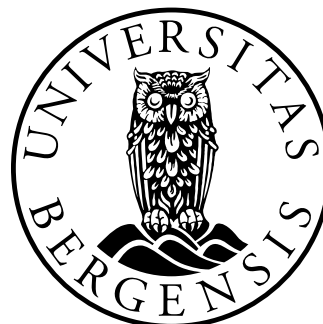
Supervisor: Tanja Barth

Bergen, Norway

Department of Engineering, Aarhus University

Supervisor: Patrick Biller

Aarhus, Denmark



October 11, 2020

Preface

This report is submitted for the Master's degree in Chemistry at the University of Bergen, Norway. The thesis is a result of a 60 ECTS master thesis, and marks the end of the Master's degree program. The experimental laboratory work was carried out at the Center for Biorefining Technologies (CBT), Foulum, Denmark, at different facilities at Aarhus University, Denmark and at different facilities at the University of Bergen, Norway.

Acknowledgements

First of all I would like to give a great thank you to my supervisors, professor Tanja Barth at the University of Bergen, and assistant professor Patrick Biller at Aarhus University, for great guidance and help throughout the thesis work.

I would also like to thank Ph.d. student Juliano Souza dos Passos for operating the GC-MS on my samples at the department of Chemistry, Aarhus University. Thank you to PostDoc Chia-Wen Carmen Hsieh for running my samples on the elemental analyzer and sending me the data from the instrument.

A huge thanks to the hydrothermal processing research group at the department of Engineering, Aarhus University, as well as the research group for renewable fuels as the department of Chemistry, University of Bergen, for great discussions and good ideas and tips for my thesis work both at the laboratory and for the analysis.

Last, but not least I would like to thank my parents and friends at the master offices both in Aarhus and Bergen, for great encouragement, helpful discussions and support during the entire laboratory work- and writing process.

Thank you

Bergen, October 2020
Tina Hemmingsen

Abstract

Hydrothermal liquefaction (HTL) is a promising technique used for production of biocrude. Along with the biocrude, there is also produced large amounts of aqueous waste containing high concentrations of both soluble organics and nutrients. This thesis focus on the aqueous phase in the HTL process since little research is done on the aqueous phase. Several analytical techniques were utilized for monitoring the product of the aqueous phase.

Feedstocks of corn stover (CS), wheat straw (WS) and sugar kelp (SK) were pretreated and processed under alkaline (KOH-catalyzed) conditions, while sewage sludge (SS) and cattle manure (CM) were processed without a catalyst present. All feedstocks were processed in a continuous flow pilot scale HTL reactor at 350 °C and 220 bar.

The samples were analyzed by ^1H and ^{13}C - nuclear magnetic resonance (NMR) spectroscopy, gas chromatography mass spectrometry (GC-MS), in addition to obtaining data from elemental analysis, Karl Fischer analysis and ash content. The GC-MS analyses showed that during the first 40-50 minutes a relatively stable composition of compounds was established in the HTL process. The GC-MS analysis provided chromatographic separation of compounds identified through MS fragmentation and library connected to the instrument, while qNMR analysis gave quantitative results of compounds of the aqueous sample characterized by unique peaks. The thesis work has focused mainly on products in the aqueous phase. The CS and WS experiments among other compounds, gave alcohols as products while the CM and SS experiments among other compounds, gave N-containing products like pyrazine and pyridine. Acetic acid was found as the major component in all aqueous phases.

Elemental analyses showed that the WS biocrude had the highest oxygen content and lowest higher heating value (HHV) for all examined feedstocks, and also the lowest sulphur and nitrogen content. The biocrudes of the other three examined feedstocks (CS, SS and CM) had oxygen content in the range 13.7 – 16.5%, and calculated HHV in the range 33.1-34.1.

Keywords: Hydrothermal liquefaction, corn stover, wheat straw, sugar kelp, sewage sludge, cattle manure, wastewater, biocrude, qNMR, GC-MS.

Abbreviations

Chemicals

CMC	Carboxymethyl cellulose
DCM	Dichloromethane
MCF	Methyl chloroformate
TSP	3-(trimethylsilyl)-propionic-2,2,3,3-d ₄ acid

Methods

HTL	Hydrothermal liquefaction
GC-MS	Gas chromatography – Mass spectrometry
NMR	Nuclear magnetic resonance
qNMR	Quantitative nuclear magnetic resonance
1D	One dimensional
2D	Two dimensional
HSQC	Heteronuclear single quantum coherence
HMBC	Heteronuclear multiple bond correlation
I	Nuclear spin

Feedstocks

CS	Corn stover
WS	Wheat straw
SS	Sewage sludge
CM	Cattle manure
SK	Sugar kelp

Others

AP	Aqueous phase
DM	Dry matter
HHV	Higher heating value
ppm	Parts per million
RT	Retention time

Table of Contents

PREFACE	III
ACKNOWLEDGEMENTS	V
ABSTRACT	VII
ABBREVIATIONS	IX
1 INTRODUCTION	1
1.1 BACKGROUND	1
1.2 HYDROTHERMAL LIQUEFACTION PROCESS	2
1.3 HTL PROCESS WATER	6
1.4 ANALYSIS OF AQUEOUS PHASE	7
1.5 PROBLEM STATEMENT	8
2 METHODS	9
2.1 HTL CONVERSION	9
2.1.1 Feedstocks	9
2.1.2 Pre-treatment	9
2.1.3 Hydrothermal liquefaction reaction	9
2.1.4 Sample retrieval	11
2.2 OIL ANALYSIS	11
2.2.1 Oil filtration	11
2.2.2 Ash	11
2.2.3 Moisture content	12
2.2.4 Elemental composition	12
2.3 GAS CHROMATOGRAPHY – MASS SPECTROMETRY	13
2.3.1 Gas chromatography – mass spectrometry theory	13
2.3.2 GC-MS procedure	14
2.4 NUCLEAR MAGNETIC RESONANCE	17
2.4.1 Nuclear magnetic resonance theory	17
2.4.2 ¹ H, HSQC and HMBC	18
2.4.3 Quantitative Nuclear Magnetic Resonance	18
2.4.4 qNMR procedure	19
3 RESULTS AND DISCUSSION	21
3.1 CORN STOVER	22
3.1.1 Aqueous phase	23
3.1.2 Biocrude	35
3.2 WHEAT STRAW	39
3.2.1 Aqueous phase	39
3.2.2 Biocrude	50
3.3 SEWAGE SLUDGE	53
3.3.1 Aqueous phase	53
3.3.2 Biocrude	61
3.4 CATTLE MANURE	65
3.4.1 Aqueous phase	65
3.4.2 Biocrude	76
3.5 SUGAR KELP	80
3.5.1 Aqueous phase	80
3.5.2 Biocrude	82
3.6 ALL FEEDSTOCKS	82
3.6.1 Comparison of results for the aqueous and biocrude phases from the experiments with all feedstocks, by use of GC-MS and NMR analyses	82
3.6.1 Elemental composition and HHV of biocrude	85
4 CONCLUSIONS	87

4.1	CONCLUSIONS	87
4.2	FURTHER WORK	90
REFERENCES		92
APPENDIX		96
APPENDIX A – CORN STOVER		96
APPENDIX B – WHEAT STRAW		101
APPENDIX C – SEWAGE SLUDGE		105
APPENDIX D – CATTLE MANURE		106
APPENDIX E – SUGAR KELP		107
APPENDIX F – ALL FEEDSTOCKS		108

1 Introduction

1.1 Background

As a result of the Paris Agreement and the United Nations Sustainable Development Goals presented to the world in 2015, the awareness surrounding climate change, environmental sustainability and independence of fossil fuels, has increased throughout the world. However, as the population increases, the demand for energy increases accordingly, contributing to higher amounts of greenhouse gases released into the atmosphere (Dong et al., 2018).

The Covid-19 pandemic and its accompanying lockdowns has led to massive emission reductions, with the daily global emissions decreased by 17 % at the peak in early April. The pandemic is causing the impact on the 2020 annual global emissions to be projected to reductions up to 8 % by multiple studies performed in April and May 2020, which is approximately the reductions required year on year over the next decades to fulfill the 1.5 °C goal of the Paris agreement (Sussmann and Rettinger, 2020). A very large share of this reduction is due to a decrease in road transport, maritime transport and aviation (Liu et al., 2020). Thus, these reductions in emissions are temporary and will most likely return to normal numbers as the lockdown is lifted, but it undeniably shows the need for green, renewable energy sources.

Currently there is not an environmentally friendly option for production of energy and fuels that is capable of covering the demand for energy in the world. However, the goal is to replace as much as possible of the traditional fossil fuel with renewable fuels. The use of available biomass, which does not compete with the food crops of the world, as building blocks together with suitable conversion processes could be an important step towards a minimized use of and need for fossil fuel (Tenenbaum, 2008, Gollakota et al., 2018).

The experimental work done on the thesis is also a part of the HyFlexFuel project, which is a European Union project with funding from the European Union's Horizon 2020 research and innovation program under grant agreement No 764734. The project is an ongoing project started 1st of October 2017, and will end 30th of September 2021 (European Commission). The main objective of the project is “... to advance the technical maturity of the hydrothermal liquefaction

technology to provide truly sustainable fuels that are compatible with existing infrastructure (drop-in capable) and that can be produced at competitive cost.” (HyFlexFuel). One of the specific objectives is to ensure efficient valorization of residual process streams, particularly of the aqueous phase from hydrothermal liquefaction (HTL) conversion, which is the most relevant objective of the thesis.

1.2 Hydrothermal liquefaction process

The conversion of biomass to oil is a process that already takes place in nature, and is currently used on a large scale as fossil fuels. The composition of oil includes carbon, hydrogen, nitrogen, sulphur and oxygen, which makes biomass very suitable for producing energy in the form of fuels. In nature, the oil is produced from biomass under pressure over millions of years, and therefore is not a renewable source of energy. As an alternative, by using available biomass and the theory behind its conversion in nature, several ways to produce fuels by more efficient and renewable technologies have been developed (Gollakota et al., 2018).

Most of the technologies that have been developed over recent years require a dry feedstock, which can be challenging to achieve. Most biomasses on Earth have a high water content, which typically lies between 25 and 50 %. It is, however, energy consuming and costly to remove the water before the process is started. Therefore, one of the major advantages of using hydrothermal liquefaction (HTL) as a conversion method is that it uses wet biomass as feedstock, and thereby does not require any drying methods of the feedstocks prior to the reaction (Biller et al., 2012, Mørup et al., 2015, Elliott et al., 2015). Another advantage of HTL is that the method does not require strong bases or acids for the production of biocrude (Arturi et al., 2016). A number of literature reviews of the HTL process are published (Akhtar and Amin, 2011, Toor et al., 2011, Elliott et al., 2015, Dimitriadis and Bezergianni, 2017, Gollakota et al., 2018).

During HTL, high temperature and pressure induce the depolymerization of biochemical components to small monomers. The monomers are further decomposed by cleavage, dehydration, decarboxylation and deamination, before a recombination and polymerization of reactive fragments can take place (Toor et al., 2011). The process yields four product parts: a gas phase of mainly CO₂, a top phase of biocrude, a bottom phase with solid residue consisting

of mainly inorganic salts and an aqueous phase with byproducts, where the oil is separated from the aqueous phase by simple centrifugation (Villadsen et al., 2012, Mørup et al., 2015).

The HTL process has been used since at least 1970, in Lawrence Berkeley Laboratory (Schaleger et al., 1982) and the Albany Biomass Liquefaction Experimental Facility. At the time it went by the terminology “Direct biomass liquefaction” (Elliott, 2007). HTL energy and fuels has not been able to economically compete with the fossil fuels and energy yet. However, with the rising focus and debate on environmental issues HTL has once again become an area of research, which is very important and interesting to improve and streamline.

For hydrothermal liquefaction most research has been done on batch reactors due to low cost, simple construction and easy handling (Dimitriadis and Bezergianni, 2017). However, these reactors limit the possibility for any post-treatment of the oil and analysis on oil and aqueous phase, as the volume in the reactor is very limited. Therefore there is a need for upscaling of the process for research. This has been done in larger scale batch reactors at the University of Bergen (Ghoreishi et al., 2019a, Ghoreishi et al., 2019b) and through continuous flow reactor system. As these types of reactors produces a larger volume of products, it is easier to analyze said products, and it is also the types of reactors that would be used in the industry, which means the reaction happens at true process conditions (Mørup et al., 2015, Ghoreishi et al., 2019a). The reactor used in the thesis is developed at Aarhus University (AU) Denmark, and is to the best of our knowledge the largest pilot-scale HTL reactor reported in peer reviewed literature (Anastasakis et al., 2018). The HTL reactor is shown in Figure 1.1.



Figure 1.1: Photo of the continuous flow pilot-scale HTL reactor placed at the Center for Biorefining Technologies (CBT) in Foulum, and belonging to Aarhus University.

There are several parameters that can impact the results of the HTL biocrude yields. These include temperature, pressure, catalysts, residence time, solvents and biomass to solvent ratio. A fair amount of research has been done on the effect of each of these parameters. The extensive reviews by Dimitriadis and Bezergianni from 2017 and Akhtar and Amin from 2011, give a good overview of the effect of the parameters (Akhtar and Amin, 2011, Dimitriadis and Bezergianni, 2017).

The studies found that the biocrude yield increased with temperature up until a certain point, where the yield level flattened or decreased (Dimitriadis and Bezergianni, 2017). The ideal temperature varies for the different feedstocks, with research done showing that the ideal temperature for pinewood was 300 °C (Liu and Zhang, 2008). The best yields from pulp/paper sludge powder was at 350 °C (Xu and Lancaster, 2008), and other research pointed to 300 °C as the ideal temperature for woody biomass (Xu and Etcheverry, 2008, Sugano et al., 2008).

Numerous variants of catalysts have been used in the HTL process, like acidic compounds, alkaline compounds and metals. The function of the catalyst is to reduce the amount of char

produced, and at the same time to increase the biocrude-yield of the process (Dimitriadis and Bezergianni, 2017). For woody biomass previous research has shown alkaline catalysts to be the most optimal catalyst considering the biocrude yield and solid residue yield. An example is the use of KOH, that more than doubled the yield of the uncatalyzed product (Nazari et al., 2015). Nazari et al. show in this paper, the effects of different catalysts HTL of woody biomass on product yields. The use of alkali catalyst promotes more base-catalyzed condensation reactions leading to aromatic oil formation, which is more favorable than acid-catalyzed polymerization reactions leading to solid product formation. (Elliott et al., 2015)

A lot of research has also been done, addressing the residence time of the reaction. The residence time is defined as the time the biomass spends at maximum temperature, not counting the heating and cooling time. From literature it appears that there is not one optimal residence time, as it depends heavily on the other parameters, such as for instance the temperature and catalyst of the reactions (Dimitriadis and Bezergianni, 2017). The literature reports that at lower temperatures, an increased residence time leads to an increased biocrude yield and conversion, while at higher temperatures, the opposite is true (Akhtar and Amin, 2011). Different reports conclude with values from 1 to 840 minutes as the optimal residence time, depending on the other parameters and feedstocks (Qu et al., 2003, Xu and Etcheverry, 2008, Zhang et al., 2009, Yip et al., 2009, Valdez et al., 2012, Ye et al., 2014).

There has also been done some research on when a reactor reaches steady state at another continuous flow HTL reactor in Aarhus. The research concludes that the steady state is reached within 3 hours for carboxylic acids, and within 4,5 hours for cyclic ketones and for pyrazines, meaning that the continuous flow reactor also reaches the steady state within 4,5 hours (Madsen et al., 2016).

The most common solvent used for thermal conversion is water, as it is the economically and environmentally best option. Other common solvents that are used for thermal conversion include methanol and ethanol. An advantage of using methanol or ethanol as solvent is that it requires lower temperature and pressure than water for the conversion to take place. However, the optimal solvent concerning the biocrude yields varies with the different feedstocks, with ethanol or methanol as solvent giving the best yields on some feedstocks, and water as solvent giving the best yield on others in the literature (Akhtar and Amin, 2011, Dimitriadis and Bezergianni, 2017).

1.3 HTL process water

The desired product through the HTL process is the crude oil, with the aqueous phase being a by-product from the conversion. This naturally leaves the aqueous phase without the massive research attention that the crude oil receives. Since the water works as both a reactant and a catalyst in the HTL process, the process includes a large amount of aqueous waste. Therefore, to ensure sustainability and energy recovery, a monitoring of both the product streams and waste streams is important. These data provide an important basis for mass balance reports, identification and quantification of all product streams, as a large amount of the aqueous by-product is generated. Previous studies have shown that the aqueous phase contains high concentrations of both soluble organics and nutrients (Gu et al., 2019, Løhre et al., Prepared for submission). Maddi et al. states that the aqueous byproduct hydrothermal liquefaction (HTL) contains around 20-50% biogenic feed carbon, which will be valuable for industrial production of commercially needed products (Maddi et al., 2017).

Some of the research that has been done on the aqueous phase from HTL of lignocellulosic feedstocks, in these examples pine forest residuals and wheat straw, mainly contains organic acids, alcohols and ketones, especially acetone and cyclopentanones (Panisko et al., 2015, Seehar et al., 2020). Research done on the sewage sludge coming from domestic waste water mainly consists of a water phase where the compounds are dissolved in water (Xu et al., 2018). It contains both toxic and nontoxic organic compounds, pathogens and minerals including heavy metals. However, its dry basis is rich in proteins, lipids, carbohydrates in addition to lignin and ash. The aqueous phase are found to contain ethanol, acetone, oxygenates and organic acids, as well as nitrogen containing compounds, most likely coming from the nitrogen containing proteins in the feedstock (Huang et al., 2014, He et al., 2014, Maddi et al., 2017). Livestock manures used as feedstock also includes a lot of proteins, which in the same way as for sewage sludge, result in nitrogen containing compounds, such as pyrazines, pyrroles and pyridines in the aqueous phase after the HTL process of the feedstock (Lu et al., 2018). Limited research is done on the aqueous phase from HTL processes using sugar kelp as feedstock, but research covering the chemical composition of the kelp concludes that sugar kelp also contains around 7 % protein, indicating nitrogen containing compounds to be expected as part of the aqueous phase from the HTL process. In addition the research shows that sugar kelp contains a larger section of ash than terrestrial feedstocks due to accumulation of mainly potassium and sodium ions (Schiener et al., 2014).

Some research has also been done on the aqueous phase from HTL using microalgae as feedstock. Under the microalgae HTL process the compounds decompose, and the heavy metals are concentrated in the solid phase (Huang and Yuan, 2016). It was found that the water phase had a decrease in TOC, and an increase in NH₃-N (decomposed organic N-compounds) with increasing temperature in the HTL process (Qian et al., 2015).

An interesting study is made by Tommasos group on HTL of aqueous products from mixed-culture wastewater algae experiments (Tommaso et al., 2015). The effect of retention time and temperatures is studied. It shows an increase of the amount of short chained fatty acids with prolonged HTL retention time at 300 °C with a maximum fatty acid amount at one hour, and also an increase with higher temperature up to 300 °C at one hour. However, extended retention times beyond one hour at 300 °C and temperatures higher than 300 °C at one hour showed a reduction of the fatty acids.

A research group at Aalborg University has examined the effect of recycling the aqueous phase, which they state as the leading challenge with the HTL process of sewage sludge. The research showed that the product yield was increased until the fifth cycle of the aqueous phase, before the yields evened out for the following cycles. It was also demonstrated that even with the recycled water on its first cycle the product yields were higher than for the experiment with an acid catalyst (Shah et al., 2020).

1.4 Analysis of aqueous phase

For the analysis of the aqueous phase from HTL several methods are currently used. A method that is commonly used is reverse phase high performance liquid chromatography (HPLC) (Tomasini et al., 2014, Becker et al., 2014, Lazzari et al., 2019, Dubuis et al., 2019). However, this method normally requires previous information on the sample content for extensive calibration curve preparations to quantify and identify the sample compounds (Løhre et al., Prepared for submission).

Another frequently used method is gas chromatography – mass spectrometry (GC-MS). GC-MS is a suitable analytical technique used both for the biocrude phase and the aqueous phase due to its versatility, and to the availability of a large library of mass spectra for compound identification. The disadvantages of using GC-MS is that only volatile compounds

can be analyzed, which leads to challenges with high molecular weight and the insufficient quantification of polar compounds. However, derivatization of the compounds can be used to overcome this problem (Villadsen et al., 2012).

Quantitative nuclear magnetic resonance (qNMR) is a method which can be used to identify and quantify the molecules in the aqueous byproduct. An advantage of qNMR is that it is directly quantitative, with no need for sample preparation including separation or derivatization. Another advantage is that it can be used for all samples containing an atom with a spin-active nucleus, which means that the atom possesses either odd mass, odd atomic number or both (Løhre et al., Prepared for submission). The main methods used in this thesis are based on GC-MS and qNMR.

1.5 Problem statement

The problem statement for this thesis is the monitoring of components in the aqueous phase during a HTL process. Both GC-MS and direct NMR profiling are used to identify the organic compounds dissolved in the HTL aqueous phase, and also to determine whether a steady state is reached for a continuous flow pilot-scale HTL reactor at approximately 350 °C and 220 bar for five different feedstocks. The feedstocks used in the thesis are corn stover, wheat straw, sewage sludge, cattle manure and sugar kelp.

2 Methods

2.1 HTL conversion

2.1.1 Feedstocks

Five different biomass feedstocks were used in the experiments: corn stover (CS), wheat straw (WS), sewage sludge (SS), cattle manure (CM), and sugar kelp (SK) were examined in the thesis work.

2.1.2 Pre-treatment

Some of the biomass feedstocks needed to be pre-treated in order to pass through the HTL reactor. The pre-treatment reduces the size of the particles, increases or decreases the dry matter (DM) content, and lowers the needed reaction time.

Sewage sludge and cattle manure are ready for HTL processing without pre-treatment, while the other feedstocks are first extruded through a twin-screw extruder (Xinda, 65 mm twin screw extruder with 2000 mm barrel length), and run through a grinder (Stephan Microcut MCH-D 60A 60 hp with double cutting) 2-3 times. Following the reduction of particle size, carboxymethyl cellulose (CMC) (around 0,25 wt% (w/w) of the slurry mass) is added to the slurry as a thickener. The CMC is added to increase the viscosity of the slurry, and to prevent removal of water from the slurry into the piston pump, which would end in a dry biomass blockage. Water is added to the slurry until it is pumpable, and KOH (about 1 wt% of slurry mass) is added to the slurry as a catalyst, in order to enhance the decomposition and reduce the amount of char and solids produced during the HTL run.

2.1.3 Hydrothermal liquefaction reaction

The pilot scale HTL reactor built by Aarhus University comprises 9 parts: (1) a feed system, (2) a heat exchanger, (3) a trim heater, (4) a reactor, (5) a filter system, (6) a cooler, (7) a take-off system, (8) a hydrocyclone and (9) a gravimetric separator. A schematic overview of the HTL pilot plant is given in Figure 2.1.

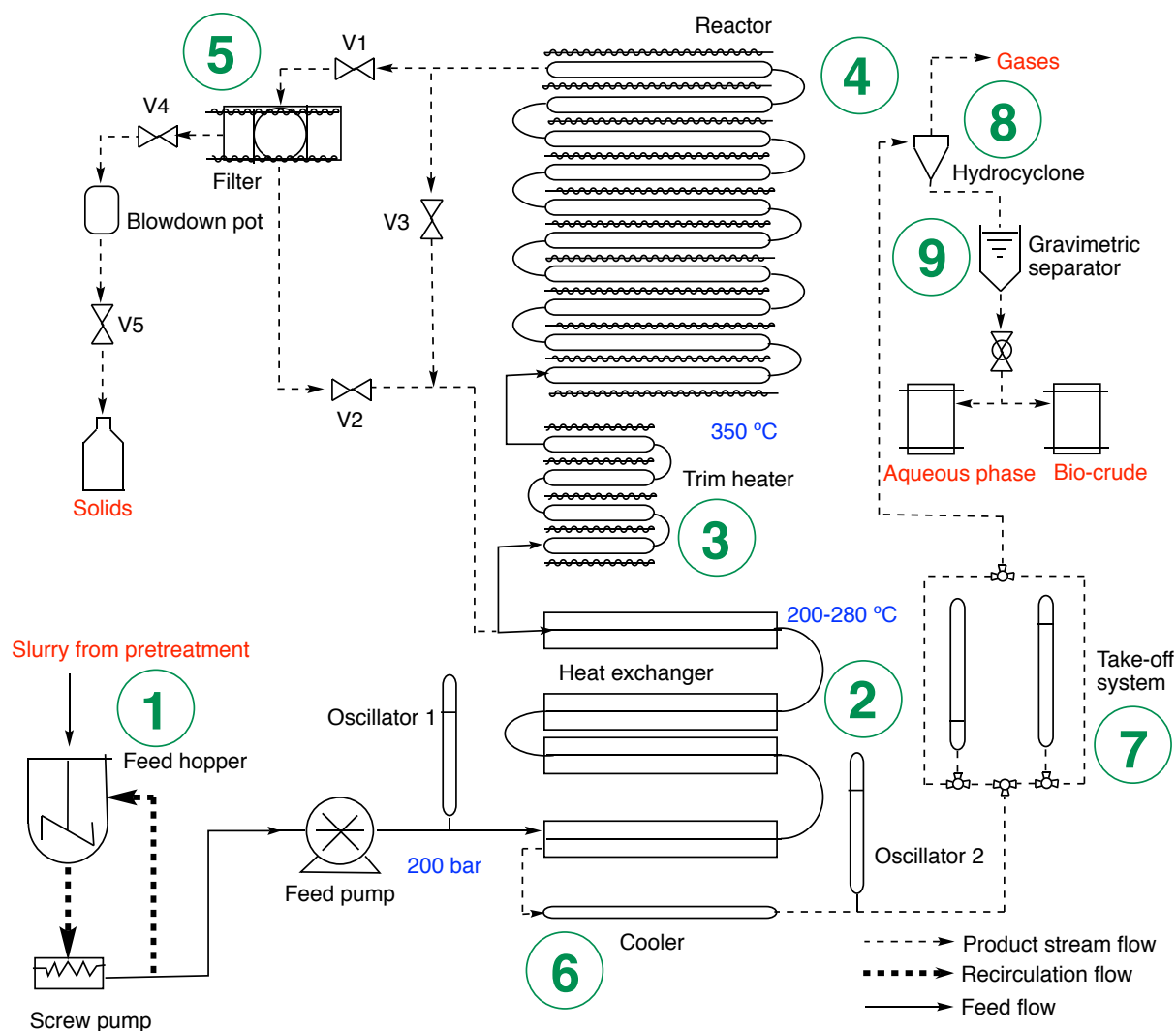


Figure 2.1: Schematic overview of the HTL pilot-scale plant belonging to Aarhus University. (1) Feed system: feed hopper, screw pump and feed pump, (2) heat exchanger, (3) trim heater, (4) reactor, (5) filter system: filter and blowdown pot, (6) cooler, (7) take-off system, (8) hydrocyclone, and (9) gravimetric separator. (Modified picture from (Anastasakis et al., 2018))

The process starts in the feed system, which consists of a feed hopper, a screw pump and a feed pump. The slurry is added to the feed hopper, where it passes through to the screw pump. The screw pump circulates the slurry to ensure the homogeneity of the slurry. The oscillators which are included in the set-up, were not used for this particular thesis project. The feed pump drives the slurry to the heat exchanger, which uses the heat of the product stream from the reactor to pre-heat the slurry, before the trim heater causes the slurry to reach 350 °C, which is the target temperature for the reactor. Thereafter, the slurry enters the reactor, consisting of 10 pipes, where the HTL chemical reactions and biomass conversion take place. After the reaction the product stream flows to the heated part of the heat exchanger to heat up and simultaneously be

cooled by the incoming slurry, before moving on to the cooler to cool down to the ideal temperature. This process is called the counter current system, which reduces the energy consumption. This is a well-known system in nature in mammalian organs, but also with temperatures for example in the breath of polar rain deer or in the feet of sea gulls. The fluid then reaches the take-off system where the pressure is released. Following the depressurization, the stream continues to the hydrocyclone where the gases are separated from the liquid phases. The stream then moves on to the gravimetric separator where the aqueous phase and the bio-crude are separated using gravity.

2.1.4 Sample retrieval

For each sample of the product from the reactor a 500mL flask is weighed, and then filled with the volume of one piston pump from the take-off system. The time, flow and cylinder count, which is the number of times the right and left cylinder in the take-off system are emptied, is noted before the flask is left to cool down. When cooled, the filled flask is weighed and approximately 14mL of the aqueous phase is decanted into a 15mL centrifuge tube twice for each sample, before the rest of the aqueous phase is poured out leaving only the remaining oil in the flask. The flask is left to evaporate before it is weighed again, and the aqueous phase is centrifuged to remove oil residue.

2.2 Oil analysis

2.2.1 Oil filtration

To a 50 mL centrifuge tube, 3 g of the oil sample and around 20 mL DCM is added and shaken until the oil is dissolved. The sample is vacuum filtrated through a pre-weighed filter, and washed with dichloromethane (DCM). The filtrate is added to a pre-weighed beaker and left for two days in the fume hood for evaporation of the DCM. The filter is then dried in an oven at 105 °C for 12 hours before the filter and the beaker with the oil is weighed.

2.2.2 Ash

The dried solid from the oil filtration of the sample is added to a pre-weighed, clean, porcelain crucible, before the crucible is weighed and covered with aluminum foil. The crucible with the

sample is heated in a muffle-oven at 550 °C for 5 hours, before it is cooled down in a desiccator and weighed.

2.2.3 Moisture content

A two-component Karl Fischer reagent system is used to measure the moisture content in the filtrated biocrude. The analysis is performed on a Hach Karl Fischer KF Series 1000. The sample solution is made by adding 5 g chloroform/methanol to 500 mg of the bio-crude. Afterwards 1 mL of the sample solution is injected, which contains 1-10 mg of water based on the original sample with 1-10 wt% water.

2.2.4 Elemental composition

The elemental analysis instrument, a Vario MACRO cube in CHNS mode with associated software, is used for measuring the content of carbon, hydrogen, nitrogen, and sulphur in the sample. The samples are combusted into CO₂, NO_x, H₂O, and SO₂, before the gases are separated by purge and trap gas chromatography columns with a specific affinity to each combustion gas and analyzed with a thermal conductivity detector. Assuming that the rest of the weight of the sample is oxygen, it is possible to calculate the content of oxygen in the sample, even though it entails some uncertainty as some inorganic compounds may occur in the samples as well. The instrument uses helium as a carrier gas. Sulfanilamide (C₆H₈N₂O₂S; 16,25 wt% N, 41,81 wt% C, 4,65 wt% H, and 18,62 wt% S) is used as a reference.

A zinc capsule is weighed and filled with 15-40 mg of the sample. For the solid samples a small amount of Tungsten (IV)-oxide is added as a catalyst before the capsule is sealed, and for the biocrude samples, no catalyst is used. The moisture content is taken into consideration for the results from the biocrude samples. The samples of both solids and biocrude are done in duplicates.

The prepared samples were analyzed in the Vario MACRO cube by postdoc Carmen Hsieh, who sent the result data used as a basis for the elemental analysis results presented in the thesis. The results from the elemental analysis is used to calculate the higher heating value (HHV) of the biocrudes and the solids. The higher heating value is used to define the energy content of the fuel, based on the fact that carbon, hydrogen and sulfur add to the energy content, and

oxygen, nitrogen and ash decrease the energy content. There are several equations formulated in literature for calculating the HHV, but after a thorough research and comparison of 22 important correlations for calculations of HHV, Equation 2.1 was concluded to be the best one (Channiwala and Parikh, 2002).

$$HHV = 0,3491C + 1,1783H + 0,1005S - 0,1034O - 0,0151N - 0,0211Ash \quad (2.1)$$

Where the higher heating value, *HHV*, is presented in MJ/kg, and the C, H, S, O, N and Ash is the concentration of the particular one present in the sample in percentage.

2.3 Gas chromatography – mass spectrometry

2.3.1 *Gas chromatography – mass spectrometry theory*

Gas chromatography (GC) is a method that utilizes the volatility and polarity of the compounds to separate them from each other. The method is based on the compounds being distributed differently between two phases; a stationary phase and a mobile phase. The mobile phase is the gas phase, usually consisting of nitrogen, helium or hydrogen, while the stationary phase is placed as a thin film on the inside of the column (Miller, 2004). The gas chromatograph is coupled to a mass spectrometer, in order to identify the compounds in the samples. In mass spectrometry (MS) the analytes, operated under high vacuum, are ionized, and sometimes fragmented. Following the ionization and fragmentation, the analytes are directed to a mass analyser where they are separated dependent on their mass to charge ratios, *m/z* (Miller, 2004). The results from the mass spectrometer are transferred to mass spectral libraries which identify the compounds.

Some groups, including carboxyl, phenols and amino groups, are responsible for low volatility of the compounds, and other phenomena that make direct GC difficult or impossible due to their polarity and tendency to form hydrogen bonds. This is especially a problem if there are several groups, whether if one or more types are present in the sample (Drozd, 1981). Chemical derivatization of the sample molecules improves the symmetry of the peak, the volatility, thermal stability and the chromatographic performance for gas chromatographic separations, which makes it possible to analyze the sample even though these polar types of functional groups are present (Grob and Barry, 2004).

Previous research on the analysis of complex aqueous phases in general in metabolomics has been using two main types of derivatizations; using either silylating reagents or chloroformates (Smart et al., 2010). Chloroformates are sufficiently stable reagents in water, which means that no prior drying is needed. The mechanism is described in Figure 2.2. Drying would be a great disadvantage as it could lead to potential condensation reactions. In addition volatile compounds cannot be detected, and semi-volatile compounds will give varying results with methods that requires complete evaporation of water (Madsen et al., 2016).

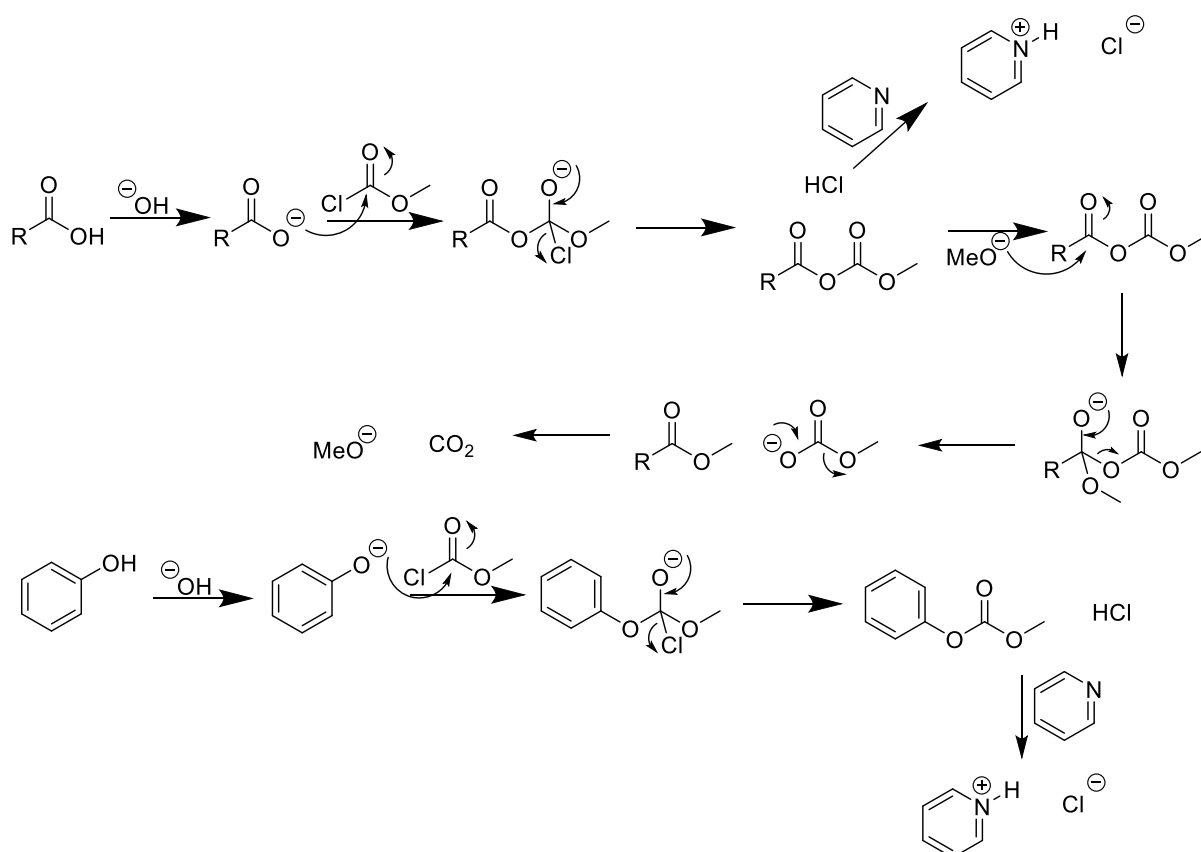


Figure 2.2: The general mechanism for derivatization of carboxylic acid and phenol with methyl chloroformate (MCF) under alkaline conditions (modified from (Madsen et al., 2016)).

2.3.2 GC-MS procedure

The method used for the samples from the aqueous phase is based on the paper by Madsen R. B. et. al. (Madsen et al., 2016) published in *Analytical and Bioanalytical Chemistry*. The concentration of the sample is diluted to be approximately 20 mg mL⁻¹. Table 2.1 lists the chemicals used for the preparation of samples for GC-MS analysis as well as their relevant specifications.

Table 2.1: List of chemicals used for GC-MS analysis as well as their specifications. All chemicals are supplied from Sigma Aldrich.

Chemicals	Specifications
MeOH	≥99,5 % purity, analytical grade
NaOH	5 %
Pyridine	≥99,5 % purity, analytical grade
MCF	99 % purity, analytical grade
CHCl ₃	≥99,5 % purity, analytical grade
4-Bromotoluene	98 % purity
NaHCO ₃	50 mM

The samples for GC-MS analyses are prepared by using chloroform with an internal standard, with composition listed in Table 2.2. The content of the GC-MS samples are added to a 2 mL vial, and the preparation components of the sample is given in Table 2.3. When all the components from Table 2.3 are added, the aqueous phase is removed with a pipette and discarded before an aliquot of 125 µL of the organic phase is transferred to a 200 µL vial with insert. All samples are made in duplicates, and the average values of the duplicates are used for the GC-MS diagrams in the results section. The accuracy limit of the equipment used to prepare the GC-MS samples are listed in Table 2.4.

Table 2.2: Composition of the chloroform containing the internal standard.

Components:	Volume (mL)	Concentration (µg mL⁻¹)
CHCl ₃ (l)	19.6	-
4-Bromotoluene (l)	0.4	20

Table 2.3: Preparation of the GC-MS samples.

Components:	Volume (µL)	Vortexed (s)
AP sample (l)	200	-
NaOH (l)	40	-
Pyridine (l)	40	Gently swirled
MCF (l)	2 x 20	2 x 30
CHCl ₃ w/internal std. (l)	400	10
NaHCO ₃ (l)	400	10

Table 2.4: The accuracy limit of the sampling equipment used for GC-MS.

Sampling equipment:	Accuracy limit
10-100 μL Finn-pipette	$\pm < 3 \%$
100-1000 μL Finn-pipette	$\pm < 1 \%$

The samples were analyzed by the use of GC-MS by Ph.d. student Juliano Souza dos Passos. 1 μL samples is injected with a split ratio 20:1 and injector temperature 280 $^{\circ}\text{C}$, split liner with quartz wool on a VF-5ms column with a 5%-phenyl, 95% dimethylpolysiloxane stationary phase with the dimensions 60 m x 0.25 mm x 0.25 μm with the dimensions 60 m x 0.25 mm x 0.25 μm . The start temperature of the oven is 40 $^{\circ}\text{C}$ (held for 1 min) and is increased by 5 $^{\circ}\text{C min}^{-1}$ to 300 $^{\circ}\text{C}$ (held for 3 min). The transfer line is maintained at 280 $^{\circ}\text{C}$. The MS is operated in scan mode (35-400 m/z) with temperatures of 250 $^{\circ}\text{C}$ and 150 $^{\circ}\text{C}$ for ion source and quadrupole, respectively. The chloroform is stabilized with amylene.

Since there is no need for derivatization of the biocrude samples, they are dissolved using methanol obtained in analytical grade, and extracted using 400 μL methanol with 4-bromotoluene (20 mg mL^{-1}) as an internal standard.

For the biocrude analysis, 1.0 μL of the aliquot retrieved from sample work-up is directly injected with a split ratio 20:1 and injector temperature 280 $^{\circ}\text{C}$, with a helium carrier gas flow of 1 mL min^{-1} , after internal standard addition (4-bromotoluene) on a VF-5ms column with an inert 5% phenylmethyl polysiloxane stationary phase with the dimensions 60 m x 0.25 mm x 0.25 μm . The following temperature program for GC oven is used: The start temperature is 60 $^{\circ}\text{C}$ (held for 2 min) and is increased by 5 $^{\circ}\text{C min}^{-1}$ to 200 $^{\circ}\text{C}$, and then increased by 20 $^{\circ}\text{C min}^{-1}$ to 320 $^{\circ}\text{C}$ (held for 5 min). The compounds are identified with authentic standards, NIST17 mass spectra library or based on literature references (Mørup et al., 2015).

2.4 Nuclear magnetic resonance

2.4.1 Nuclear magnetic resonance theory

Nuclear magnetic resonance (NMR) is one of the most important analytical methods for determining the structure of a compound, as the technique provides information about the exact placement of the atoms in a molecule.

In NMR the absorption of electromagnetic radiation by the nuclei is measured. The phenomenon occurs when a static magnetic field (B_0) is applied in the presence of certain nuclei and is also exposed to another, oscillating field (B_1). To absorb the electromagnetic radiation, the nucleus must have a nuclear spin (I), which makes the nucleus behave like a bar magnet. When the nucleus is in the presence of a magnetic field, the nuclear magnets may assume one of $2I + 1$ orientations relative to the applied field. In organic chemistry, the most important nuclei with $I = \frac{1}{2}$ are ^1H , ^{13}C , ^{19}F , ^{29}Si and ^{31}P (Fleming and Williams, 2019).

Individual, unpaired electrons, protons and neutrons has a spin of $\frac{1}{2}$ (+ or -), which gives them two orientations in the presence of a magnetic field; aligned with the applied field or opposed to the applied field. The orientation that is aligned with the applied field is the low-energy orientation, and opposed to the applied field is the high-energy orientation. If nuclei in the low-energy orientation are exposed to a radio-frequency signal applied to the system, which matches the rotation frequency of the nuclei, the nuclei will absorb the energy and excite to the high-energy orientation, called resonance. The nuclei are shielded by the electrons around them, and difference in the electron density leads to different resonance frequency. As a result, NMR spectroscopy can provide information regarding the type of nuclei, the environment of the nuclei and stereochemistry (Pavia, 2015).

A typical NMR spectrum is a plot of resonance frequency against signal intensity. The frequency axis gives the chemical shift (δ) and is shown in parts per million (ppm), and the scale is calibrated relative to the signal of a reference compound, whose frequency is set to 0 ppm (Field et al., 2015). In the thesis the reference compound used, was 3-(trimethylsilyl)-propionic-2,2,3,3-d₄ acid (TSP). For signals with multiple peaks, the distance between them is called a coupling constant (J), and is measured in Hz. The coupling constant gives information on which atoms are coupled, and the position between them (Field et al., 2015).

2.4.2 ^1H , HSQC and HMBC

The one-dimensional (1D) proton specter is the most simple specter and the quickest to obtain. It gives information about chemical shifts, coupling constants (J_{HH}) and integration signals. The ^1H spectra are mainly used to decide the number of and type of protons (Pavia, 2015). Heteronuclear single quantum coherence (HSQC) is a two-dimensional (2D) NMR experiment which shows 1J -couplings between carbon and hydrogen atoms. As it only shows couplings directly between carbon and protons, quaternary carbons will not be shown in the spectra. Heteronuclear multiple bond correlation (HMBC) is a 2D NMR experiment which shows nJ -couplings (mainly 2J - and 3J -couplings) between carbon and hydrogen atoms. In these spectra the quaternary carbons will also be detected (Field et al., 2015).

2.4.3 Quantitative Nuclear Magnetic Resonance

To be able to perform quantitative nuclear magnetic resonance (qNMR) on the aqueous phase a method developed by postdoc Camilla Løhre and associate professor Jarl Underhaug, *noesygpprd1*, was used. The method uses proton spectra with water signal suppression using pre-saturation pulses during relaxation delay. For the quantification part of the analysis emphasis is placed on the ^1H NMR, as it is present in most molecules of interest, has a short relaxation time and gives a strong signal. In addition, a ^{13}C spectra was recorded for one of the samples from each of the feedstocks, recorded for HSQC and HMBC, to be used for the qualitative part of the analysis.

Some aspects should be taken into consideration when using qNMR to obtain accurate and precise quantitative results. The most important of these aspects is the relaxation delay of at least five times the relaxation time, T_1 , of the slowest relaxing signal of interest in the spectrum, to ensure that all spin has reached equilibrium before supplying a new pulse (Amin and Claridge, 2017). The aspects are added to the method used for recording the qNMR spectra.

The compounds of interest in this thesis are quantified using the integral of the added internal standard in the procedure, dimethyl sulfone ($(\text{CH}_3)_2\text{SO}_2/\text{DMSO}_2$) (Løhre et al., Prepared for submission).

The concentration of each component, M_A , was calculated using Equation 2.2:

$$M_A = \frac{I_A \times n_{DMSO_2}}{n_A \times I_{DMSO_2}} \times M_{DMSO_2} \quad (2.2)$$

Where I_A is an integral of the component and n_A is the number of protons giving rise to the signal. I_{DMSO_2} is the integral of the DMSO₂ signal, n_{DMSO_2} is the number of protons giving rise to the DMSO₂ signal (6 protons), and M_{DMSO_2} is the concentration of DMSO₂ in the NMR sample ($101,2 \times 10^{-3}$ M) (Løhre et al., Prepared for submission).

2.4.4 qNMR procedure

Table 2.5 lists the chemicals used for the preparation for qNMR analysis as well as their specifications. The method used is based on earlier work at the University of Bergen. (Halleraker and Barth, 2020)

Table 2.5: Chemicals used for qNMR analysis. All chemicals are supplied from Sigma Aldrich.

Chemicals	Specifications
Na ₂ HPO ₄ ·2H ₂ O (s)	≥99,0 %
H ₂ O (l)	Distilled
D ₂ O (l)	99,9 atom % D Contains 0,05 wt% TSP, sodium salt
HCl	1,0 M
NaOH	1,0 M
DMSO ₂ (s)	Standard for quantitative NMR, TraceCERT®

The qNMR samples are prepared using a 20 % D₂O stock solution and an internal standard. The composition for both are listed in Table 2.6 and 2.7, respectively. The composition of the qNMR samples are listed in Table 2.8. The accuracy limit of the equipment used to prepare the qNMR samples are listed in Table 2.9.

Table 2.6: List of the composition of the prepared 20 % D₂O stock solution.

Components:	Volume (mL)	Mass (g)	pH
Na ₂ HPO ₄ ·2H ₂ O (s)	-	0,445	-
Distilled H ₂ O (l)	50,0	-	-
D ₂ O (l)	200,0	-	-
1,0M HCl/1,0M NaOH	-	-	Adjusted to 7,4

Table 2.7: List of the composition of the internal standard.

Components:	Volume (mL)	Mass (g)	Concentration (M)
DMSO ₂ (s)	-	1,0	2,125
Distilled H ₂ O (l)	5,0	-	-

Table 2.8: List of the composition of the NMR samples.

Components:	Volume (mL)	pH
AP sample (l)	4,0	-
Internal standard (l)	0,250	-
D ₂ O (l)	5,250	-
1,0M HCl/1,0M NaOH	-	Adjusted to 7,4

Table 2.9: The accuracy limit of the sampling equipment used for NMR.

Sampling equipment:	Accuracy limit
Weight	± 0,3 mg
50 mL volumetric flask	± 0,05 mL
200 mL volumetric flask	± 0,1 mL
100-1000 µL Finn pipette	± < 1 %
500-5000 µL Finn pipette	± < 2 %

The samples are analyzed with qNMR on a Bruker 850 MHz AVANCE III HD NMR spectrometer equipped with a 5 mm TCI Cryoprobe, using the standard conditions for methods *zgesgpppe*, *noesygppr1d*, and *cpmgpr1d*. The spectra are analyzed with Bruker's Topspin software 3.6.2.

3 Results and discussion

The aqueous phase (AP) from the experiments with corn stover (CS), wheat straw (WS), sewage sludge (SS), cattle manure (CM) and sugar kelp (SK) as feedstock were all analyzed by GC-MS and NMR. Table 3.1 presents the analyses done on the samples from the different experiments. The corn stover and wheat straw experiments produced the best looking biocrude, meaning black in color, high amount, lower viscosity and had a lower level of sand in the crude, and therefore they were chosen to be the two series that were focused most on in terms of analyses. From these two experiments all aqueous samples were analyzed by GC-MS. For sewage sludge and cattle manure three aqueous samples from each experiment were analyzed by GC-MS: the first sample that gave a significant biocrude-yield, the last sample from the experiment, and the one midway between the other two. The GC-MS samples for the aqueous phase from the sugar kelp experiment were also prepared for GC-MS analyses, but were not analyzed because of lockdown in Aarhus due to Covid-19. All aqueous samples were analyzed by NMR. In the same way as for the aqueous phase samples from the sewage sludge and cattle manure experiments, three biocrude samples from each of the corn stover, wheat straw, sewage sludge and cattle manure experiments were also analyzed by GC-MS. For the sugar kelp experiment, no biocrude analysis was done as the amount of biocrude produced was not enough to allow an analysis. An elemental analysis was performed on the biocrude samples and on solid residue in addition to analysis of ash content in the solid residue and moisture content in the biocrude.

Table 3.1: Analyses done on the samples from the different experiments.

Feedstock	CS	WS	SS	CM	SK
AP GC-MS all samples	X	X	-	-	-
AP GC-MS three example samples	X	X	X	X	X
AP NMR all samples	X	X	X	X	X
Biocrude GC-MS three example samples	X	X	X	X	-
Biocrude elemental analysis	X	X	X	X	-
Solid residue elemental analysis	X	X	X	X	-

3.1 Corn stover

Figure 3.1 shows the average and maximum temperatures and flow rates in the HTL experiment with corn stover as feedstock. The sensor, on the reactor which recorded the maximum temperatures were approximately 12 °C higher than the average temperature of the measuring on all the sensors on the reactor, and the temperature was stable over the main process period (30-220 min). The other HTL experiments were performed under similar and stable temperature and flow conditions.

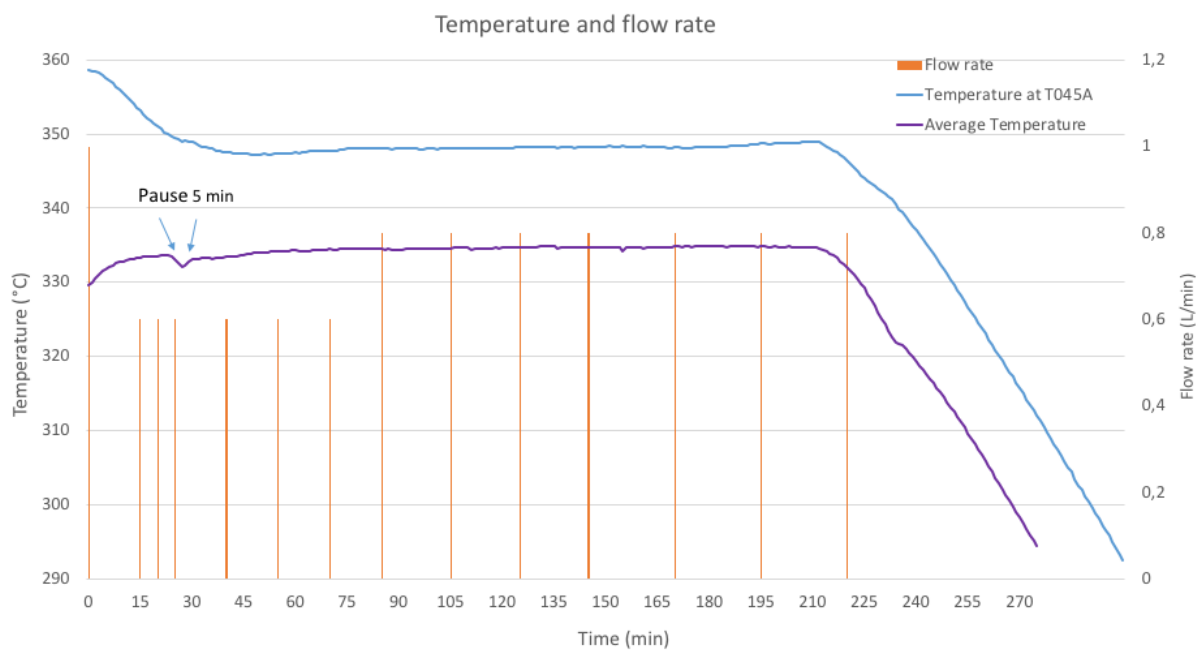


Figure 3.1: Graph of the average and maximum temperatures in the reactor during the run of the corn stover experiment, with flow rate bars at the times samples were retrieved.

3.1.1 Aqueous phase

GC-MS

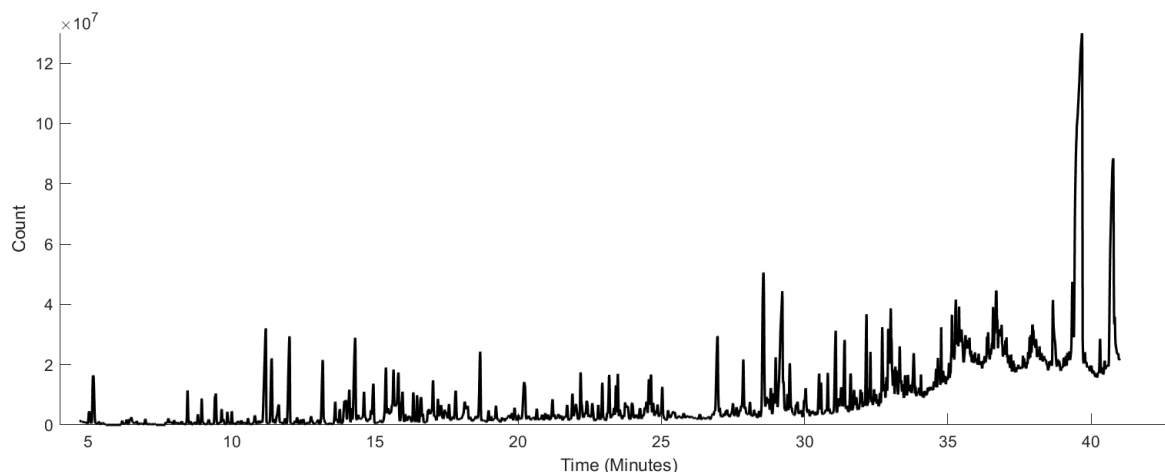
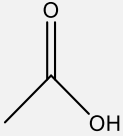
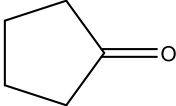
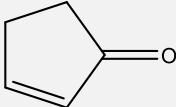
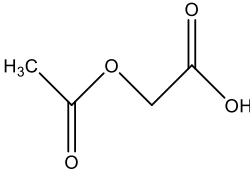
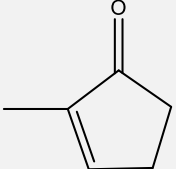
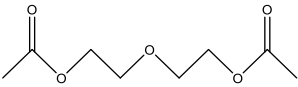
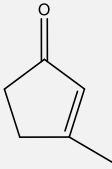
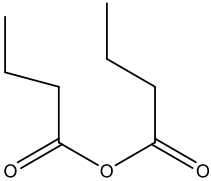


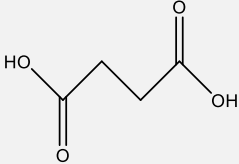
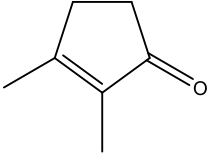
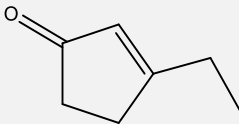

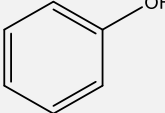
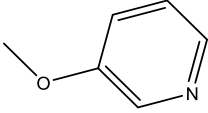
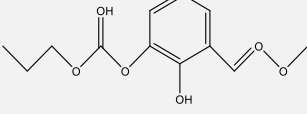
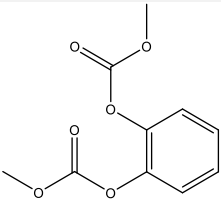
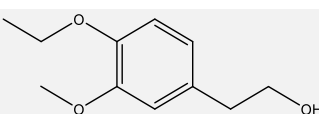
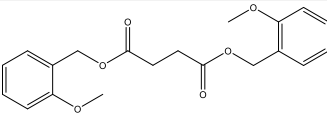
Figure 3.2: Chromatogram from the GC-MS analysis of the aqueous phase taken after 220 minutes from the corn stover experiment.

GC-MS analysis was performed on the aqueous phase from all feedstock experiments using derivatization with MCF. The results are presented as the origin compounds before derivatization, cf. Figure 2.2 on page 17 (in method section). The chromatogram from the GC-MS analysis of the aqueous phase taken after 220 minutes from the corn stover experiment is shown in Figure 3.2. 4-bromotoluene was used as an internal standard, and the peak is used to correct the chromatogram. The internal standard has a retention time of around 15,8 minutes for the aqueous phase samples, and around 18,2 minutes for the biocrude phase samples. The major compounds giving peaks in the chromatogram, as well as the structure of the compounds, the retention time and the peak areas are shown in Table 3.2. The structure of the compounds given in the table are interpreted from the GC-MS library. The largest area shown in Table 3.2 is acetic acid at retention time 5,222 minutes. Peaks were also found for other acids in the aqueous phase, such as acetoxy acetic acid and succinic acids, shown more detailed in Figure 3.5. The ketones found in the aqueous phase from the corn stover experiment were mainly cyclopentanones. Some monoaromatic compounds were also detected from the GC-MS analysis. In addition to the peaks discussed, there is a large non identified peak at retention time around 39 minutes. A relatively high content of butanoic acid, anhydride is also detected, but the interpretation from the GC-MS library might be questionable as an anhydride is not expected in the aqueous phase samples because acid anhydrides would normally hydrolyze in

water to form carboxylic acids. The table shows that the majority of compounds are oxygenated with a high abundance of organic acids, ketones - especially cyclopentanones, and phenols.

Table 3.2: Compounds with respective retention times and peak areas from GC-MS analysis of the aqueous phase with corn stover as feedstock.

Name of compound	Structure	Retention time (min)	Area ($\times 10^6$)
Acetic acid		5,222	11,31
Cyclopentanone		8,456	1,72
2-Cyclopenten-1-one		9,444	1,11
Acetoxyacetic acid		11,114	2,33
2-Cyclopenten-1-one, 2-methyl-		11,369	2,67
Ethanol, 2,2'-oxybis-, diacetate		11,954	3,55
2-Cyclopenten-1-one, 3-methyl-		13,196	1,78
Butanoic acid, anhydride		14,242	4,34

Succinic acid		14,941	0,68
2-Cyclopenten-1-one, 2,3-dimethyl-		15,369	1,30
2-Cyclopenten-1-one, 3-ethyl-		16,645	0,37
Glutaric acid		18,225	0,18
Phenol		18,661	0,96
Pyridine, 3-methoxy-		19,970	0,76
1,2-Benzenediol, O-methoxycarbonyl-O'-propoxycarbonyl-		26,866	2,12
1,2-Benzenediol, O,O'-di(methoxycarbonyl)-		29,409	2,95
4-Ethoxy-3-methoxyphenethyl alcohol		31,261	0,75
Succinic acid, di(2-methoxybenzyl) ester		32,100	2,39

Samples were taken at different time intervals of the aqueous phase with corn stover as feedstock throughout the experiment, and an overview figure of the composition of identified compounds is included in Figure A1 in Appendix A. The figure shows that significant amounts of compounds are not formed until sample number five, taken 40 minutes after the start of pumping of the feedstock into the heat exchanger. The amount of the compounds (based on GC-MS signal area) in all the aqueous phase samples from the liquefaction with corn stover as

feedstock is also shown in the figure. Both Figure 3.3 and Figure A1 in Appendix A shows results that implies that the reactor reaches a steady state very abruptly after around 40 minutes after the feeding starts up. There is a decline in the areas in the graph at the sample taken after 125 minutes, which can be explained by a clogging of the filter and a pressure build-up which might have inhibited the amount of compounds to pass through the filter to reach the take-off system. A few minutes later the filter fell off due to the pressure, and the compound concentration restabilized.

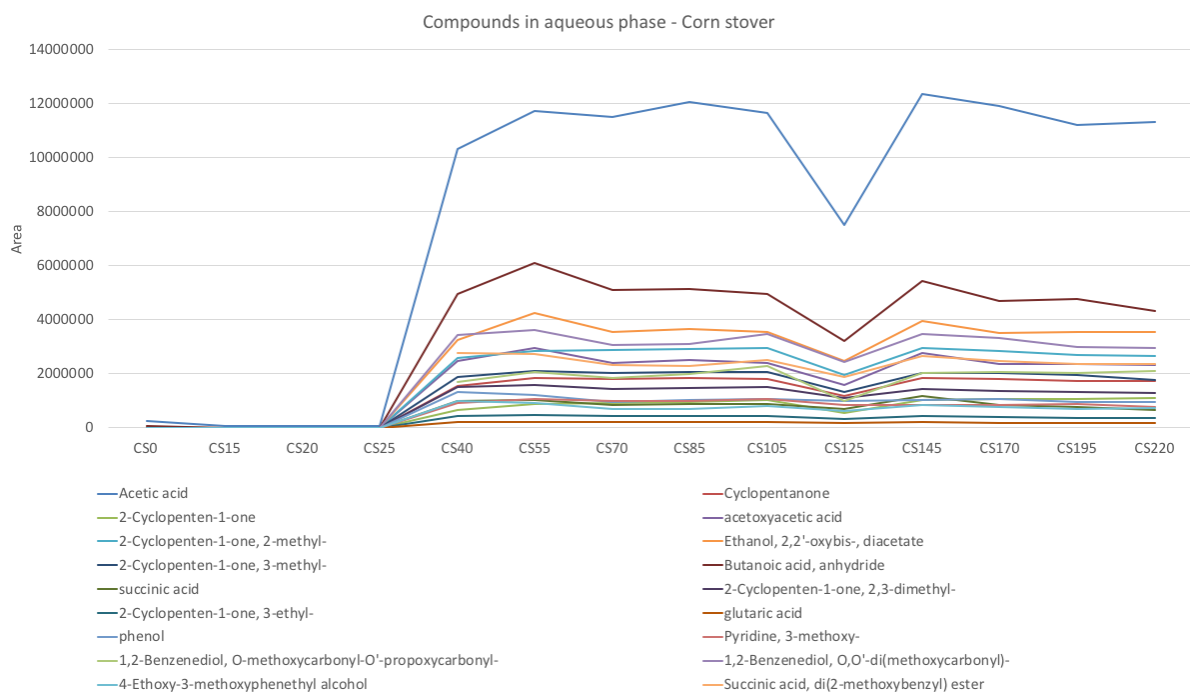


Figure 3.3: Component composition in the aqueous phase for all samples with corn stover as feedstock obtained from the GC-MS analyses.

Figure 3.4 shows the amount of the compounds in the aqueous phase for the last sample point at 220 minutes for corn stover feedstock, which is based on the data from Table 3.2, but gives a more visual comparison. This figure shows a very similar composition compared to the other sample points in the experiment, as is also shown in Figure A1 in Appendix A. Figure 3.4 also shows that acetic acid is the noticeably dominating compound of the aqueous phase from the HTL with corn stover as feedstock.

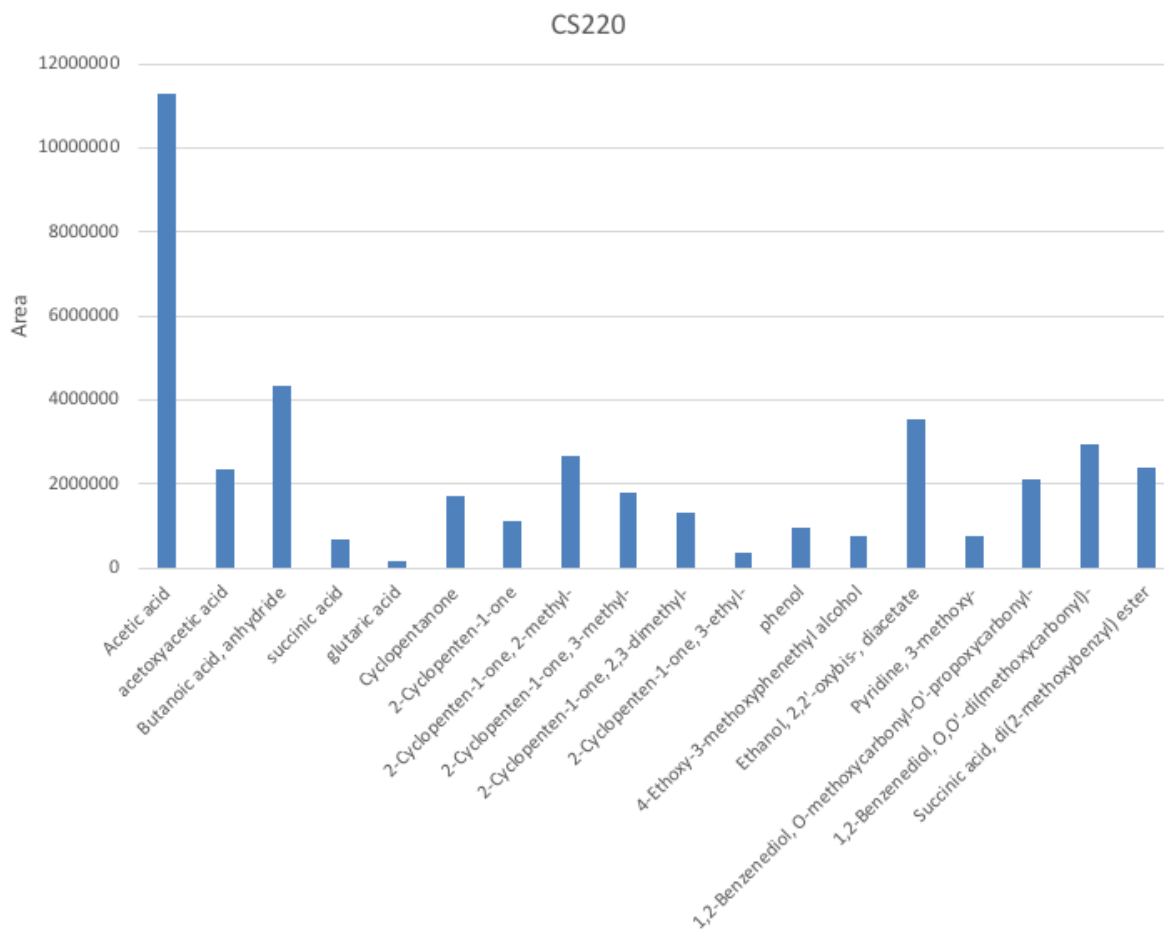


Figure 3.4: Component composition in the aqueous phase for the sample with corn stover as feedstock obtained from the GC-MS analyses after 220 minutes.

To simplify the discussion, the components in the results from the GC-MS analyses of the aqueous phase, the results are divided into four categories, based on the functional groups of the components; carboxylic acids, ketones with a predominance of cyclopentanones, alcohols and a mixed group of compounds which do not fall into the other three categories. Figures 3.4 to 3.7 show diagrams where the compounds in these categories are plotted as the peak area from the GC-MS chromatogram, respectively for carboxylic acids, ketones, alcohols and other compounds. The results are based on the GC-MS analyses of the aqueous phase of the experiment with corn stover used as feedstock. Each diagram is divided into three parts, where the first section is the first sample that gave a significant biocrude yield, the third section is the final sample taken from the experiment, and the second section is the sample taken midway between the other two samples. The first, second and third sections are from the samples taken 40, 105 and in the end at 220 minutes after the feedstock was pumped to the reactor. The trend over time based on these samples showed a marginal increase in fatty acids, fairly stable ketone

fraction with a minimal increase of 2-cyclopenten-1-one. The alcohol fraction with phenol decreased around 30% which might be due to a esterification reaction. A small increase in the concentration of Ethanol, 2,2'-oxybis-, diacetate (also called diethylene glycol diacetate), probably through an esterification reaction was also observed in Figure 3.8.

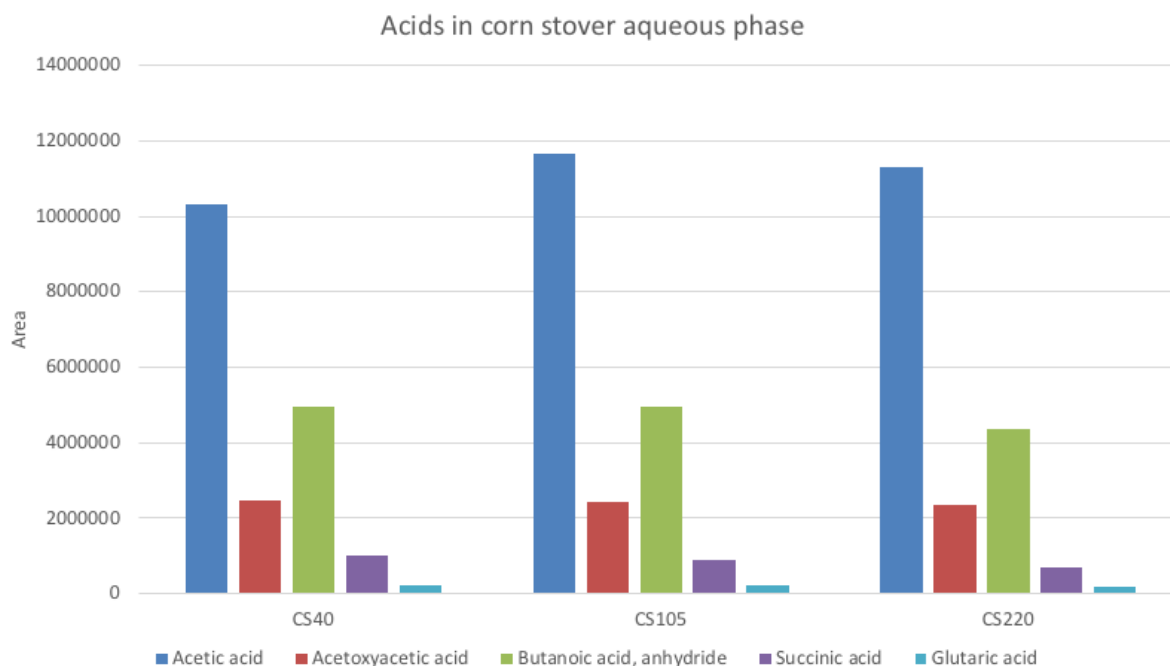


Figure 3.5: Component composition of the carboxylic acids in the aqueous phase for the samples with corn stover as feedstock obtained from the GC-MS analyses after 40, 105 and 220 minutes.

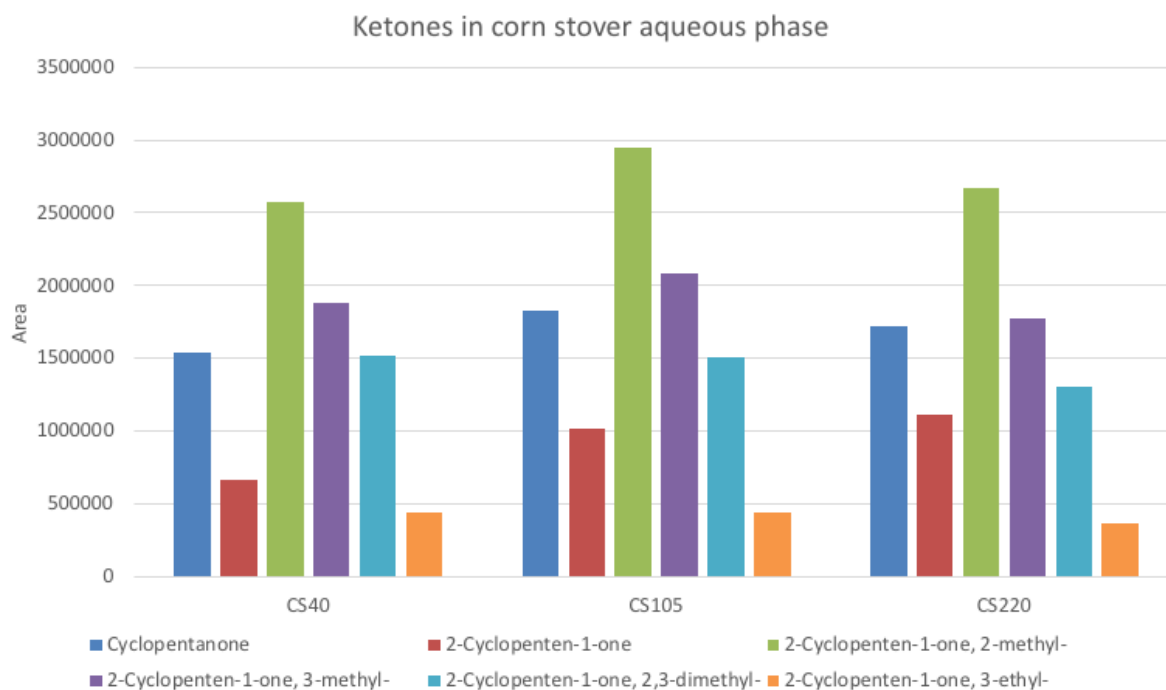


Figure 3.6: Component composition of the ketones in the aqueous phase for the samples with corn stover as feedstock obtained from the GC-MS analyses after 40, 105 and 220 minutes.

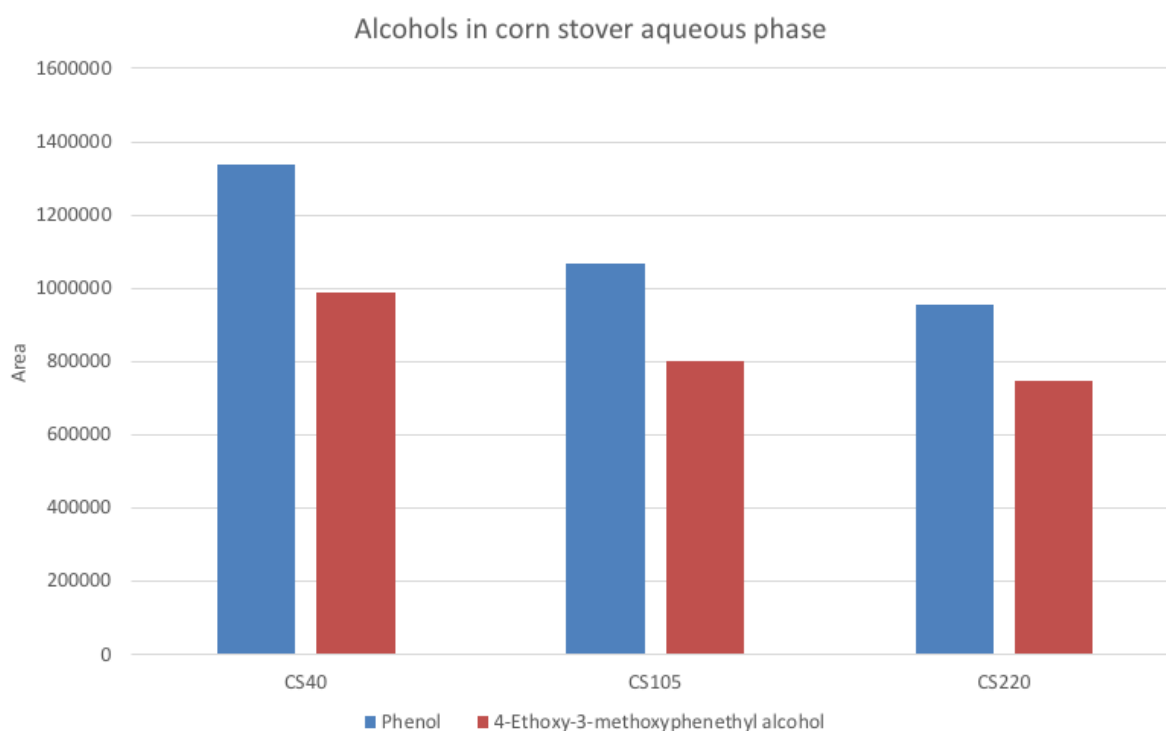


Figure 3.7: Component composition of the alcohols in the aqueous phase for the samples with corn stover as feedstock obtained from the GC-MS analyses after 40, 105 and 220 minutes.

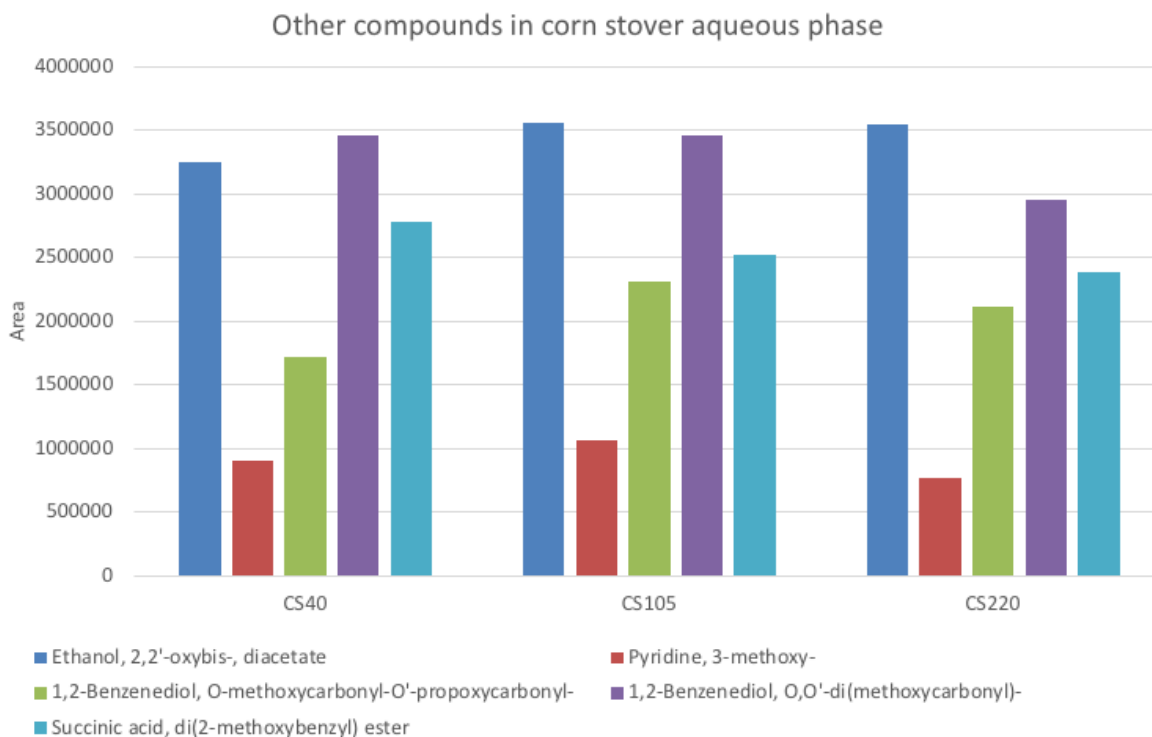


Figure 3.8: Component composition of the other compounds in the aqueous phase for the samples with corn stover as feedstock obtained from the GC-MS analyses after 40, 105 and 220 minutes.

qNMR

The GC-MS derivatization method has a risk of incomplete reactions and formation of multiple derivatives. The method is also quite complex, which gives lower reproducibility. In addition, the GC-MS methods used were not able to detect small organic compounds like methanol and dimethyl ether, as the compounds with low boiling points are not detectable by use of standard GC-MS procedures due to short retention times. Therefore, the aqueous samples were also analyzed by qualitative and quantitative NMR spectroscopy, in order to reduce the uncertainty of the results. (Løhre et al., Prepared for submission)

The full proton spectrum for the aqueous phase from the corn stover experiment is shown in Figure 3.9.

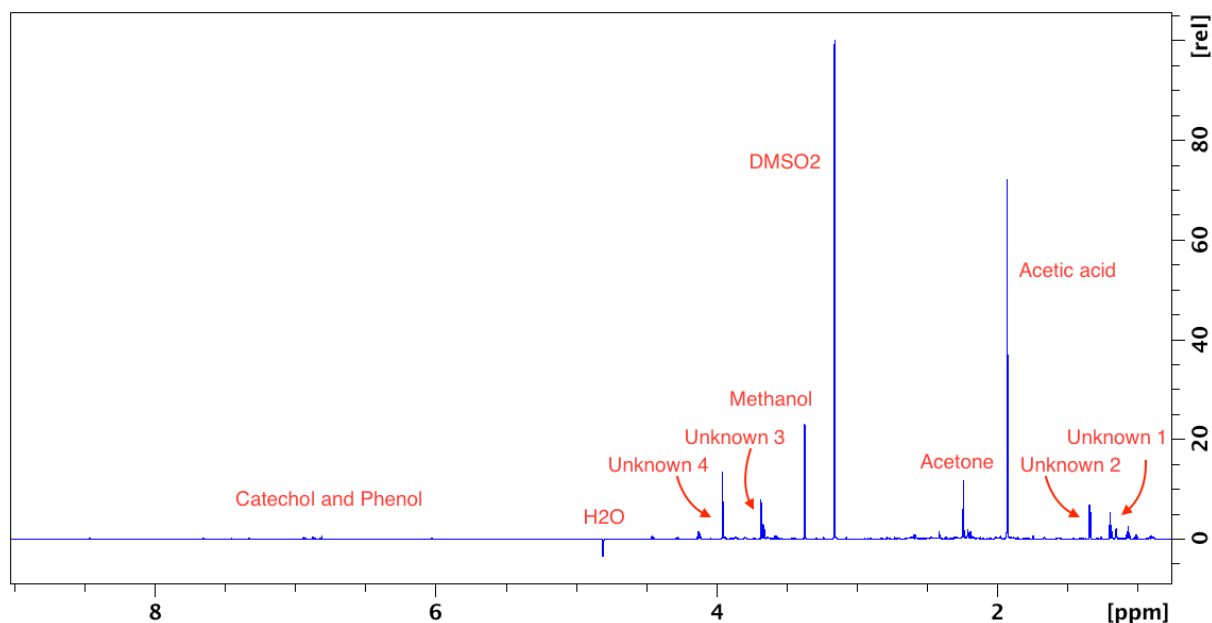


Figure 3.9: ^1H spectrum of the aqueous phase from the experiment with corn stover as feedstock.

HSQC and HMBC spectra were also recorded for each of the feedstock experiments, where Figure 3.10 is showing the full HSQC spectrum of the aqueous phase from the corn stover experiment. The proton spectrum is the horizontal spectrum on top, and the carbon spectrum the vertical spectrum to the left. The parallel axis shows the corresponding chemical shifts. The peaks of phenol and catechol are zoomed in on and shown in Figure 3.11.

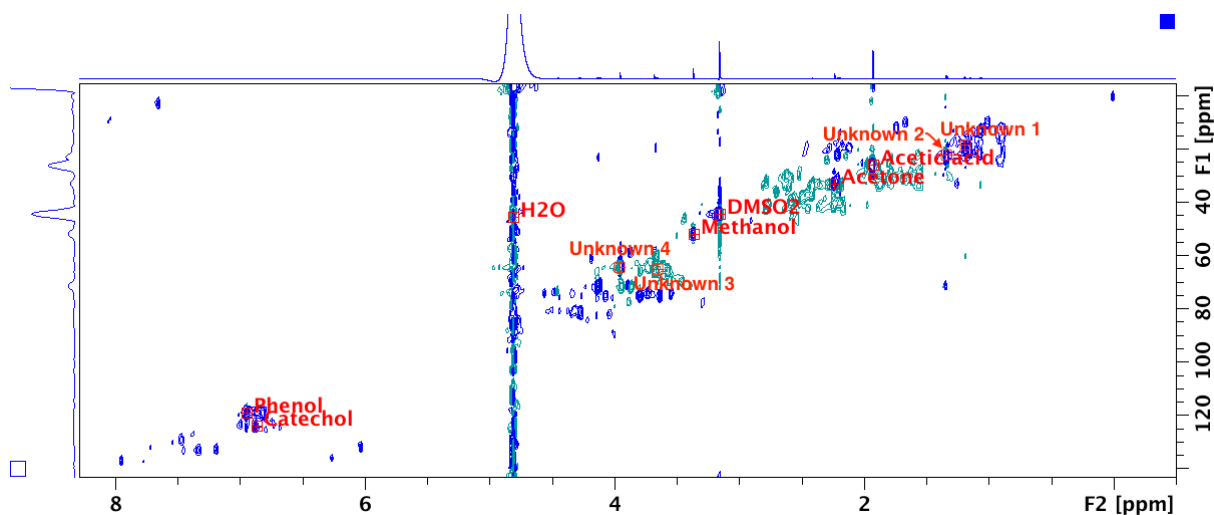


Figure 3.10: HSQC spectrum of the aqueous phase from the experiment with corn stover as feedstock.

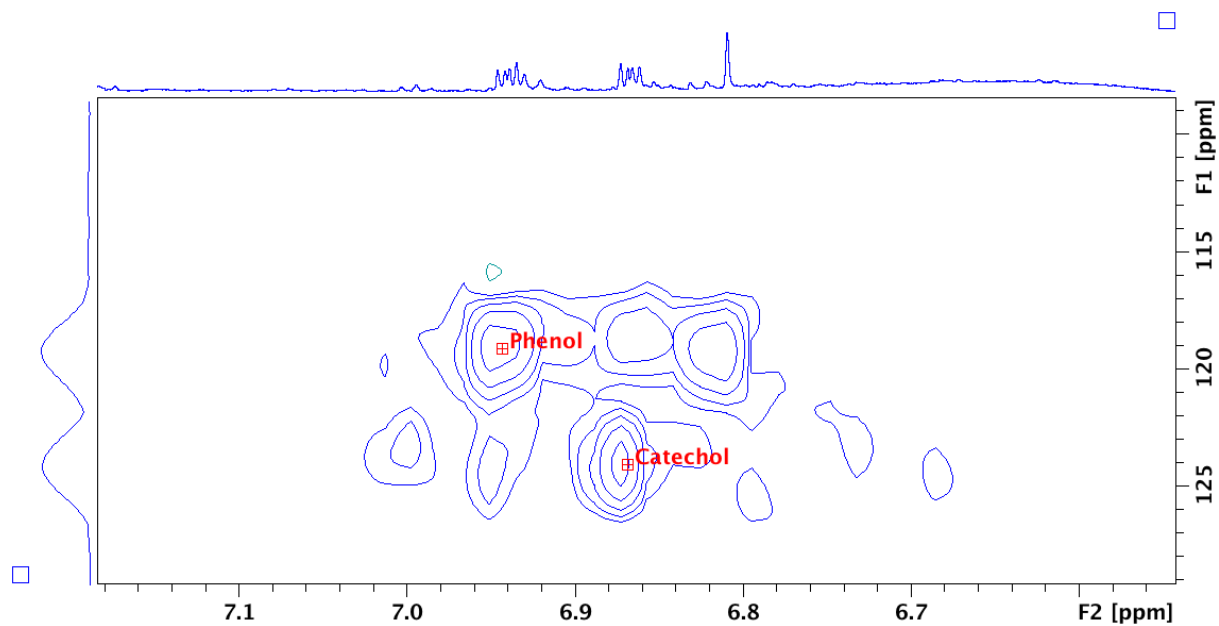


Figure 3.11: HSQC spectrum of the aqueous phase from the experiment with corn stover as feedstock, showing the peaks for phenol and catechol.

The values from the spectra were analyzed and included into Table 3.3, showing the most probable compounds that represent each peak, the proton or carbon which is represented and their corresponding chemical shifts.

Table 3.3: Peak assignment for the NMR of the aqueous sample taken after 55 minutes with corn stover as feedstock.

Compound	¹ H chemical shift ppm		¹³ C chemical shift ppm	
DMSO ₂ (IS)	CH ₃	3,15	CH ₃	44,4
Unknown compound 1	Aliphatic	1,19		19,0
Unknown compound 2	Aliphatic	1,34		22,8
Acetic acid	CH ₃	1,92	CH ₃	26,1
Acetone	CH ₃	2,24	CH ₃	33,2
Methanol	CH ₃	3,37	CH ₃	51,9
Unknown compound 3	Isolated	3,68		65,5
Unknown compound 4	Isolated	3,95		64,2
Catechol	Ph-H (pos. 4 & 5)	6,87	Aromatic C (pos. 3 & 6)	123,9
Phenol	Ph-H (pos. 2 & 6)	6,94	Aromatic C (pos. 2 & 6)	118,4

The peaks were integrated, and the integrals, relative to the internal standard (DMSO₂) were used to calculate the concentration of the compounds in the sample. The major components from the GC-MS chromatogram was searched for with respect to the proton and the carbon spectra for all feedstocks based on literature spectra, without being able to detect the matching compound in the NMR spectra for most of them. Some of the most prominent peaks in the NMR spectra were difficult to determine, and would need to be examined more. These compounds are named Unknown compound and are numbered. Unknown compound 1 gives a triplet in the proton spectrum at 1,19 ppm, while unknown compound 2 gives a doublet at 1,34 ppm. Both of these are so far upfield that they are most likely part of an aliphatic chain, where the triplet in unknown compound 1 suggest that the proton(s) giving the signal has two neighboring protons, most likely in a CH₂ as part of an aliphatic chain. The doublet in unknown compound 2 suggest that the proton(s) giving the signal has one neighboring proton, most likely a CH proton as part of a aliphatic chain, where the carbon is a tertiary carbon. The tertiary carbon is most likely bonded to an extra carbon as the signal would be more downfield is it was bonded to a more electronegative atom like for instance an oxygen or halogen atom. Unknown compounds 3 and 4 both gives singlets, which means that they do not have any neighboring protons, making them isolated protons. The chemical shifts of 3,68 ppm and 3,95 ppm

respectively, suggesting that the carbon they are bonded to is also bonded to something slightly more electronegative than just an aliphatic chain. Table 3.4 shows the integrals and number of protons that the peak represents, as well as the calculated concentrations. The concentrations are given in mM since the ratio of proton signal in NMR is based on a mol ratio. Since the literature most often uses concentration in mg/L this unit is also added in the table. Acetic acid is shown to have the highest concentration, with a concentration of 121,8 mM, which supports the results from the GC-MS analysis shown in Table 3.2 and Figures 3.3 and 3.4. Methanol was detected in the NMR analysis, but not in the GC-MS analysis. The reason for the methanol not providing a peak in the GC-MS chromatogram, is that the compound is too volatile for a GC-MS analysis. Based on the NMR spectra, the aqueous phase seem to have a very low concentration of catechol and phenol.

Table 3.4: Peak assignment for the NMR of the aqueous sample taken after 55 minutes with corn stover as feedstock.

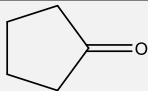
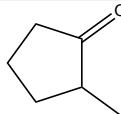
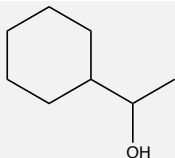
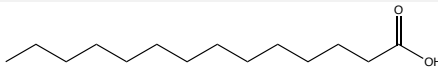
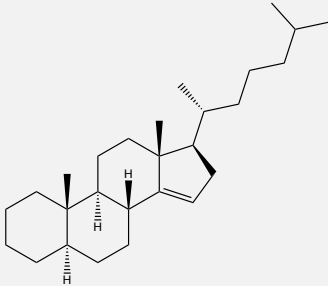
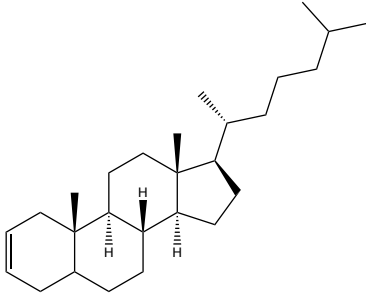
Compound		Number of protons	Integral (rel)	Concentration (mM)	Concentration (mg/L)
DMSO ₂ (IS)	CH ₃	6	1,0000	101,2	9525,96
Unknown compound 1			0,0267		
Unknown compound 2			0,0506		
Acetic acid	CH ₃	3	0,6017	121,8	7314,33
Acetone	CH ₃	6	0,0537	5,4	313,63
Methanol	CH ₃	3	0,1003	20,3	650,41
Unknown compound 3			0,0305		
Unknown compound 4			0,0625		
Catechol	Ph-H (pos. 4 & 5)	2	0,0103	3,1	341,31
Phenol	Ph-H (pos. 2 & 6)	2	0,0094	2,9	272,92

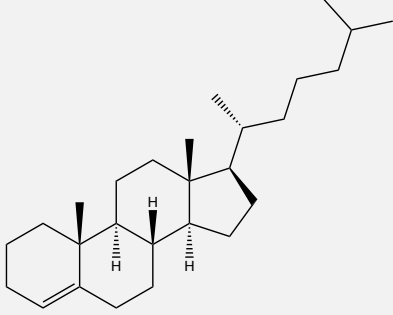
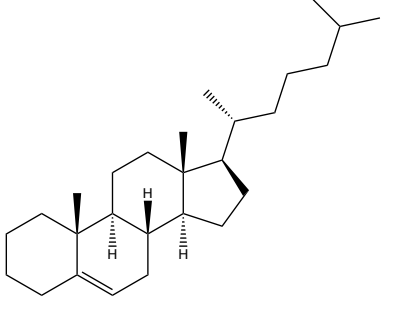
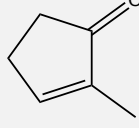
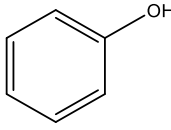
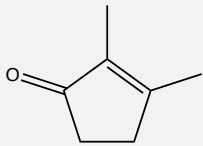
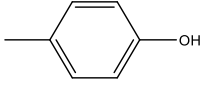
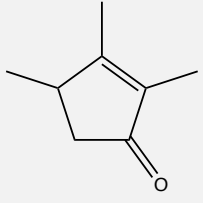
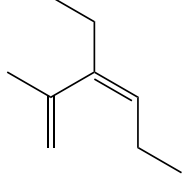
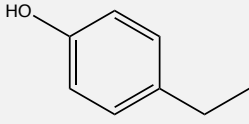
3.1.2 Biocrude

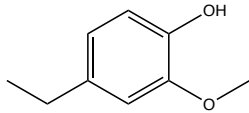
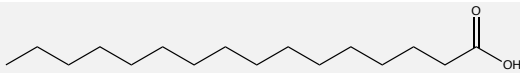
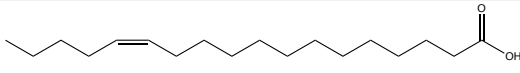
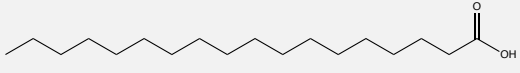
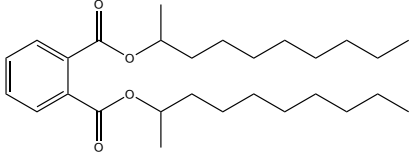
GC-MS

The biocrude was also analyzed by GC-MS, but no derivatization method was used to perform the analyses on the biocrude. The compounds, structures, retention times and areas of the peaks are listed in Table 3.5. The chromatogram where these values are taken from is shown in Figure A6 in Appendix A.

Table 3.5: Compounds with respective retention times and peak areas from GC-MS of the biocrude with corn stover as feedstock.

Name of compound	Structure	Retention time (min)	Area (x10 ⁶)
Cyclopentanone		11,296	5,02
Cyclopentanone, 2-methyl-		12,563	3,34
1-Cyclohexylethanol		14,193	1,77
Tetradecanoic acid		15,016	0,30
Cholest-14-ene, (5.alpha.)-		16,069	1,00
Cholest-2-ene		17,798	0,42

Cholest-4-ene		18,777	0,22
Cholest-5-ene		19,295	0,35
2-Cyclopenten-1-one, 2-methyl-		20,563	18,99
Phenol		21,534	36,12
2-Cyclopenten-1-one, 2,3-dimethyl-		25,130	29,89
p-Cresol		39,154	17,95
2-Cyclopenten-1-one, 2,3,4-trimethyl-		44,322	26,67
1,3-Hexadiene, 3-ethyl-2-methyl-, (Z)-		48,528	11,93
Phenol, 4-ethyl-		49,021	153,99

Phenol, 4-ethyl-2-methoxy-		58,765	59,32
n-Hexadecanoic acid		61,399	17,02
cis-13-Octadecenoic acid		62,197	5,89
Octadecanoic acid		62,469	1,48
Didecan-2-yl phthalate		62,831	5,74

The results from the GC-MS analyses of the biocrude are presented in the diagram in Figure 3.12, where the compounds are plotted against their corresponding peak areas. The values of the component bars to the left of the dotted line in the diagram show their area values at the left axis, and values of the component bars to the right of the dotted line in the diagram show their area values at the right axis. The sample analyses that are plotted from left to right on both sides of the line belongs to the samples taken after 55, 125 and 220 minutes after the feedstock was inserted to the reactor. The less polar compounds were found in the biocrude, where unsubstituted, alkylated phenols along with cyclopentenones and p-cresol were the dominating compounds. Also, some higher fatty acids were detected in this phase. 4-ethyl-phenol is detected as the major compound in the biocrude from the corn stover experiment. After 125 minutes a stable production of compounds is reached. It also seems to be a small reduction at 220 minutes which could be explained by further degradation.

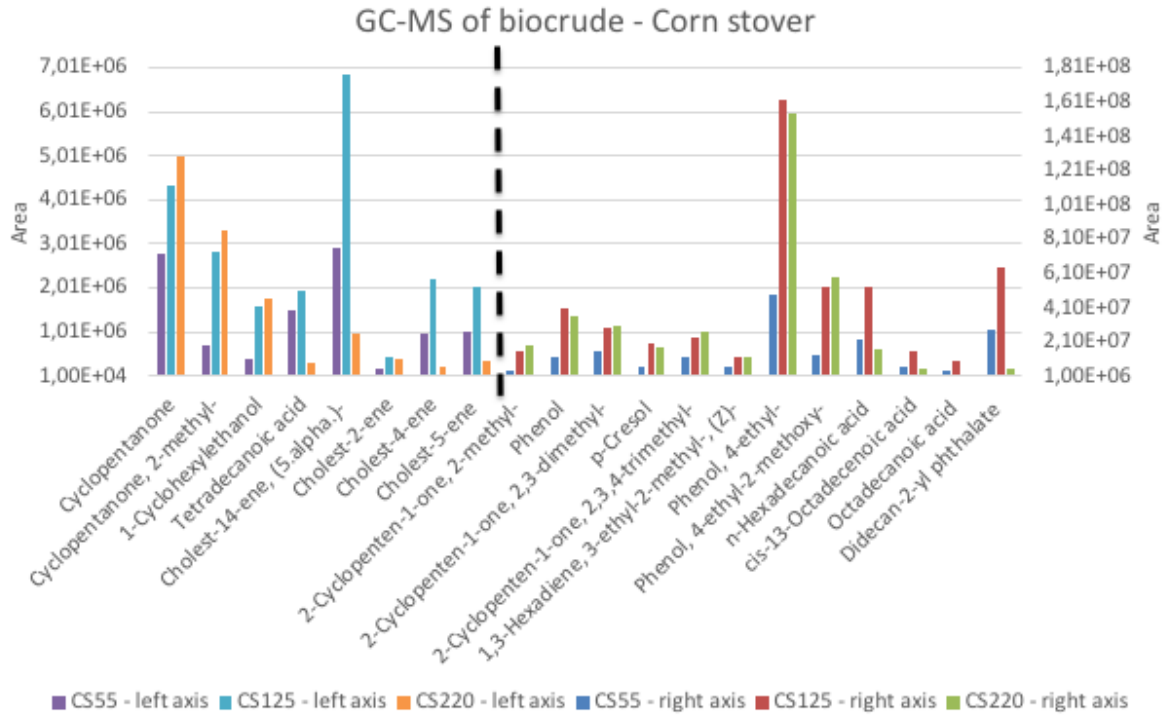


Figure 3.12: Component composition in the biocrude for the samples with corn stover as feedstock obtained from the GC-MS analyses after 55, 125 and 220 minutes. The values of the component bars to the left of the dotted line in the diagram show their area values at the left axis for lower concentrations, and values of the component bars to the right of the dotted line in the diagram show their area values at the right axis for higher concentrations.

3.2 Wheat straw

3.2.1 Aqueous phase

GC-MS

Figure 3.13 shows the GC-MS chromatogram of the last aqueous phase sample taken from the wheat straw experiment, taken 250 minutes after the feedstock was pumped to the reactor.

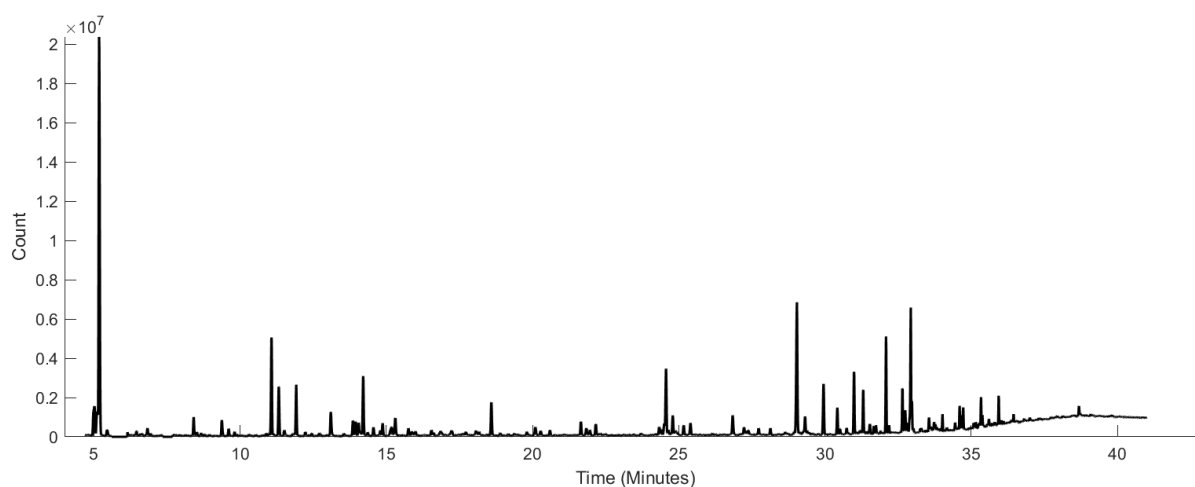
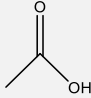
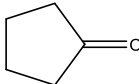
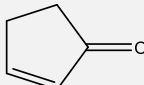
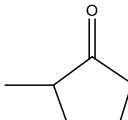

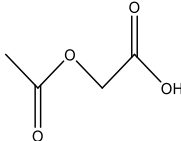
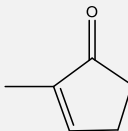
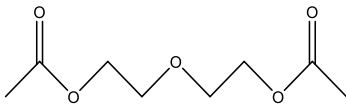
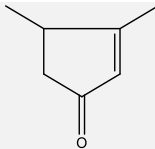
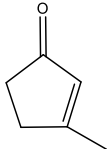
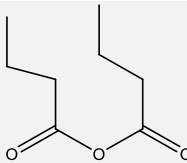
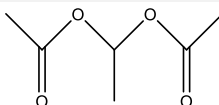
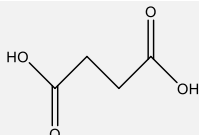
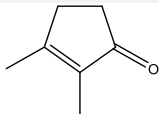
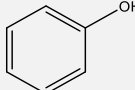
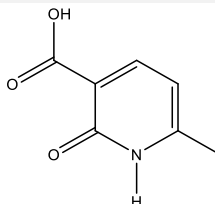
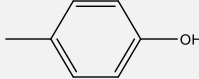
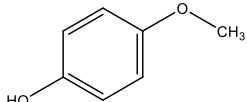
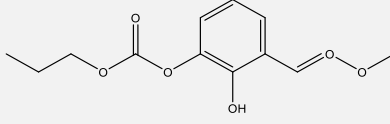

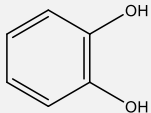
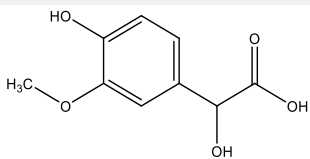
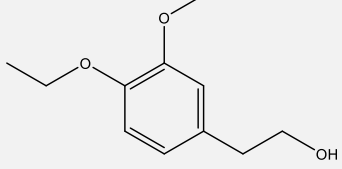
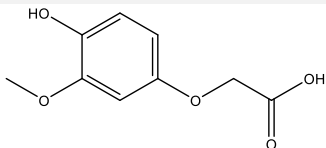


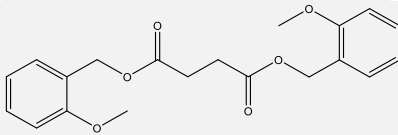
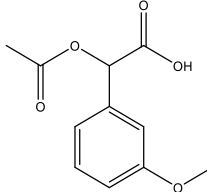
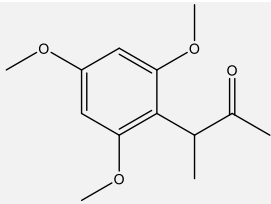
Figure 3.13: GC-MS chromatogram of the aqueous phase from the hydrothermal liquefaction of wheat straw for the sample taken after 250 minutes.

The compounds detected, their structures, the peak retention times and areas from the GC-MS analysis are listed in Table 3.6. Figure 3.13 and Table 3.6 also show that acetic acid is the noticeably dominating compound of the aqueous phase from the HTL with wheat straw as feedstock. In addition to acetic acid, other acids are also detected, such as succinic acid and acetoxy acetic acid. Similarly to the aqueous phase from the corn stover experiment, butanoic acid, anhydride is also detected, but the interpretation from the GC-MS library might be questionable as an anhydride is not expected in the aqueous phase samples. Cyclopentenones, catechol and phenol are also found in smaller amounts in these samples.

Table 3.6: Compounds with respective retention times and peak areas from GC-MS of the aqueous phase with wheat straw as feedstock.

Name of compound	Structure	Retention time (min)	Area ($\times 10^6$)
Acetic acid		5,205	1,02
Cyclopentanone		8,415	0,38
2-Cyclopenten-1-one		9,386	0,89
Cyclopentanone, 2-methyl-		9,608	0,11
2-Heptanol		9,896	0,19
Acetoxyacetic acid		11,081	1,92
2-Cyclopenten-1-one, 2-methyl-		11,328	1,80
Ethanol, 2,2'-oxybis-, diacetate		11,921	1,83
2-Cyclopenten-1-one, 3,4-dimethyl-		12,234	0,06
2-Cyclopenten-1-one, 3-methyl-		13,106	7,90
Butanoic acid, anhydride		14,209	3,70
Ethane-1,1-diol dipropanoate		14,563	0,49

Succinic acid		14,875	0,43
2-Cyclopenten-1-one, 2,3-dimethyl-		15,312	0,48
Phenol		18,595	0,69
2-Hydroxy-6-methylpyridine-3-carboxylic acid		20,101	0,28
<i>p</i> -Cresol		20,595	0,11
4-methoxyphenol		24,562	1,90
1,2-Benzenediol, O-methoxycarbonyl-O'-propoxycarbonyl-		26,841	0,44
2,5,8,11,14,17-Hexaoxaoctadecane		28,134	0,35
Pyrocatechol		29,047	2,49
2-hydroxy-2-(4-hydroxy-3-methoxyphenyl)acetic acid		29,952	1,44
4-Ethoxy-3-methoxyphenethyl alcohol		30,421	0,40
(4-Hydroxy-3-methoxyphenoxy)acetic acid		31,532	0,22

Succinic acid, di(2-methoxybenzyl) ester		32,084	2,79
2-acetoxy-2-(3-methoxyphenyl)acetic acid		33,730	0,30
2-Propanone, 1-methyl-1-(2,4,6-trimethoxyphenyl)		35,335	0,40

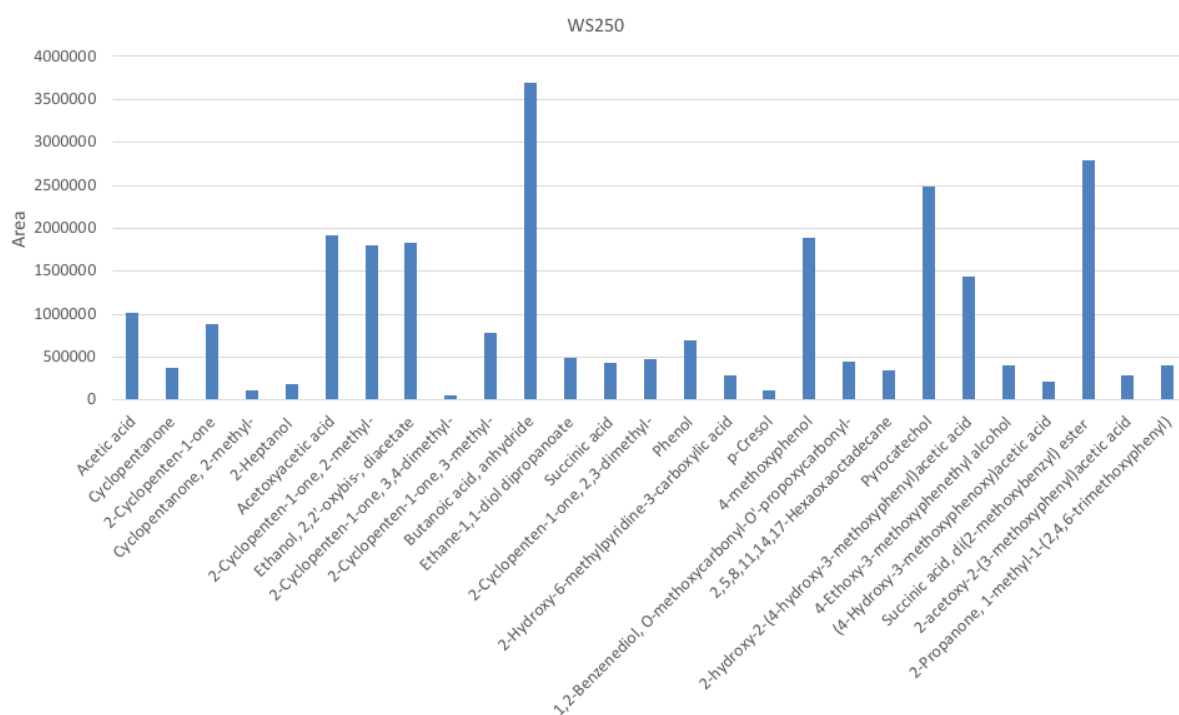


Figure 3.14: Component composition in the aqueous phase for the sample with wheat straw as feedstock obtained from the GC-MS analyses after 250 minutes.

All the components that gave a significant area on the GC-MS peaks from the last sample taken after 250 minutes, are shown in Figure 3.14. The figure is based on the data from Table 3.6, and gives a more visual presentation of the data. Figures 3.15 to 3.18 show the peak areas of

the carboxylic acids, the ketones, the alcohols and the other compounds respectively in the three distributed samples, taken after 75, 150 and 250 minutes. In Figure 3.17 the pyrocatechol seems to have the highest concentration midway, also compared with 4-methoxyphenol, and might have been degraded later in the process. In Figure 3.18, O-methoxycarbonyl-O'-propoxycarbonyl- 1,2-Benzenediol, which is a derivative of catechol, showed the same increase and decrease in concentration in this period. It should be noted that the sample point at 150 after minutes had elevated concentration values for unknown reasons, and therefore is not quite reliable.

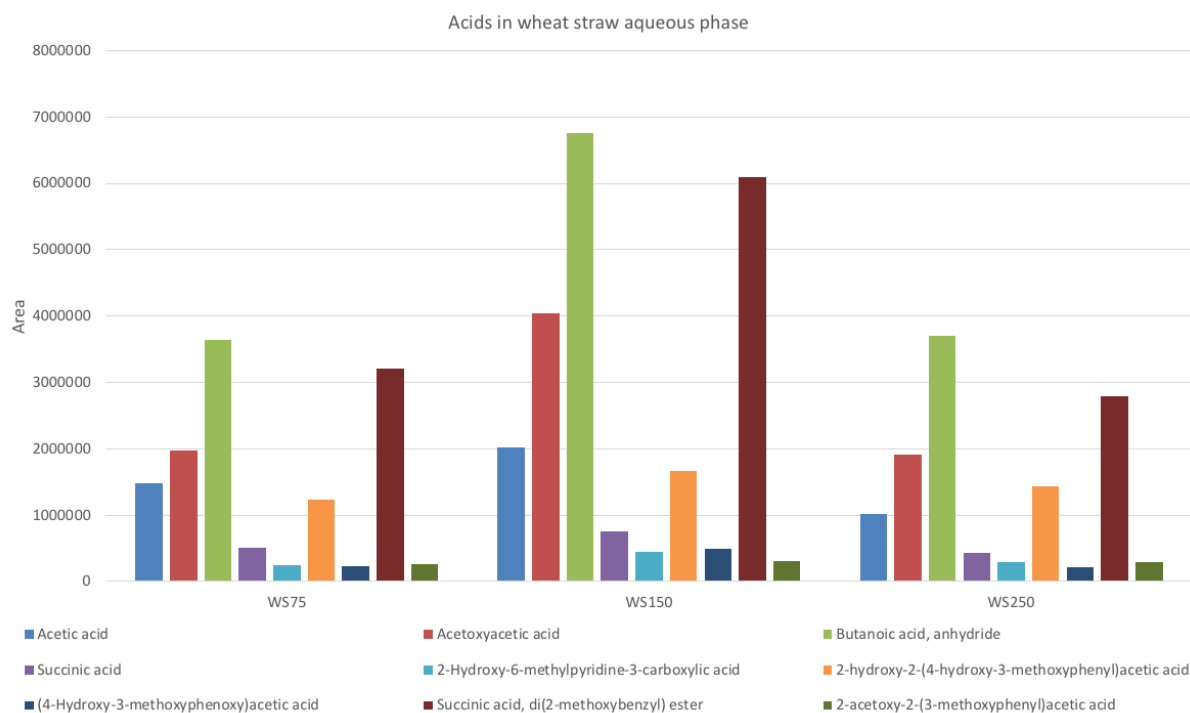


Figure 3.15: Component composition of the carboxylic acids in the aqueous phase for the samples with wheat straw as feedstock obtained from the GC-MS analyses respectively 75, 150 and 250 minutes.

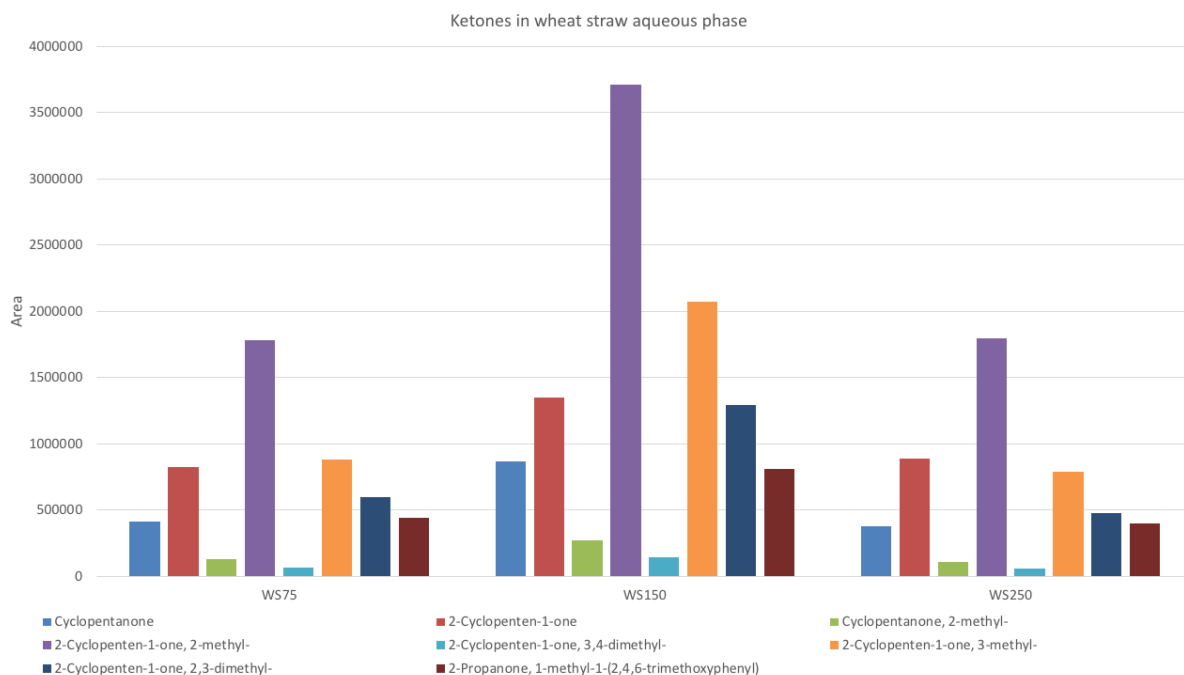


Figure 3.16: Component composition of ketones in the aqueous phase for the samples with wheat straw as feedstock obtained from the GC-MS analyses respectively 75, 150 and 250 minutes.

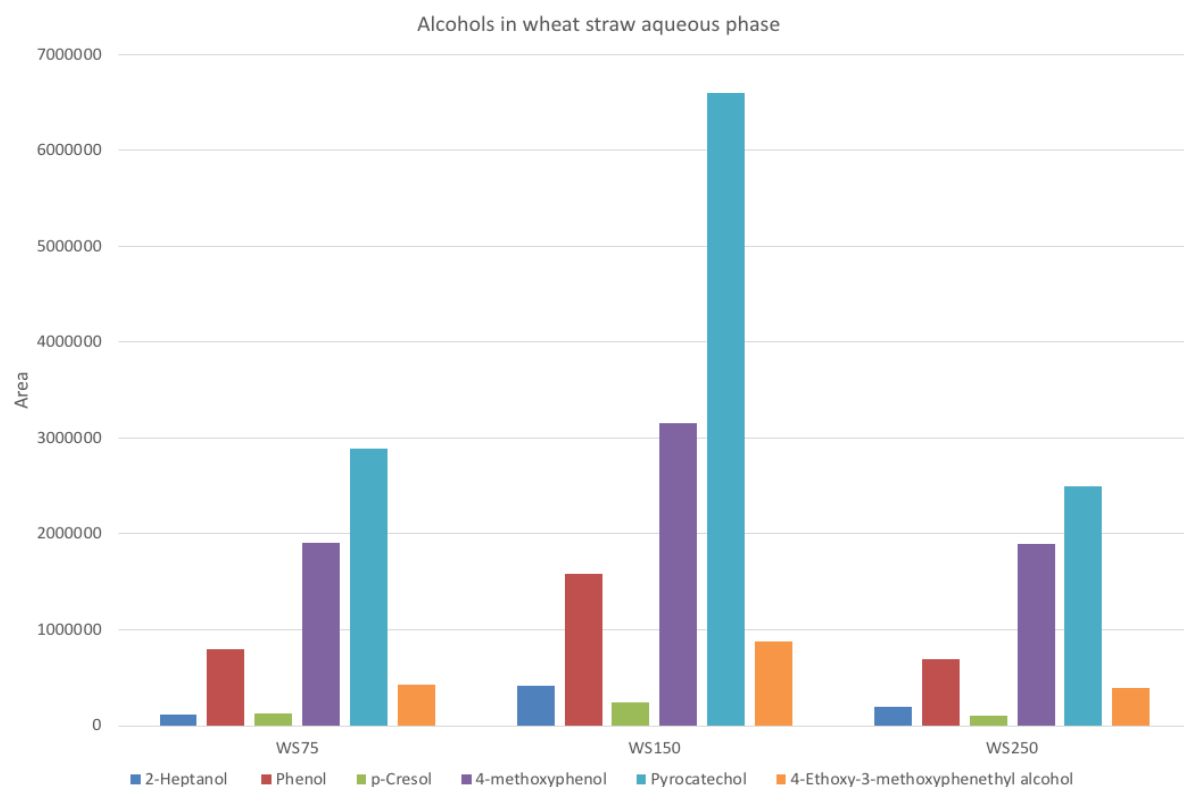


Figure 3.17: Component composition of alcohols in the aqueous phase for the samples with wheat straw as feedstock obtained from the GC-MS analyses respectively 75, 150 and 250 minutes.

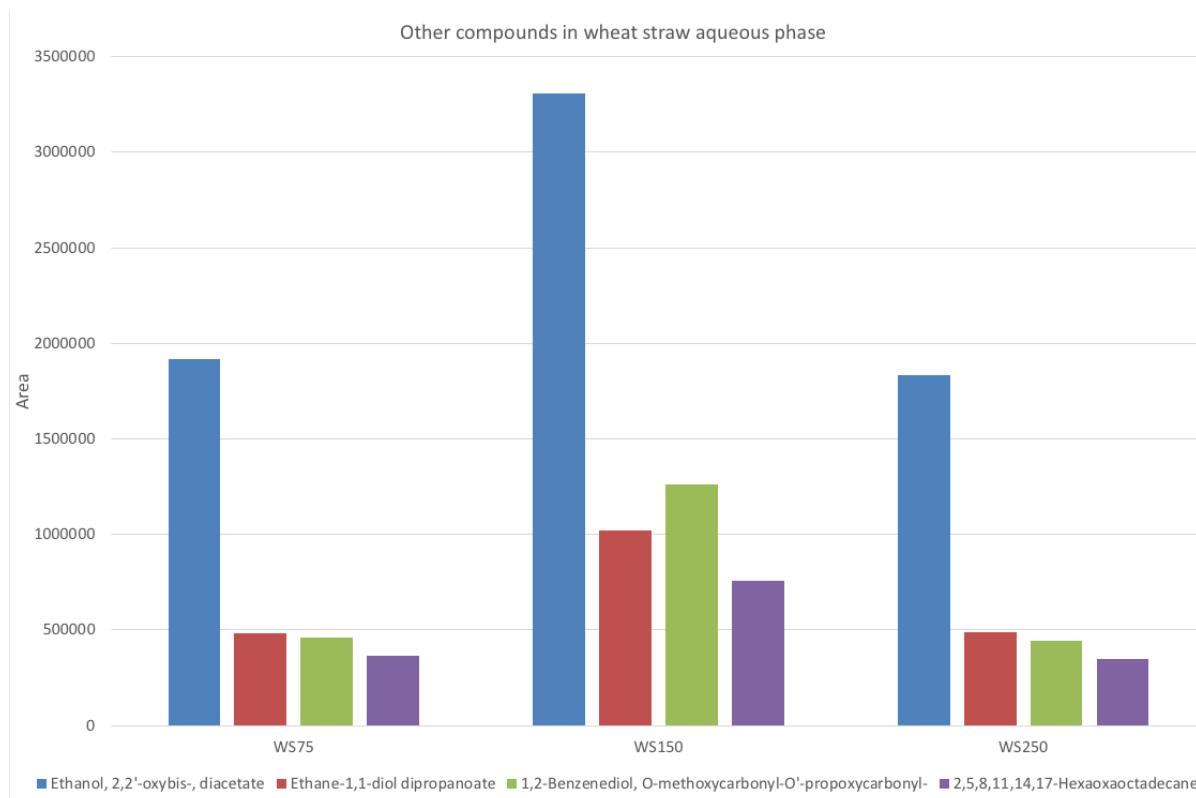


Figure 3.18: Component composition of other compounds in the aqueous phase for the samples with wheat straw as feedstock obtained from the GC-MS analyses respectively 75, 150 and 250 minutes.

The areas from the GC-MS analyses of compounds in the aqueous phase are also plotted in graphs in Figure 3.19, which shows the distribution of the concentrations in the aqueous phase over time. The concentration is fairly stable after approximately 40 minutes, with a somewhat higher concentration at 150 minutes which not easily could be explained. This indicates that the reactor reaches a steady state quite early in the process, in a similar way as observed in the corn stover experiment.

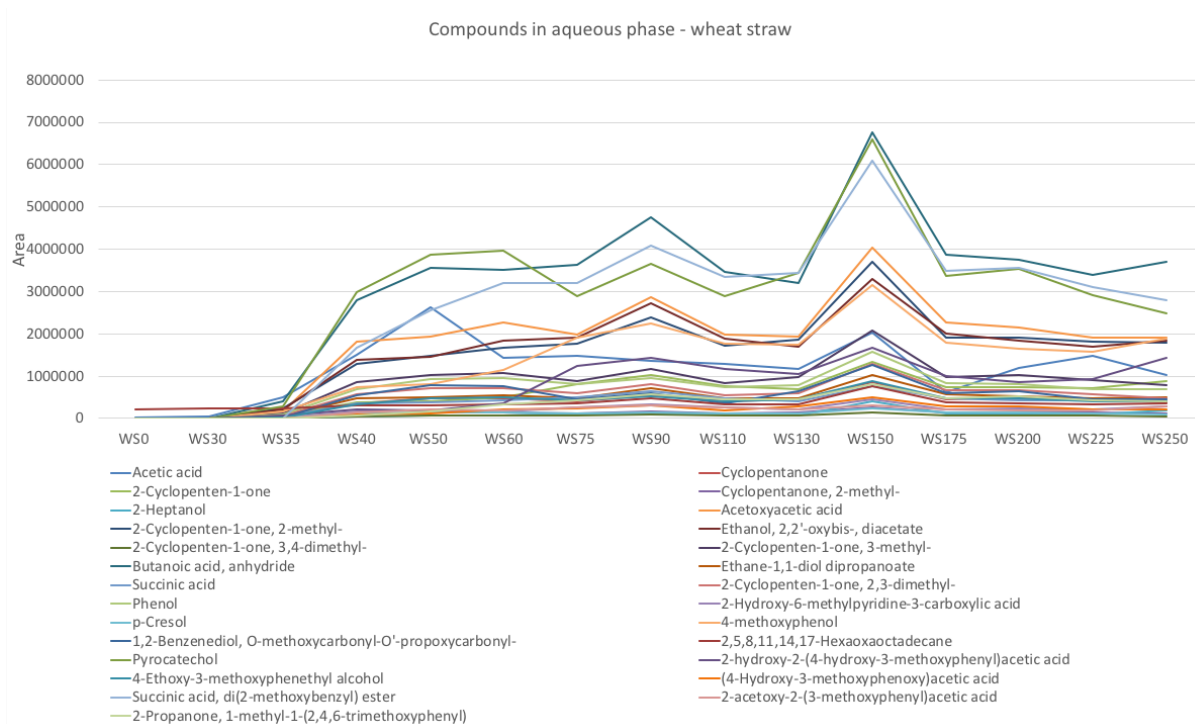


Figure 3.19: Component composition in the aqueous phase for all samples with wheat straw as feedstock obtained from the GC-MS analyses.

qNMR

The full spectrum from the proton NMR analysis from the aqueous phase sample of the wheat straw experiment taken after 60 minutes is shown in Figure 3.20.

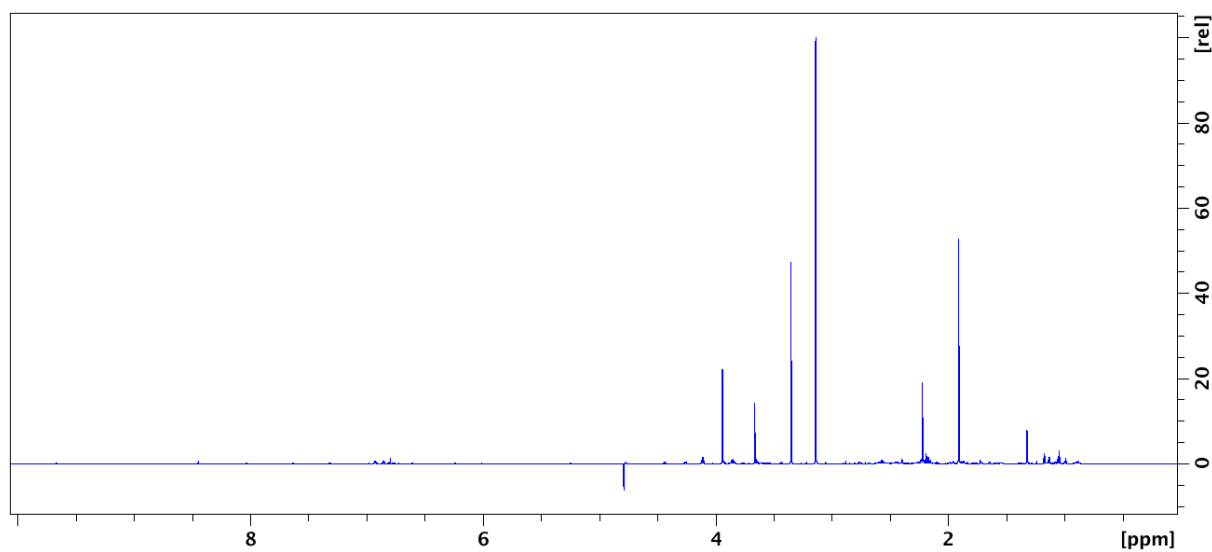


Figure 3.20: ^1H spectrum of the aqueous phase from the experiment with wheat straw as feedstock.

Figure 3.21 shows the full HSQC spectrum of the aqueous phase from the wheat straw experiment.

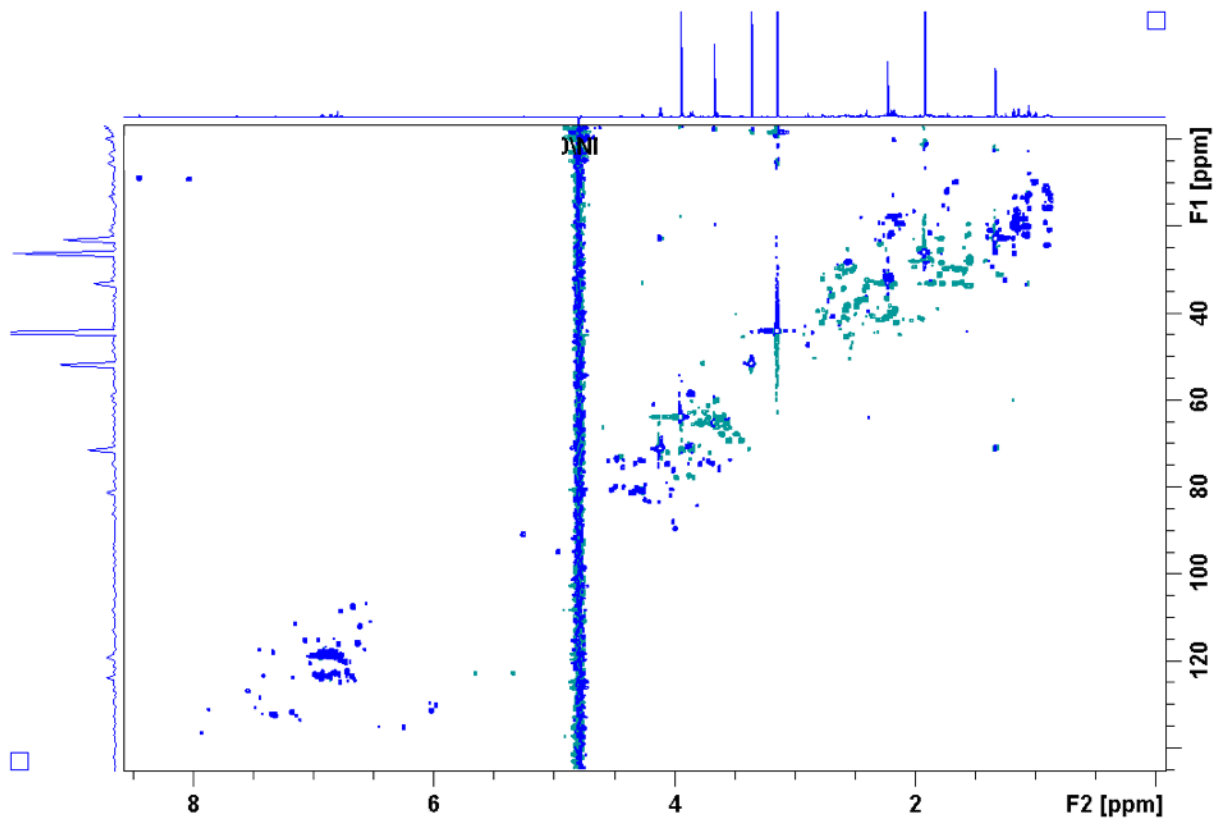


Figure 3.21: HSQC spectrum of the aqueous phase from the experiment with wheat straw as feedstock.

The compounds detected, the represented proton and carbon, as well as their chemical shifts are shown in Table 3.7.

Table 3.7: Peak assignment for the NMR of the aqueous sample taken after 60 minutes with wheat straw as feedstock.

Compound	¹ H chemical shift		¹³ C chemical shift	
		ppm		ppm
DMSO ₂ (IS)	CH ₃	3,14	CH ₃	44,4
Unknown compound 2	Aliphatic	1,32		22,8
Acetic acid	CH ₃	1,91	CH ₃	26,1
Acetone	CH ₃	2,22	CH ₃	33,1
Methanol	CH ₃	3,35	CH ₃	51,9
Unknown compound 3	Isolated	3,66		65,4
Unknown compound 4	Isolated	3,94		64,2
Catechol	Ph-H (pos. 4 & 5)	6,85	Aromatic C (pos. 3 & 6)	123,9
Phenol	Ph-H (pos. 2 & 6)	6,93	Aromatic C (pos. 2 & 6)	119,1*

*Had a shoulder peak at 118,3, which matches the literature.

Table 3.8 lists the number of protons represented in each peak in the spectrum, the integral of the peak as well as the calculated concentration of the detected compound. The unknown compounds 2, 3 and 4 present in the spectra from the aqueous phase from the wheat straw experiment have very similar proton and carbon peaks compared to the compounds in the analysis from the aqueous phase from the corn stover experiment given the same names, thus is most likely the same compounds. The compound with the highest concentration in the qNMR proton spectrum of the aqueous phase from the wheat straw experiment was acetic acid with a concentration of 123,9 mM shown in Table 3.8, which supports the results of the GC-MS analysis of the aqueous phase from the same experiment, shown in Figure 3.14 and Table 3.6. The aqueous phase samples from the wheat straw experiment have a much higher concentration of methanol than the aqueous phase samples from the corn stover experiment shown in Figure 3.9 and Table 3.4. Other than that, most of the compounds have similar concentrations in the wheat straw experiment and the corn stover experiment.

Table 3.8: Peak assignment for the NMR of the aqueous sample taken after 60 minutes with wheat straw as feedstock.

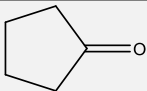
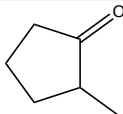
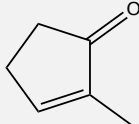
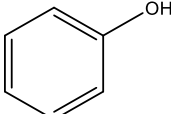
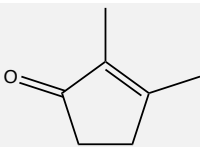
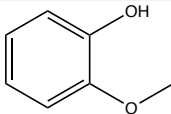
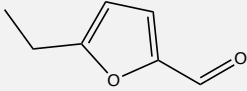
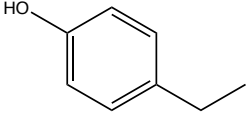
Compound		Number of protons	Integral (rel)	Concentration (mM)	Concentration (mg/L)
DMSO ₂ (IS)	CH ₃	6	1,0000	101,2	9525,96
Unknown compound 2			0,3403		
Acetic acid	CH ₃	3	0,6121	123,9	7440,44
Acetone	CH ₃	6	0,1520	15,4	894,43
Methanol	CH ₃	3	0,4317	87,4	2800,30
Unknown compound 3			0,1938		
Unknown compound 4			0,4995		
Catechol	Ph-H (pos. 4 & 5)	2	0,0287	8,7	957,87
Phenol	Ph-H (pos. 2 & 6)	2	0,0303	9,2	865,81

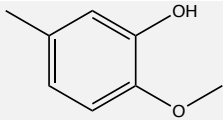
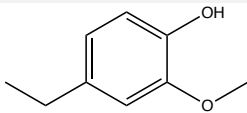
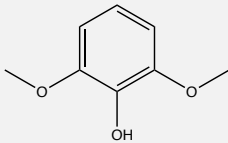
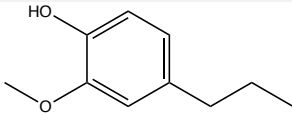
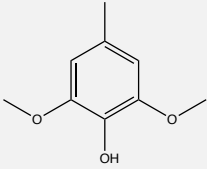
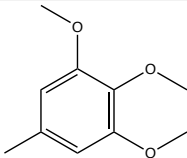
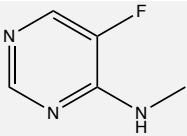
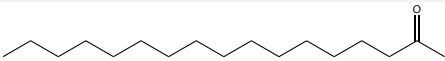
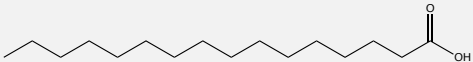
3.2.2 Biocrude

GC-MS

The compounds detected from the GC-MS analyses of the biocrude samples are shown in Table 3.9, along with the structures of the compounds, and the retention times and areas of the peaks in the chromatogram which is presented in Figure B6 in Appendix B.

Table 3.9: Compounds with respective retention times and peak areas from GC-MS of the biocrude with wheat straw as feedstock.

Name of compound	Structure	Retention time (min)	Area (x10 ⁷)
Cyclopentanone		11,288	0,35
Cyclopentanone, 2-methyl-		12,333	0,40
2-Cyclopenten-1-one, 2-methyl-		14,176	1,74
Phenol		16,053	1,55
2-Cyclopenten-1-one, 2,3-dimethyl-		17,789	1,45
Phenol, 2-methoxy-		19,287	5,88
5-Ethyl-2-furaldehyde		20,554	0,54
Phenol, 4-ethyl-		21,525	5,45

2-Methoxy-5-methylphenol		22,447	1,15
Phenol, 4-ethyl-2-methoxy-		25,122	12,48
Phenol, 2,6-dimethoxy-		27,418	5,05
Phenol, 2-methoxy-4-propyl-		27,928	2,28
3,5-Dimethoxy-4-hydroxytoluene		30,340	0,93
Benzene, 1,2,3-trimethoxy-5-methyl-		32,677	2,14
4-Pyrimidinamine, 5-fluoro-N-methyl-2-(1-pyrrolidinyl)-		35,129	2,28
2-Heptadecanone		42,915	0,31
n-Hexadecanoic acid		44,371	0,19

The compounds with significant peak area in the three biocrude samples taken after 110, 150 and 250 minutes are shown in Figure 3.22 respectively from left to right on both sides of the dotted line in the diagram. The columns left of the line show the areas on the left axis, and the columns right of the line show the areas on the right axis. The main products in biocrude phase were methoxyphenols, cyclopentenones, and N-compounds, but not high yield of longer chained fatty acids like in the biocrude from the corn stover experiment. 4-ethyl-2-methoxyphenol is detected as the major compound in the biocrude from the wheat straw experiment.

The compounds have a higher concentration after 110 minutes, than later in the experiment, which could be explained by further degradation.

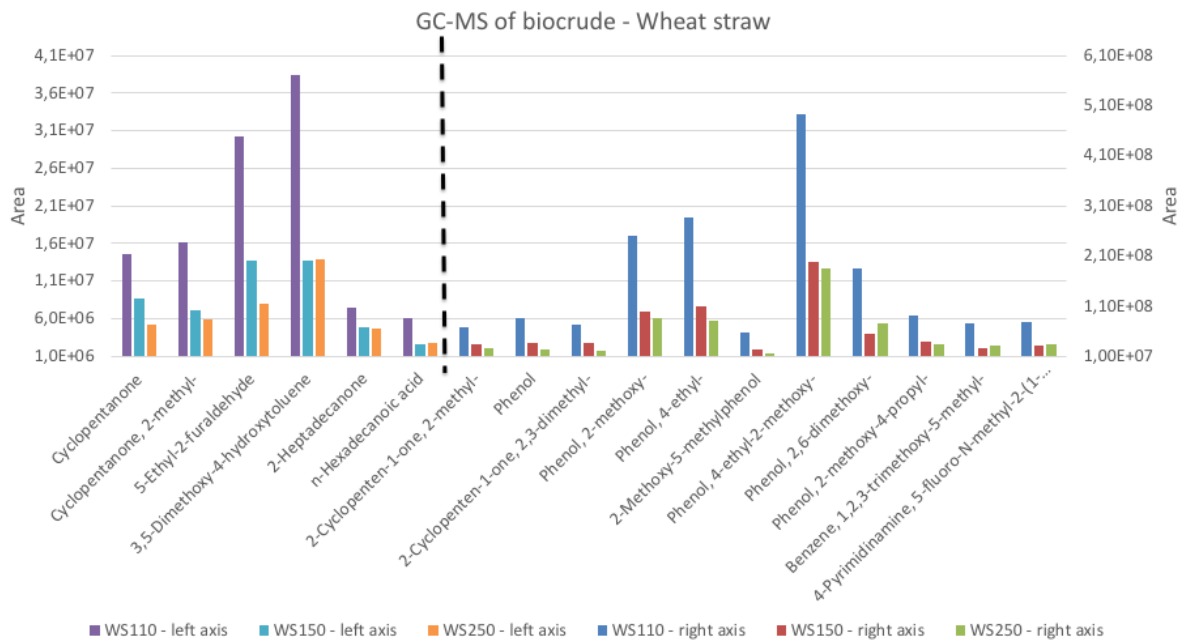


Figure 3.22: Component composition in the biocrude for the samples with wheat straw as feedstock obtained from the GC-MS analyses after 110, 150 and 250 minutes.

3.3 Sewage sludge

3.3.1 Aqueous phase

GC-MS

The chromatogram of the aqueous phase sample taken after 205 minutes after sewage sludge was inserted as feedstock is shown in Figure 3.23.

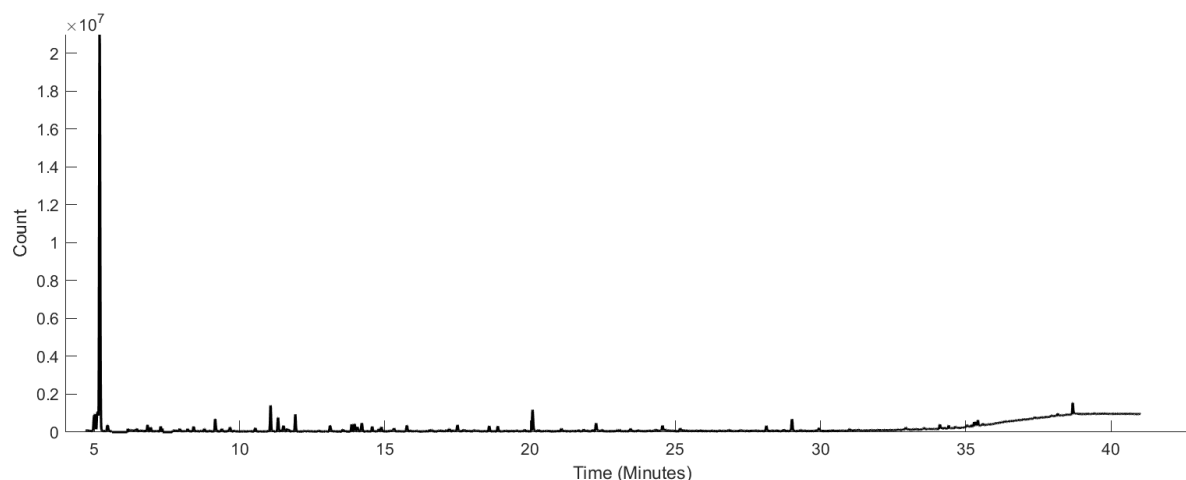
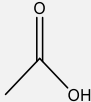
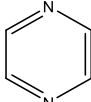
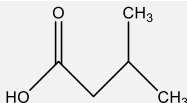
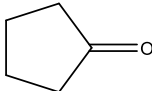
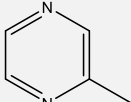
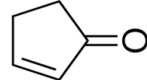
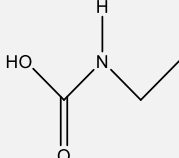
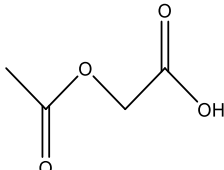
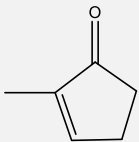
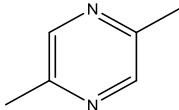
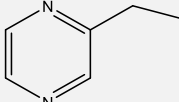
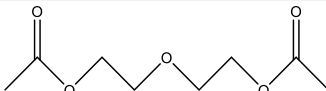


Figure 3.23: GC-MS chromatogram of the aqueous phase from the hydrothermal liquefaction of sewage sludge for the sample taken after 205 minutes.

Table 3.10 shows the compounds detected in the GC-MS analysis of the aqueous phase from the sewage sludge experiment, with the structures of the compounds, the retention time and area of the peaks in the chromatogram. Acetic acid is the dominating product. Pyrazines, cyclopentenones and diethylene glycol diacetate are also major compounds in this phase. The fact that there is detected a lot more nitrogen containing compounds in the aqueous phase from this experiment, than for the others, is supported by the literature which states that sewage sludge contains a lot of protein, which is broken down to nitrogen containing compounds in the HTL process (Toor et al., 2011, He et al., 2014, Huang et al., 2014).

Table 3.10: Compounds with respective retention times and peak areas from GC-MS of the aqueous phase with sewage sludge as feedstock.

Name of compound	Structure	Retention time (min)	Area (x10 ⁵)
Acetic acid		5,181	118,10
Pyrazine		7,279	3,55
Isovaleric acid		7,938	0,55
Cyclopentanone		8,423	1,95
Pyrazine, methyl-		9,156	7,49
2-Cyclopenten-1-one		9,386	1,37
Ethylcarbamic acid		9,674	2,26
Acetoxyacetic acid		11,073	5,33
2-Cyclopenten-1-one, 2-methyl-		11,328	4,07
Pyrazine, 2,5-dimethyl-		11,509	2,92
Pyrazine, ethyl-		11,633	1,35
Ethanol, 2,2'-oxybis-, diacetate		11,921	10,35

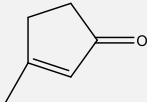
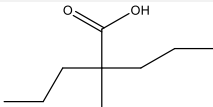
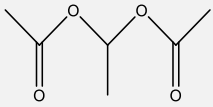
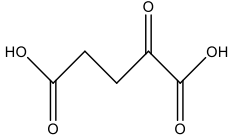
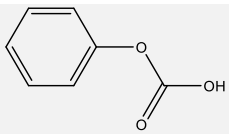
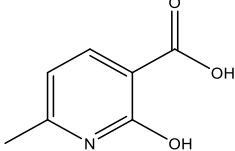
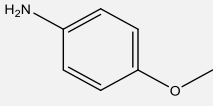
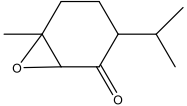
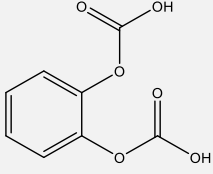
2-Cyclopenten-1-one, 3-methyl-		13,122	2,47
Pentanoic acid, 2-methyl-2-propyl-		14,209	4,35
Ethane-1,1-diol dipropanoate		14,563	3,21
2-Oxopentanedioic acid		14,884	1,99
Phenyl hydrogen carbonate		18,595	1,12
2-Hydroxy-6-methylpyridine-3-carboxylic acid		20,085	7,49
Benzenamine, 4-methoxy-		22,274	2,28
7-Oxabicyclo[4.1.0]heptan-2-one, 6-methyl-3-(1-methylethyl)-		25,163	0,05
1,2-phenylene bis(hydrogen carbonate)		29,022	2,62

Figure 3.24 shows the areas from the peaks of the compounds with noteworthy area in the GC-MS spectrum of the aqueous sample from the sewage sludge experiment taken after 205 minutes. The figure is based on the data from Table 3.10, and gives a more visual presentation of the data. The first peak represents acetic acid and has a value of $118,1 \times 10^5$, which is so prominent that all other peaks were barely visible in comparison. Therefore the full zoomed out diagram is shown in the top of the other diagram, and the large diagram shows a zoomed in version where the acetic acid peak rises above the maximum area value shown on the y-axis, to better show the results of the other compounds.

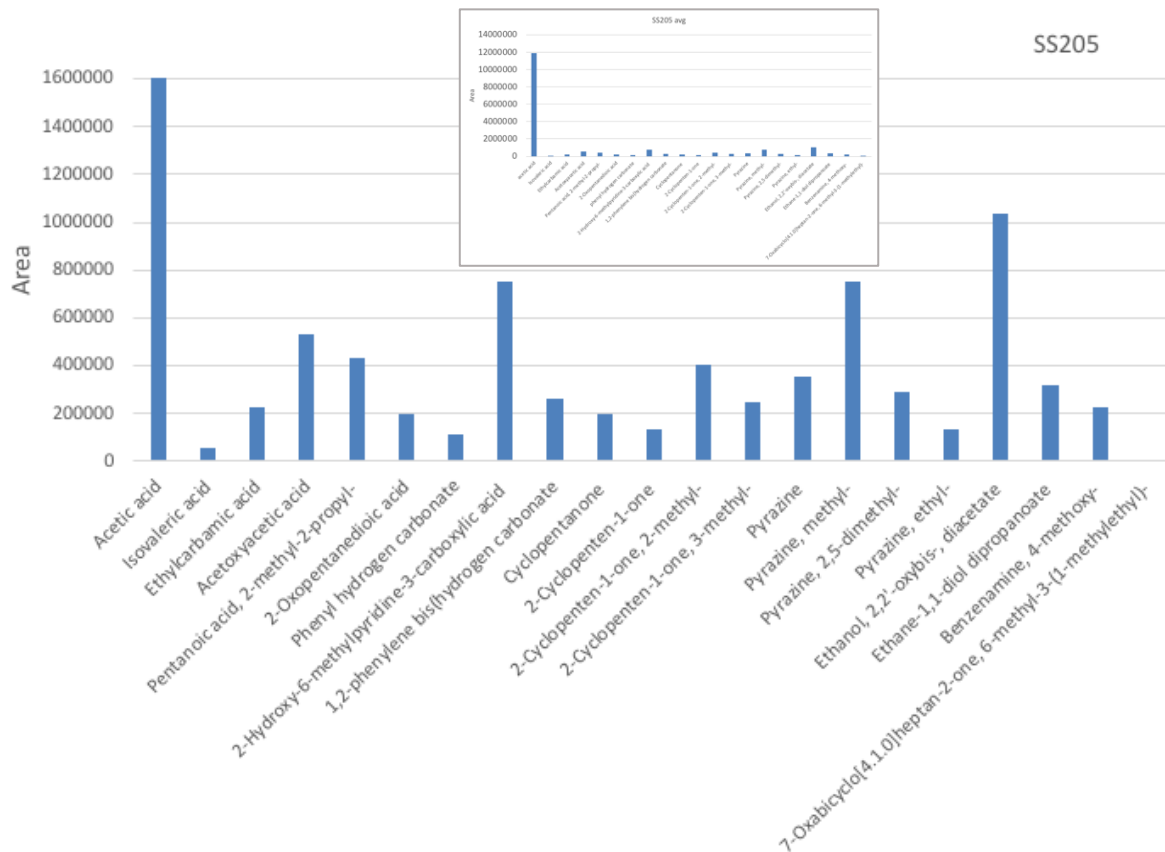


Figure 3.24: Component composition in the aqueous phase for the sample with sewage sludge as feedstock obtained from the GC-MS analyses after 205 minutes.

Figures 3.25 to 3.27 shows the areas of the carboxylic acids, ketones and other compounds respectively, from the aqueous samples taken after 30, 175 and 205 minutes of the sewage sludge experiment. As there were no alcohols with significant peak areas in these samples, there is no diagram showing alcohols. This is different from the aqueous phase from the corn stover and wheat straw experiments. In Figure 3.25 which shows the carboxylic acids, the acetic acid is not present in the beginning of the process at 30 minutes, but again so prominent in the other two sample analyses that the large diagram is zoomed in to not show the top of that peak, to better show the results of the other carboxylic acids, while the zoomed out diagram is shown in the top left corner.

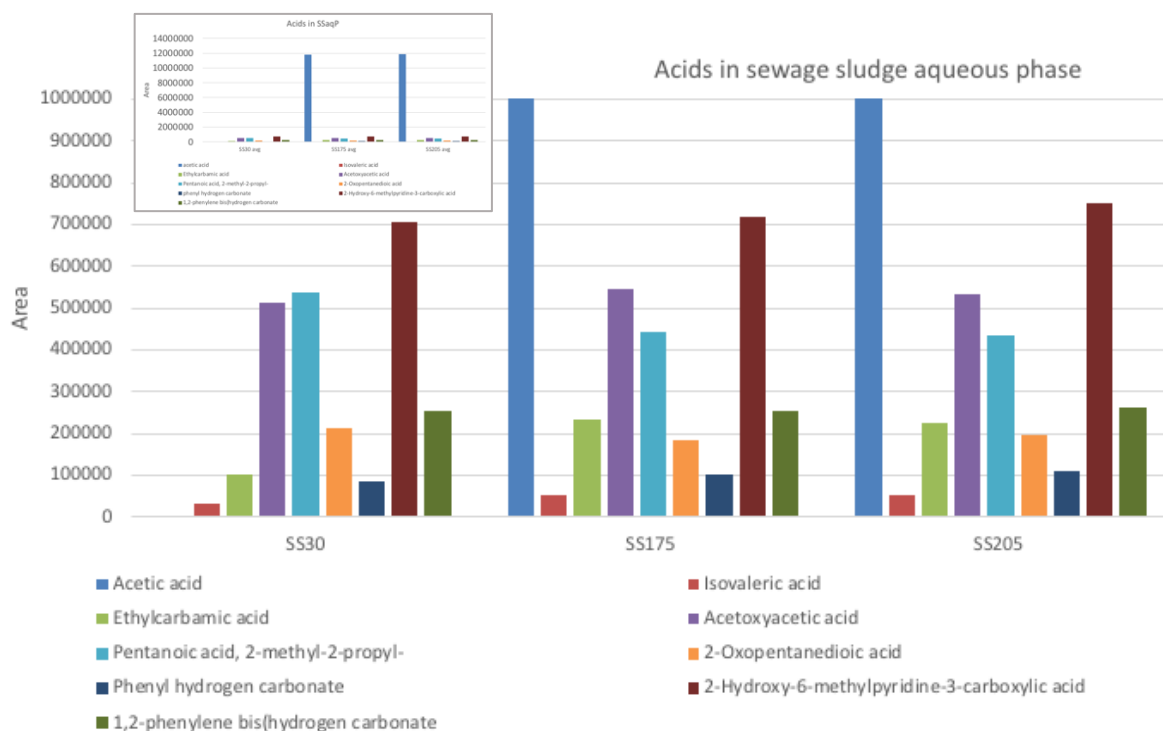


Figure 3.25: Component composition of the carboxylic acids in the aqueous phase for the samples with sewage sludge as feedstock obtained from the GC-MS analyses after 30, 175 and 205 minutes respectively.

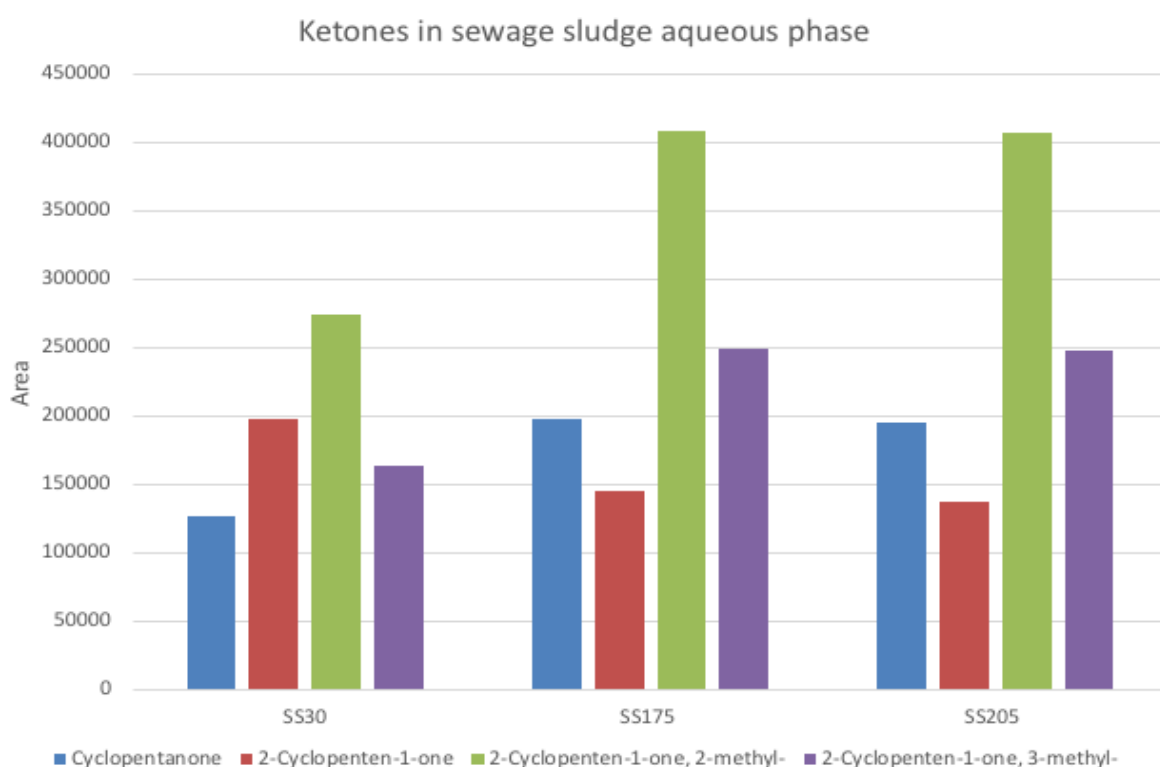


Figure 3.26: Component composition of the ketones in the aqueous phase for the samples with sewage sludge as feedstock obtained from the GC-MS analyses after 30, 175 and 205 minutes respectively.

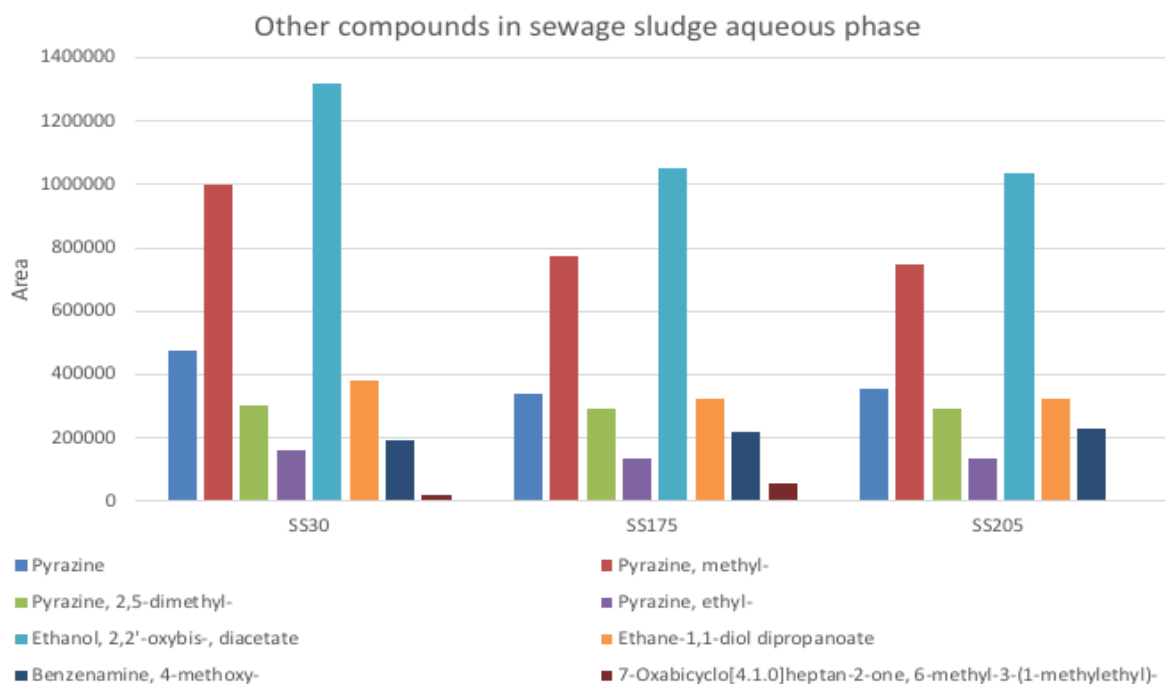


Figure 3.27: Component composition of the other compounds in the aqueous phase for the samples with sewage sludge as feedstock obtained from the GC-MS analyses after 30, 175 and 205 minutes respectively.

qNMR

The full proton spectrum of the aqueous phase sample taken after 90 minutes from the sewage sludge experiment is shown in Figure 3.28.

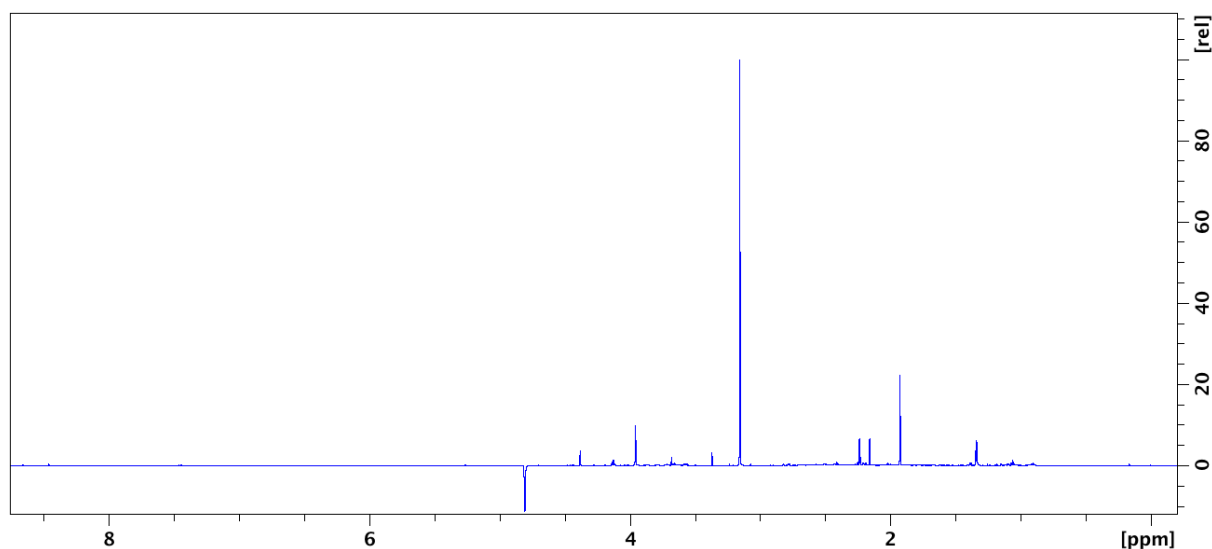


Figure 3.28: ^1H spectrum of the aqueous phase from the experiment with sewage sludge as feedstock.

Figure 3.29 shows the full HSQC spectrum of the aqueous phase sample taken after 90 minutes from the sewage sludge experiment.

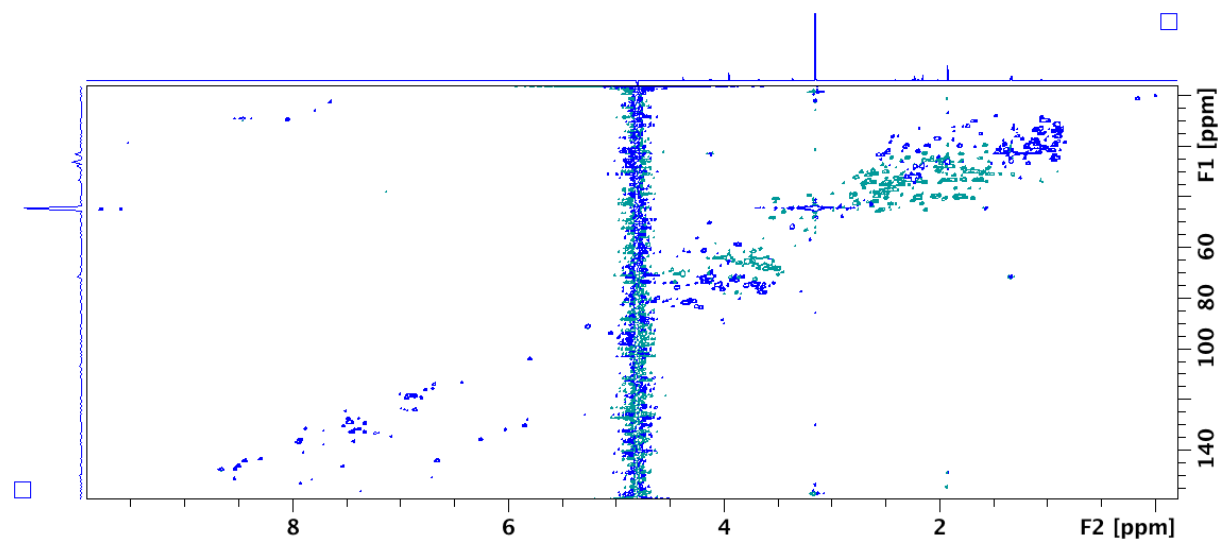


Figure 3.29: HSQC spectrum of the aqueous phase from the experiment with sewage sludge as feedstock.

The detected compounds and the represented protons and carbons are shown in Table 3.11, along with the chemical shifts of their peaks in the spectra.

Table 3.11: Peak assignment for the NMR of the aqueous sample taken after 90 minutes with sewage sludge as feedstock.

Compound		¹ H chemical shift ppm		¹³ C chemical shift ppm
DMSO ₂ (IS)	CH ₃	3,16	CH ₃	44,4
Unknown compound 2	Aliphatic	1,34		22,9
Acetic acid	CH ₃	1,93	CH ₃	26,2
Unknown compound 5	Isolated	2,16		27,7
Acetone	CH ₃	2,24	CH ₃	33,1
Methanol	CH ₃	3,37	CH ₃	51,9
Unknown compound 4	Isolated	3,95		65,0
Unknown compound 6	Isolated	4,38		70,3

Unknown compound 2 and 4 are most likely the same compounds as in the aqueous phase from the corn stover and wheat straw experiments. Unknown compound 5 and 6 gives singlets in the proton NMR spectrum, which means that the protons represented by the peaks have no neighboring protons. Unknown compound 5 gives a peak at 2,16 ppm, while unknown compound 6 gives a peak at 4,38 ppm. The peak from unknown compound 6 is more downfield, suggesting that the surroundings of the proton(s) giving this peak are more electronegative than the surroundings of the proton(s) giving the peak to unknown compound 5. The number of protons represented in the qNMR spectrum peaks is shown in Table 3.12, as well as the integral of the peaks and the calculated concentrations. As seen in Table 3.12 and Figure 3.29, catechol and phenol are not found in the NMR spectrum for this experiment, which is different from the other experiments. Acetic acid has a concentration of 49,4 mM, which makes it the most concentrated compound in the sample besides the internal standard, and which supports the GC-MS analysis results of the aqueous phase from the same experiment, shown in Figure 3.24 and Table 3.10. Neither phenol, nor catechol was detected in the aqueous phase from the sewage sludge experiment, which is also true for the GC-MS analysis from the same experiment.

Table 3.12: Peak assignment for the NMR of the aqueous sample taken after 90 minutes with sewage sludge as feedstock.

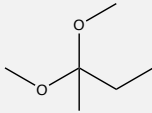
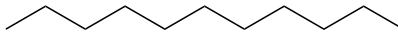
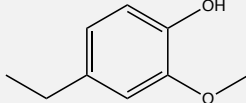
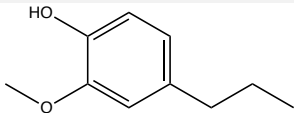
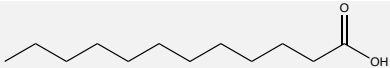
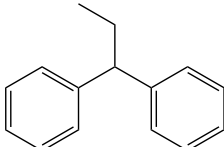
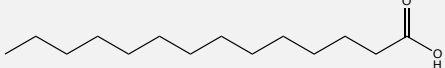
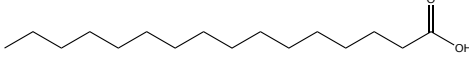
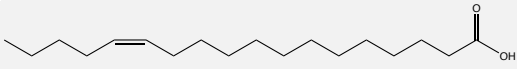
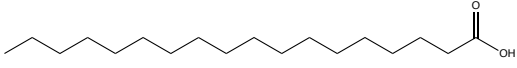
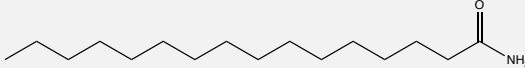
Compound		Number of protons	of Integral (rel)	Concentration (mM)	Concentration (mg/L)
DMSO ₂ (IS)	CH ₃	6	1,0000	101,2	9525,96
Unknown compound 2			0,1897		
Acetic acid	CH ₃	3	0,2442	49,4	2966,57
Unknown compound 5			0,0881		
Acetone	CH ₃	6	0,0665	6,7	389,14
Methanol	CH ₃	3	0,0302	6,1	195,44
Unknown compound 4			0,1782		
Unknown compound 6			0,0586		

3.3.2 Biocrude

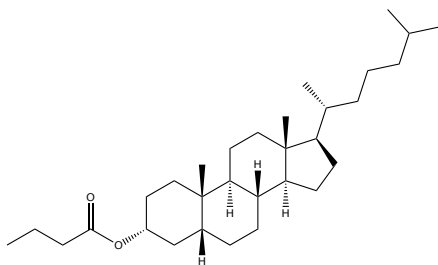
GC-MS

The detected compounds from the GC-MS analysis of the biocrude from the sewage sludge experiment are presented in Table 3.13 with the structure of each compound, and the retention time and the area of the peaks. The chromatogram where these values are taken from is shown in Figure C1 in Appendix C.

Table 3.13: Compounds with respective retention times and peak areas from GC-MS of the biocrude with sewage sludge as feedstock.

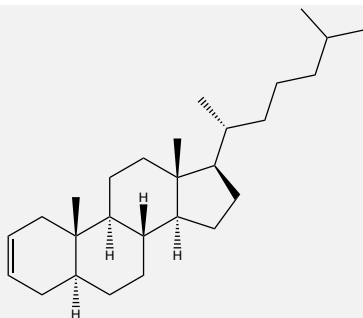
Name of compound	Structure	Retention time (min)	Area (x10 ⁷)
2,2-Dimethoxybutane		10,308	0,16
Undecane		19,361	0,51
Phenol, 4-ethyl-2-methoxy-		25,138	0,78
Phenol, 2-methoxy-4-propyl-		27,936	1,08
Dodecanoic acid		34,035	0,02
Benzene, 1,1'-propylidenebis-		35,129	0,53
Tetradecanoic acid		39,154	0,38
n-Hexadecanoic acid		44,330	8,56
cis-13-Octadecenoic acid		48,536	2,89
Octadecanoic acid		49,021	1,74
Hexadecanamide		49,556	0,87

5-.beta.-cholestan-
3.alpha.-ol, butyrate



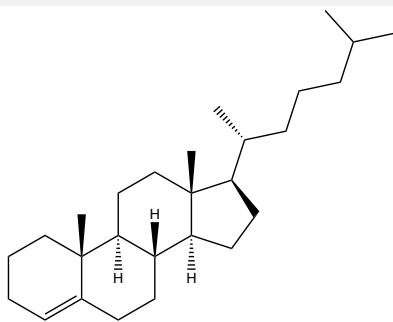
61,679 0,95

Cholest-2-ene, (5.alpha.)-



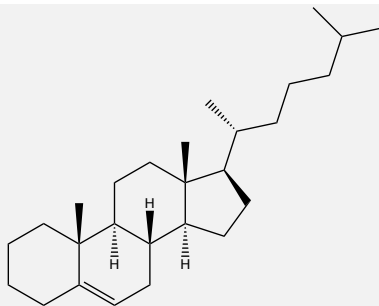
62,189 0,34

Cholest-4-ene



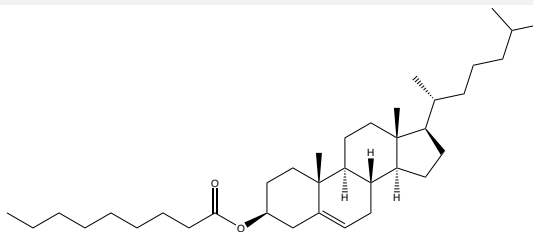
62,452 0,17

Cholest-5-ene



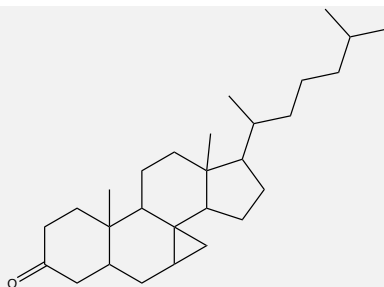
62,724 0,17

Cholest-5-en-3-ol
(3.beta.)-, nonanoate



63,687 0,07

Cyclopropa[7,8]cholestan-
3-one, 3',7-dihydro-,
(5.alpha.,7.beta.,8.alpha.)-



65,588 0,28

Figure 3.30 shows the peak areas from the GC-MS chromatogram of the compounds in the biocrude samples taken after 30, 130 and 300 minutes respectively from the sewage sludge experiment, from left to right on both sides of the dotted line in the diagram. The compounds to the left of the line show their area values on the left y-axis, while the compounds to the right of the line show their area values on the right y-axis. The main products in the biocrude phase were longer chained fatty acids, similar to the aqueous phase from the corn stover experiment, but different from the wheat straw experiment. Methoxyphenols and small amounts of cholestene compounds were also detected, which is in line with both the former experiments discussed. Cyclopentenones was not found in this phase. n-Hexadecanoic acid was found to be the main product in the biocrude from the sewage sludge experiment. For most of the compounds in the aqueous phase of the sewage sludge the concentration seem to be decreasing with time, which could be explained by further degradation.

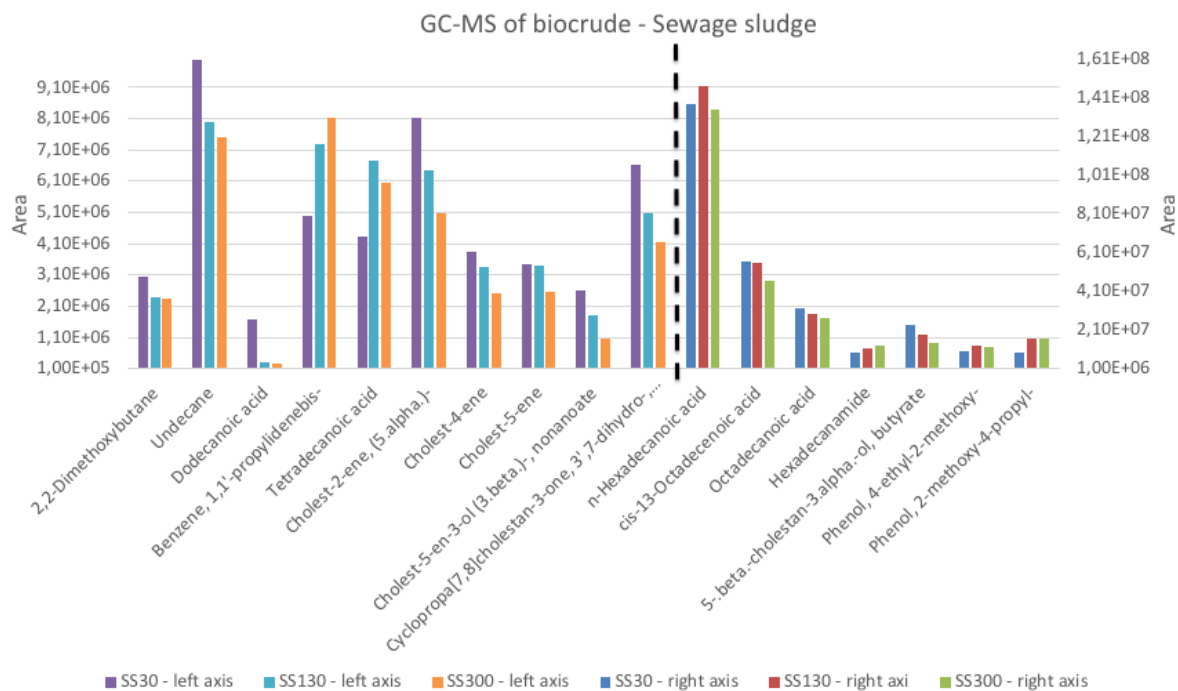


Figure 3.30: Component composition in the biocrude for the samples with sewage sludge as feedstock obtained from the GC-MS analyses after 30, 130 and 300 minutes.

3.4 Cattle manure

3.4.1 Aqueous phase

GC-MS

The GC-MS chromatogram of the aqueous phase sample taken after 240 minutes from the cattle manure experiment is presented in Figure 3.31.

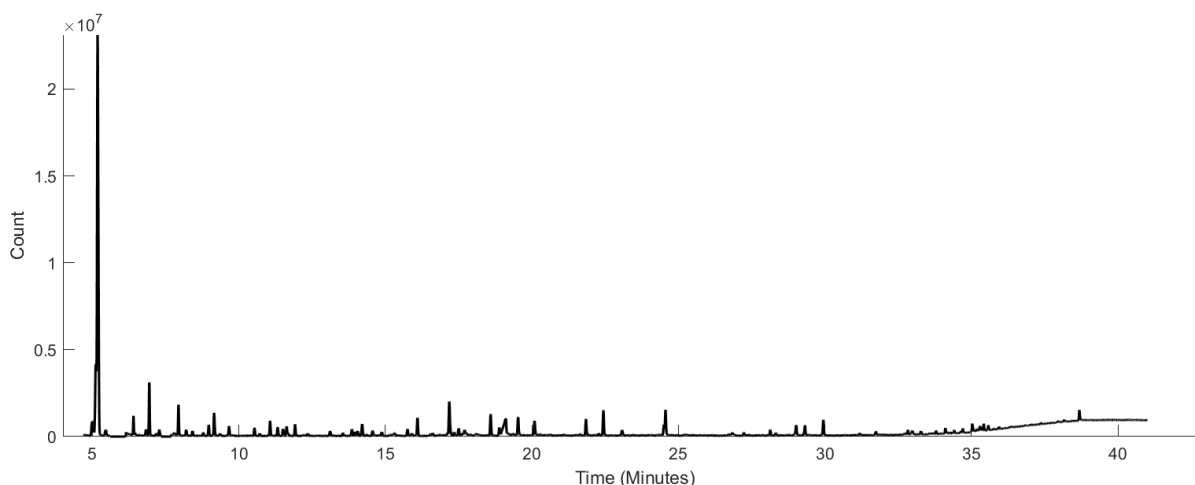
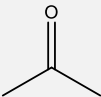
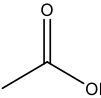
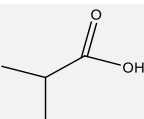
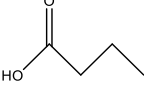
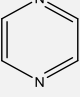
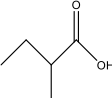
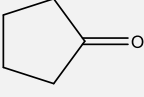
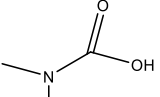
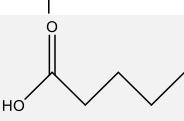
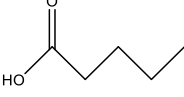
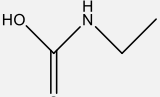
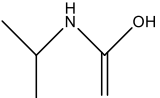


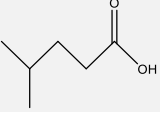
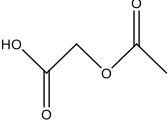
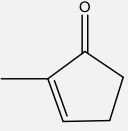
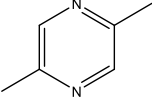
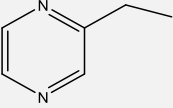
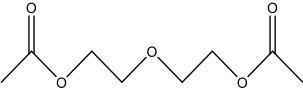
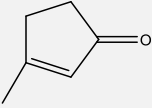
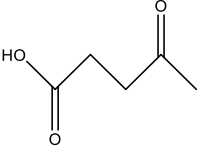
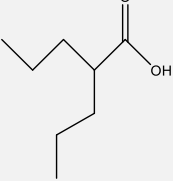
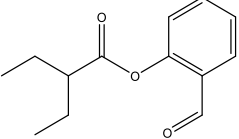
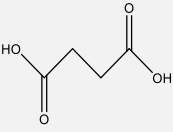
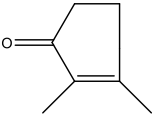
Figure 3.31: GC-MS chromatogram of the aqueous phase from the hydrothermal liquefaction of cattle manure for the sample taken after 240 minutes.

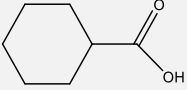
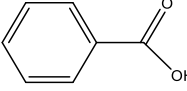
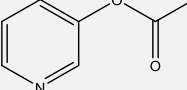
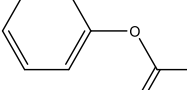
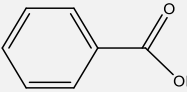
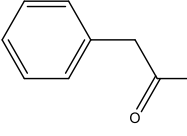
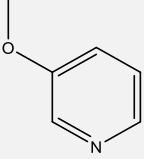
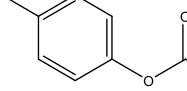
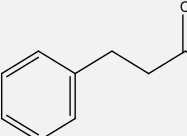
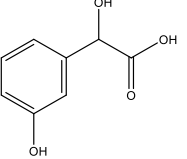
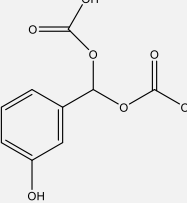
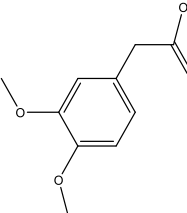
The detected compounds with their structures, and the retention times and areas of the peaks in the chromatogram is shown in Table 3.14. Acetic acid was the dominating compound in the aqueous phase from the cattle manure experiment. The table shows benzoic acid twice, at retention time 17,180 min and retention time 19,064 min. The one at 17 minutes was the converted benzoic acid, meaning it came out in the mass spectrometer as benzoic acid, methyl ester, while the one at 19 minutes just came out as benzoic acid. It was not expected to find both benzoic acid, methyl ester and benzoic acid in the analyzed sample. The reason might be a high concentration of benzoic acid, leading it to not be completely derivatized, or that the benzoic acid, methyl ester is an unstable compound, and hydrolysis back to benzoic acid. In addition to benzoic acid and acetic acid, a high number of other acids like hydroxymandelic acid and dimethylcarbamid acid were present in the aqueous phase. Similar to the aqueous phase from the sewage sludge experiment, quite a lot of nitrogen consisting compounds are detected, such as pyrazines and pyridine, in the aqueous phase from the cattle manure experiment. This was expected, as, according to previous research, cattle manure, in the same

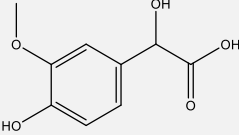
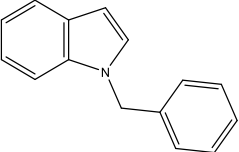
way as sewage sludge, contains a lot of protein, which is broken down to nitrogen containing compounds during the HTL process.

Table 3.14: Compounds with respective retention times and peak areas from GC-MS of the aqueous phase with cattle manure as feedstock.

Name of compound	Structure	Retention time (min)	Area ($\times 10^5$)
Acetone		5,024	8,86
Acetic acid		5,205	56,85
Isobutyric acid		6,407	2,77
Butanoic acid		6,942	13,54
Pyrazine		7,287	4,84
2-methylbutanoic acid		7,938	6,01
Cyclopentanone		8,415	1,25
Dimethylcarbamic acid		8,785	0,85
Valeric acid		8,975	3,37
Pyrazine, methyl-		9,156	12,85
Ethylcarbamic acid		9,666	4,65
Isopropylcarbamic acid		10,538	2,88

4-Methylpentanoic acid		10,711	0,48
Acetoxyacetic acid		11,328	2,48
2-Cyclopenten-1-one, 2-methyl-		11,328	3,32
Pyrazine, 2,5-dimethyl-		11,509	3,95
Pyrazine, ethyl-		11,633	3,93
Ethanol, 2,2'-oxybis-, diacetate		11,921	4,57
2-Cyclopenten-1-one, 3-methyl-		13,114	1,62
4-oxopentanoic acid		13,559	0,58
2-propylpentanoic acid		13,550	0,22
2-Ethylbutyric acid, 2-formylphenyl ester		14,209	5,82
Succinic acid		14,884	1,63
2-Cyclopenten-1-one, 2,3-dimethyl-		15,311	0,88

Cyclohexanecarboxylic acid		16,093	3,10
Benzoic acid		17,180	19,66
3-Hydroxypyridine monoacetate		17,706	2,27
Phenyl hydrogen carbonate		18,595	4,62
Benzoic acid (not converted from the methyl ester)		19,064	16,72
Phenylacetic acid		19,533	10,98
Pyridine, 3-methoxy-		20,093	5,23
<i>p</i> -tolyl hydrogen carbonate		21,846	3,09
Phenylpropanoic acid		22,438	9,09
3-Hydroxymandelic acid		24,562	6,06
1,2-phenylene bis(hydrogen carbonate)		29,014	2,04
Homoveratric acid		29,319	3,81

Vanillylmandelic acid		29,952	3,03
1-benzylindole		38,684	4,76

The peak areas of the compounds with a significant peak area value from the aqueous phase sample taken after 240 minutes from the cattle manure experiment are shown in Figure 3.32. The peak area value of acetic acid was $5,69 \times 10^6$ and was so prominent that the rest of the peaks were barely noticeable in comparison. Therefore, like in the sewage sludge results, the full diagram is shown in the top right corner, while the diagram where the maximum value of the area on the y-axis is set to 2500000, which makes the areas of the rest of the compounds visually comparable, but does not show the top of the acetic acid peak.

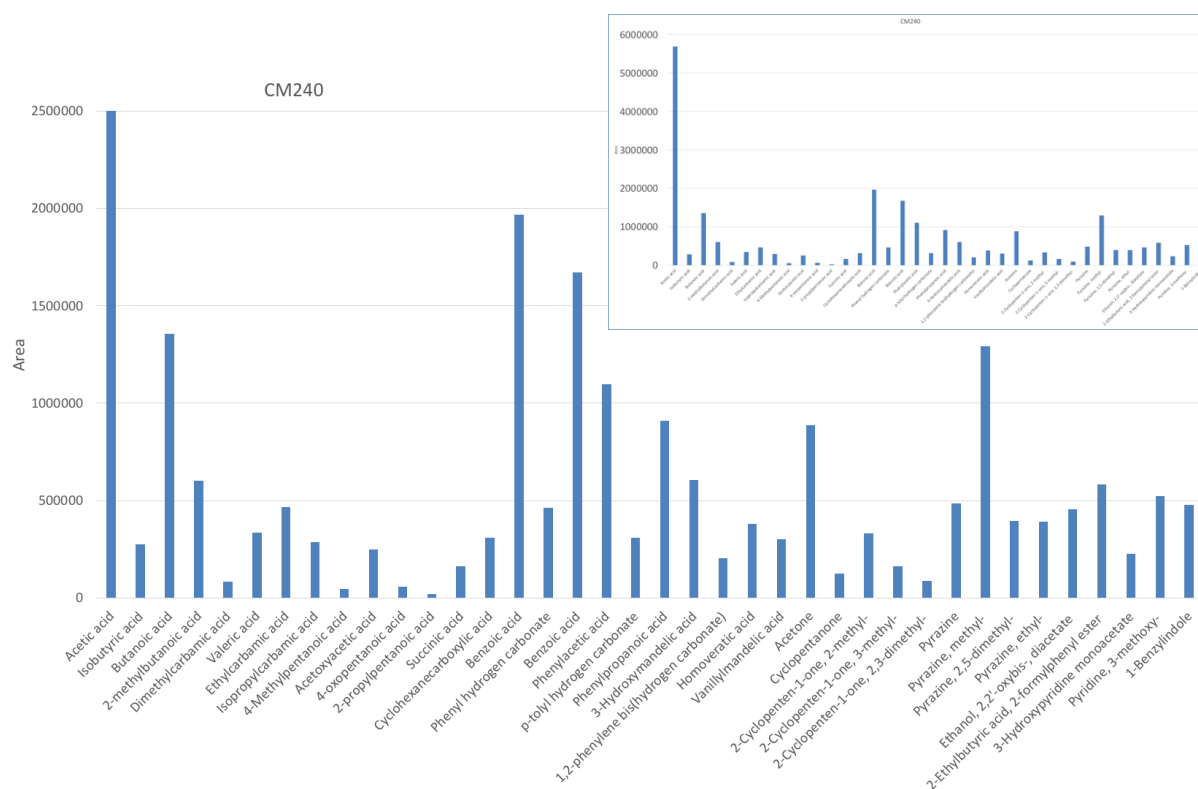


Figure 3.32: Component composition in the aqueous phase for the sample with cattle manure as feedstock obtained from the GC-MS analyses after 240 minutes.

Figures 3.33 to 3.35 show the areas of the peaks of the carboxylic acids, ketones and other compounds from the aqueous samples taken after 95, 165 and 240 minutes respectively from the cattle manure experiment. There are no alcohols of significant amounts in these samples, thus there is no diagram showing the alcohols. The diagram showing the carboxylic acids in this experiment in Figure 3.33, again shows that the rest of the carboxylic acid results are not readable when the area axis is set to a maximum which shows the entire acetic acid peak. This is solved by showing this full diagram in the top right corner, and a diagram which is better showing the rest of the peaks, while the acetic acid peak rises above the maximum area value on the y-axis.

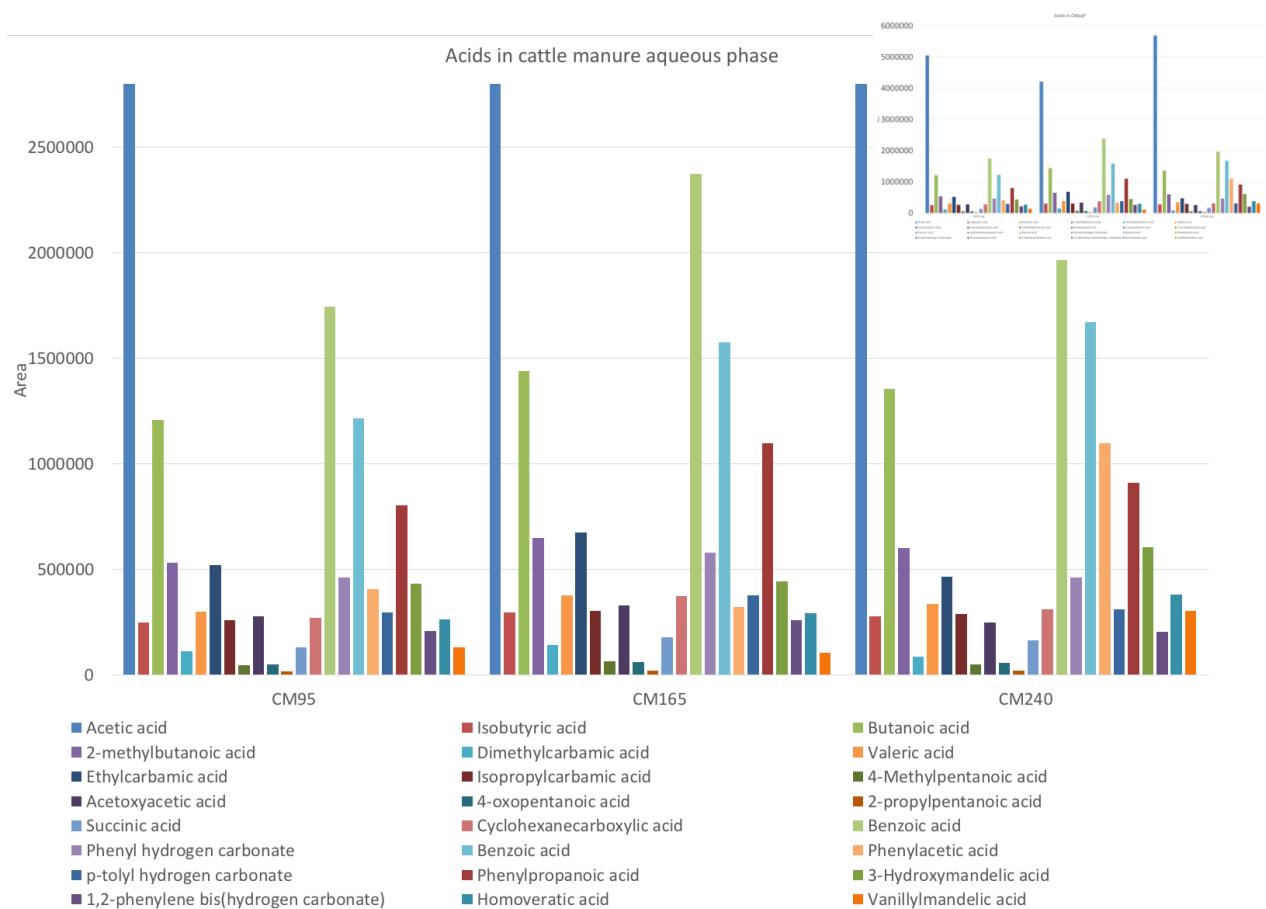


Figure 3.33: Component composition of the carboxylic acids in the aqueous phase for the samples with cattle manure as feedstock obtained from the GC-MS analyses after respectively 95, 165 and 240 minutes.

Areas from the GC-MS spectra of the carboxylic acids in the aqueous phase for the samples taken after 95, 165 and 240 minutes respectively with cattle manure as feedstock.

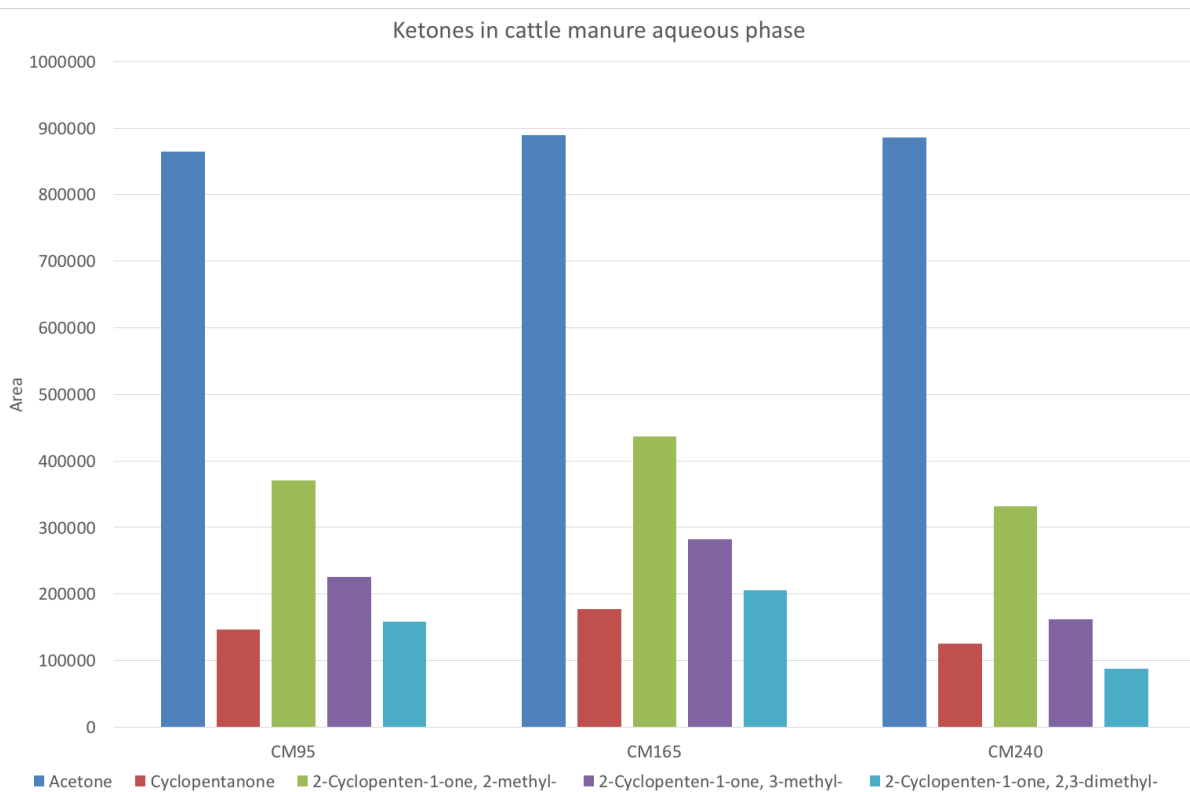


Figure 3.34: Component composition of the ketones in the aqueous phase for the samples with cattle manure as feedstock obtained from the GC-MS analyses after 95, 165 and 240 minutes respectively.

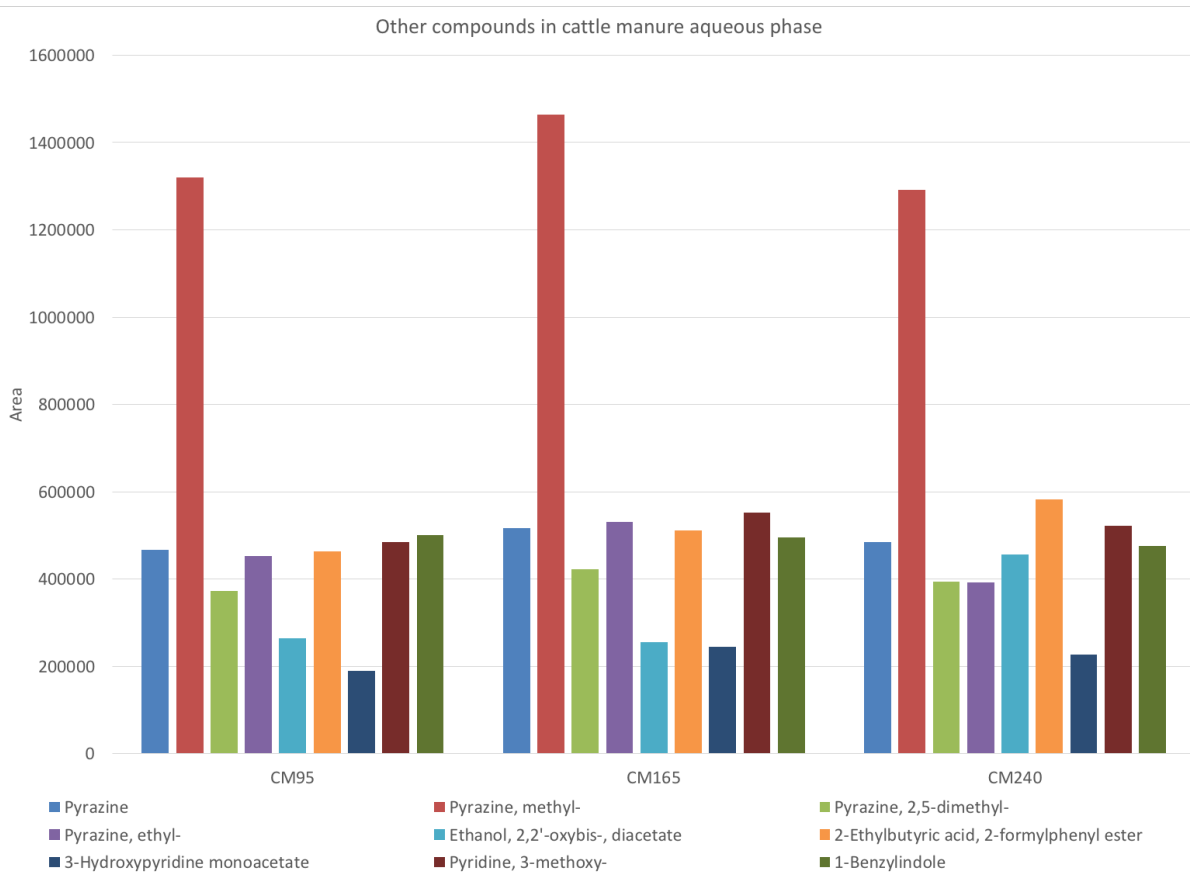


Figure 3.35: Component composition of the other compounds in the aqueous phase for the samples with cattle manure as feedstock obtained from the GC-MS analyses after 95, 165 and 240 minutes respectively.

qNMR

The full proton spectrum of the aqueous phase sample taken after 60 minutes from the cattle manure experiment is shown in Figure 3.36.

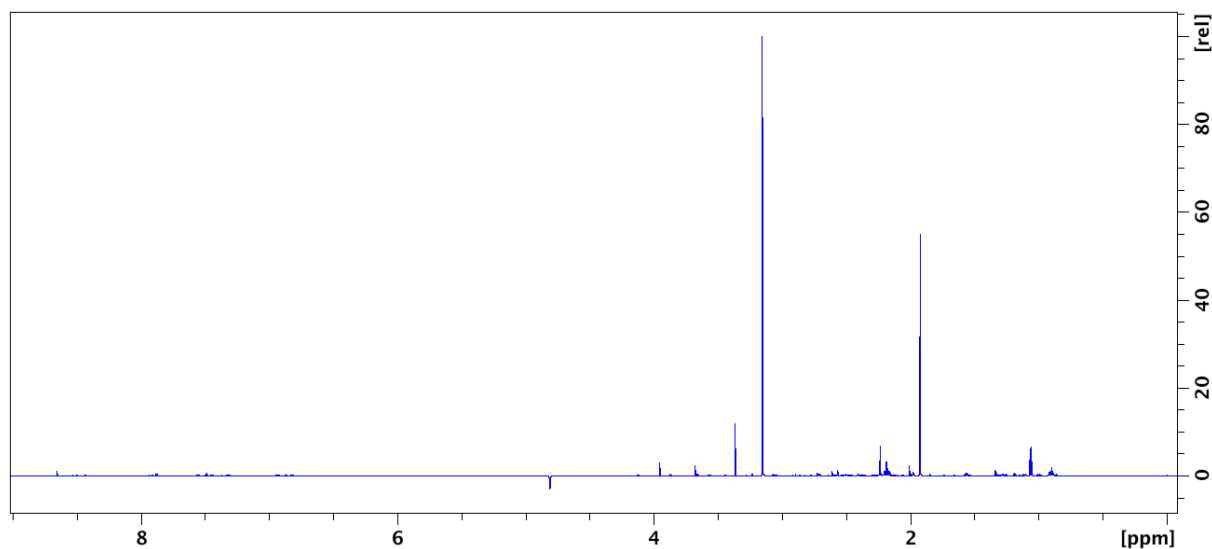


Figure 3.36: ^1H spectrum of the aqueous phase from the experiment with cattle manure as feedstock.

Figure 3.37 presents the full HSQC spectrum of the aqueous phase sample taken after 60 minutes from the cattle manure experiment.

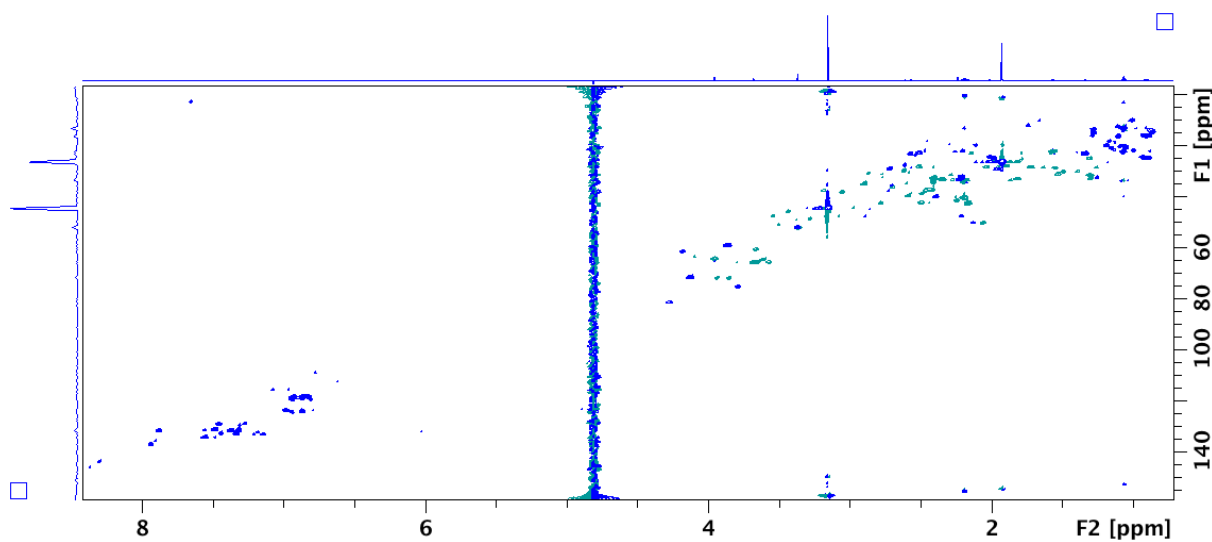


Figure 3.37: HSQC spectrum of the aqueous phase from the experiment with cattle manure as feedstock.

The detected compounds and the protons and carbons represented in the peaks are listed in Table 3.15, as well as their chemical shifts. Unknown compound 2, 3 and 4 are most likely the same compounds giving peaks to the spectra from the aqueous phases from the corn stover, wheat straw and sewage sludge experiments with the same names.

Table 3.15: Peak assignment for the NMR of the aqueous sample taken after 60 minutes with cattle manure as feedstock.

Compound	¹ H chemical shift ppm		¹³ C chemical shift ppm	
DMSO ₂ (IS)	CH ₃	3,15	CH ₃	44,4
Unknown compound 2	Aliphatic	1,34		22,8
Acetic acid	CH ₃	1,92	CH ₃	26,1
Acetone	CH ₃	2,24	CH ₃	33,1
Methanol	CH ₃	3,37	CH ₃	51,9
Unknown compound 3	Isolated	3,68		65,4
Unknown compound 4	Isolated	3,96		64,2
Catechol	Ph-H (pos. 4 & 5)	6,87	Aromatic C (pos. 3 & 6)	123,9
Phenol	Ph-H (pos. 2 & 6)	6,94	Aromatic C (pos. 2 & 6)	119,1*

*Had a shoulder peak at 118,3, which matches the literature.

The number of protons representing the peaks in the proton spectrum are listed in Table 3.16, along with the integral of the peaks and the concentration of the compounds. The most prominent compound in the aqueous phase from the cattle manure result is acetic acid with a concentration of 121,8 mM, shown in Table 3.16. This supports the results from the GC-MS analysis of the aqueous phase from the same experiment shown in Figure 3.32 and Table 3.14.

Table 3.16: Peak assignment for the NMR of the aqueous sample taken after 60 minutes with cattle manure as feedstock.

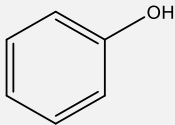
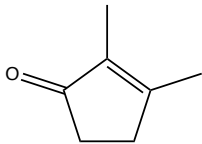
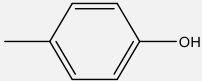
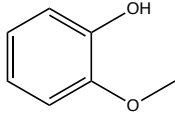
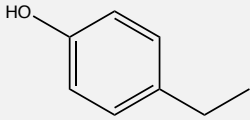
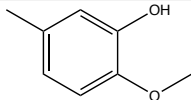
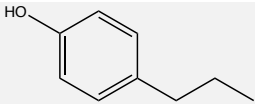
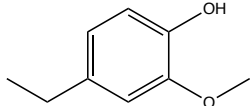
Compound		Number of protons	Integral (rel)	Concentration (mM)	Concentration (mg/L)
DMSO ₂ (IS)	CH ₃	6	1,0000	101,2	9525,96
Unknown compound 2			0,0506		
Acetic acid	CH ₃	3	0,6017	121,8	7314,33
Acetone	CH ₃	6	0,0537	5,4	313,63
Methanol	CH ₃	3	0,1003	20,3	650,41
Unknown compound 3			0,0305		
Unknown compound 4			0,0625		
Catechol	Ph-H (pos. 4 & 5)	2	0,0103	3,1	341,31
Phenol	Ph-H (pos. 2 & 6)	2	0,0094	2,9	272,92

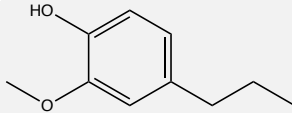
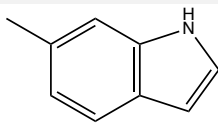
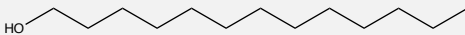
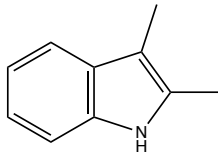
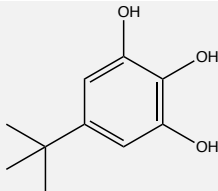
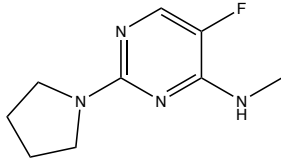
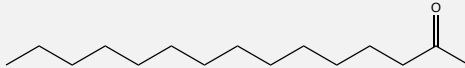
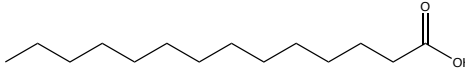
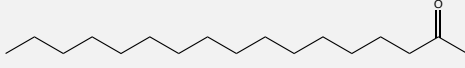
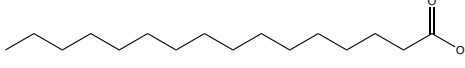
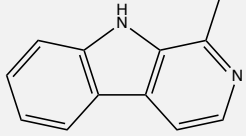
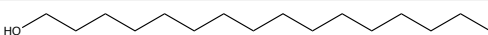
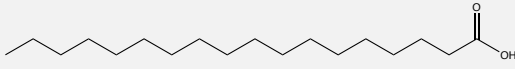
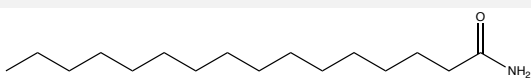
3.4.2 Biocrude

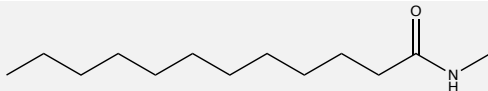
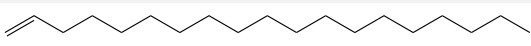
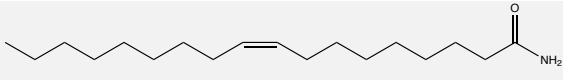
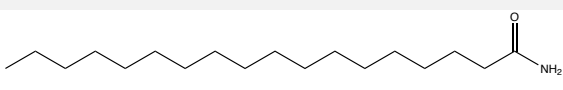
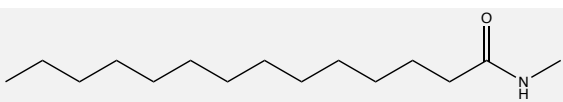
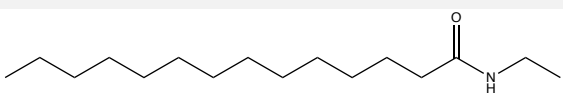
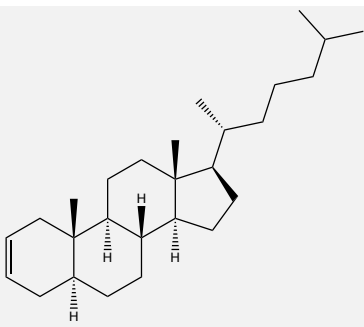
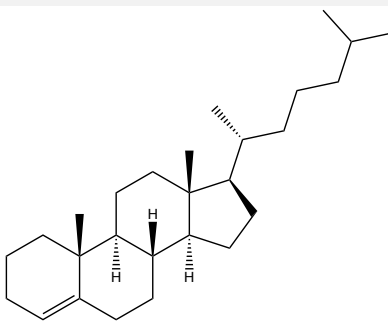
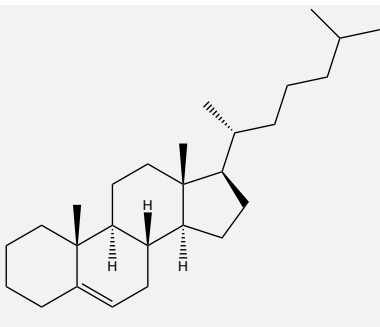
GC-MS

The compounds detected in the GC-MS spectrum of the biocrude sample from the cattle manure experiment are listed in Table 3.17 with the structures, and the retention times and areas from the peaks, which are shown in the chromatogram in Figure D1 in Appendix D.

Table 3.17: Compounds with respective retention times and peak areas from GC-MS of the biocrude with cattle manure as feedstock.

Name of compound	Structure	Retention time (min)	Area ($\times 10^7$)
Phenol		16,061	2,82
2-Cyclopenten-1-one, 2,3-dimethyl-		17,806	0,28
p-Cresol		18,752	5,22
Phenol, 2-methoxy-		19,295	2,38
Phenol, 4-ethyl-		21,526	17,39
2-Methoxy-5-methylphenol		22,456	0,89
Phenol, 4-propyl-		24,447	1,28
Phenol, 4-ethyl-2-methoxy-		25,122	13,75

Phenol, 2-methoxy-4-propyl-		27,928	11,31
1H-Indole, 6-methyl-		28,941	3,52
n-Tridecan-1-ol		31,541	0,25
1H-Indole, 2,3-dimethyl-		32,126	0,62
5-tert-Butylpyrogallol		32,677	3,05
4-Pyrimidinamine, 5-fluoro-N-methyl-2-(1-pyrrolidinyl)-		35,129	8,17
2-Pentadecanone		37,582	0,70
Tetradecanoic acid		39,154	0,76
2-Heptadecanone		42,915	0,96
n-Hexadecanoic acid		44,306	1,08
9H-Pyrido[3,4-b]indole, 1-methyl-		45,343	3,42
1-Hexadecanol		47,441	0,17
Octadecanoic acid		49,005	1,02
Hexadecanamide		49,548	3,00

N-Methyldodecanamide		50,313	0,66
1-Nonadecene		51,828	0,47
9-Octadecenamide, (Z)-		53,465	2,37
Octadecanamide		53,943	4,17
Myristamide, N-methyl-		54,618	1,17
Myristamide, N-ethyl-		55,399	0,82
Cholest-2-ene, (5.alpha.)-		62,189	0,17
Cholest-4-ene		62,461	0,20
Cholest-5-ene		62,732	0,28

The areas from the GC-MS chromatogram of the compounds in the biocrude samples taken after 95, 165 and 240 minutes from the cattle manure experiment are shown in Figure 3.38, respectively from left to right on both sides of the dotted line in the diagram. The compounds

to the left of the line show their area values on the left y-axis, while the compounds to the right of the line show their values on the right y-axis. The major compound in the biocrude sample from the cattle manure experiment is 4-ethyl-phenol. The main products in the biocrude phase were longer chained fatty acids, similar to the aqueous phase from the corn stover experiment, and sewage sludge experiment, but different from the wheat straw experiment. Methoxyphenols and small amounts of cholestene compounds were also detected, which is in line with all three former experiments discussed. Cyclopentenones were not found in this phase. For some of the compounds in the aqueous phase of the cattle manure experiment the concentration seem to be decreasing with time, which could be explained by further degradation, but there was not a very clear trend in this experiment, compared to the other experiments.

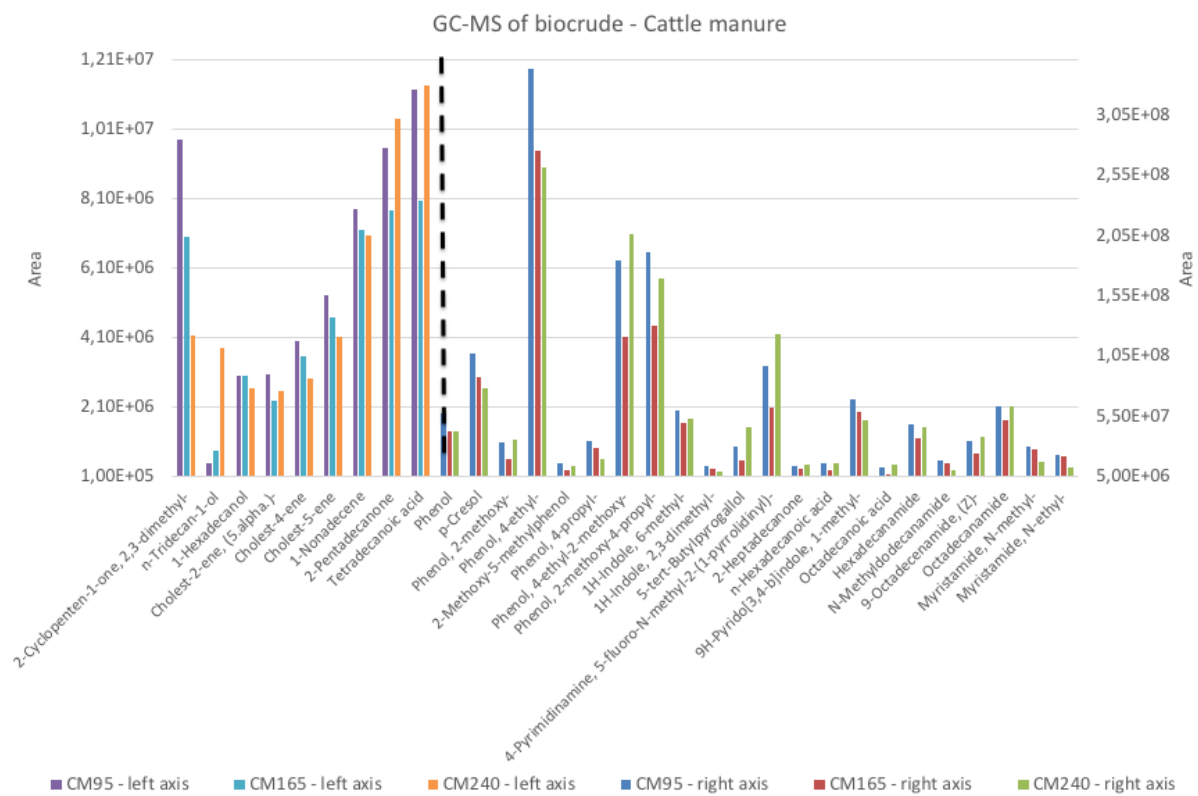


Figure 3.38: Component composition in the biocrude for the samples with cattle manure as feedstock obtained from the GC-MS analyses 95, 165 and 240 minutes.

3.5 Sugar kelp

3.5.1 Aqueous phase

GC-MS

The GC-MS samples for the aqueous phase from the sugar kelp experiment were prepared for GC-MS analysis, but were not analyzed because of lockdown in Aarhus, due to Covid-19.

qNMR

The full proton NMR spectrum of the sample of the aqueous phase taken after 65 minutes from the sugar kelp experiment is shown in Figure 3.39.

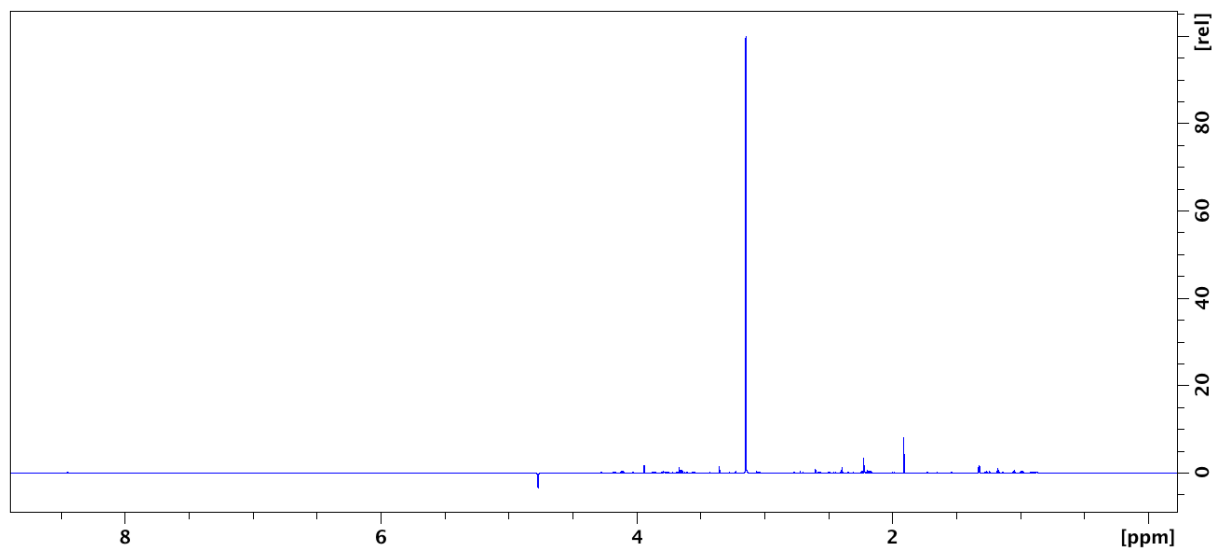


Figure 3.39: ^1H spectrum of the aqueous phase from the experiment with sugar kelp as feedstock.

The full HSQC spectrum of the aqueous phase taken after 65 minutes from the sugar kelp experiment is shown in Figure 3.50.

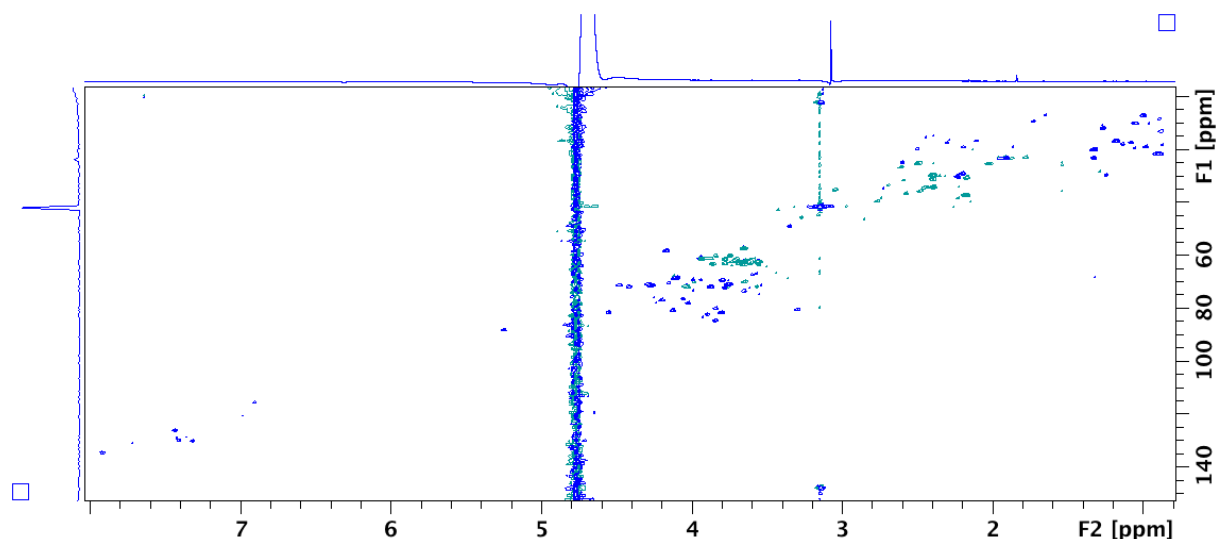


Figure 3.40: HSQC spectrum of the aqueous phase from the experiment with sugar kelp as feedstock.

The detected compounds are presented in Table 3.18, with the represented proton and carbon as well as the belonging chemical shifts. Unknown compound 3 and 4 are most likely the same compounds as in the aqueous phases from the corn stover, wheat straw, sewage sludge and cattle manure experiments.

Table 3.18: Peak assignment for the NMR of the aqueous sample taken after 65 minutes with sugar kelp as feedstock.

Compound	¹ H chemical shift ppm		¹³ C chemical shift ppm	
DMSO ₂ (IS)	CH ₃	3,14	CH ₃	44,4
Acetic acid	CH ₃	1,91	CH ₃	26,1
Acetone	CH ₃	2,22	CH ₃	33,1
Methanol	CH ₃	3,35	CH ₃	51,9
Unknown compound 3	Isolated	3,66		65,4
Unknown compound 4	Isolated	3,94		64,2

*Had a shoulder peak at 118,3, which matches the literature.

The number of protons represented in the peaks, as well as the integrals of the peaks and the calculated concentrations are shown in Table 3.19. Acetic acid was the compound with the a concentration of 18,1 mM, which makes it the compound with the highest concentration in the aqueous phase sample from the sugar kelp experiment, besides the internal standard.

Table 3.19: Peak assignment for the NMR of the aqueous sample taken after 65 minutes with sugar kelp as feedstock.

Compound		Number of protons	Integral (rel)	Concentration (mM)	Concentration (mg/L)
DMSO ₂ (IS)	CH ₃	6	1,0000	101,2	9525,96
Acetic acid	CH ₃	3	0,0896	18,1	1086,94
Acetone	CH ₃	6	0,0293	3,0	174,24
Methanol	CH ₃	3	0,0135	2,7	86,51
Unknown compound 3			0,0195		
Unknown compound 4			0,0232		

3.5.2 Biocrude

Due to too low biocrude production from the sugar kelp experiment, it was not possible to obtain any analyses on this fraction.

3.6 All feedstocks

3.6.1 Comparison of results for the aqueous and biocrude phases from the experiments with all feedstocks, by use of GC-MS and NMR analyses

The samples were analyzed by ¹H and ¹³C-NMR spectroscopy, GC-MS, in addition to obtaining data for elemental analyses. The main focus in the thesis was the aqueous phase with NMR and GC-MS data, but also GC-MS data for the biocrude phase and elemental analyses for biocrude phase and the solid residue phase was obtained. GC-MS gave more detailed information for the qualitative part of the analyses and a wider spectrum of the components in the aqueous phase, while qNMR gave a more exact quantitative analyses of the identified compounds in the aqueous phase, when the signal was separately detected. An overview over the compounds identified by the GC-MS library from all the experiments except the sugar kelp experiment is shown in Table F2 in Appendix F for the aqueous phase, and Table F3 in Appendix F for the biocrude phase. The concentration of the compounds from the aqueous phase of all the

experiments detected by qNMR are presented in Figure 3.41. As the concentrations of the compounds in the samples seemed to reach a steady state, the samples presented in the figure is the sample from the middle of the experiment for all the feedstocks.

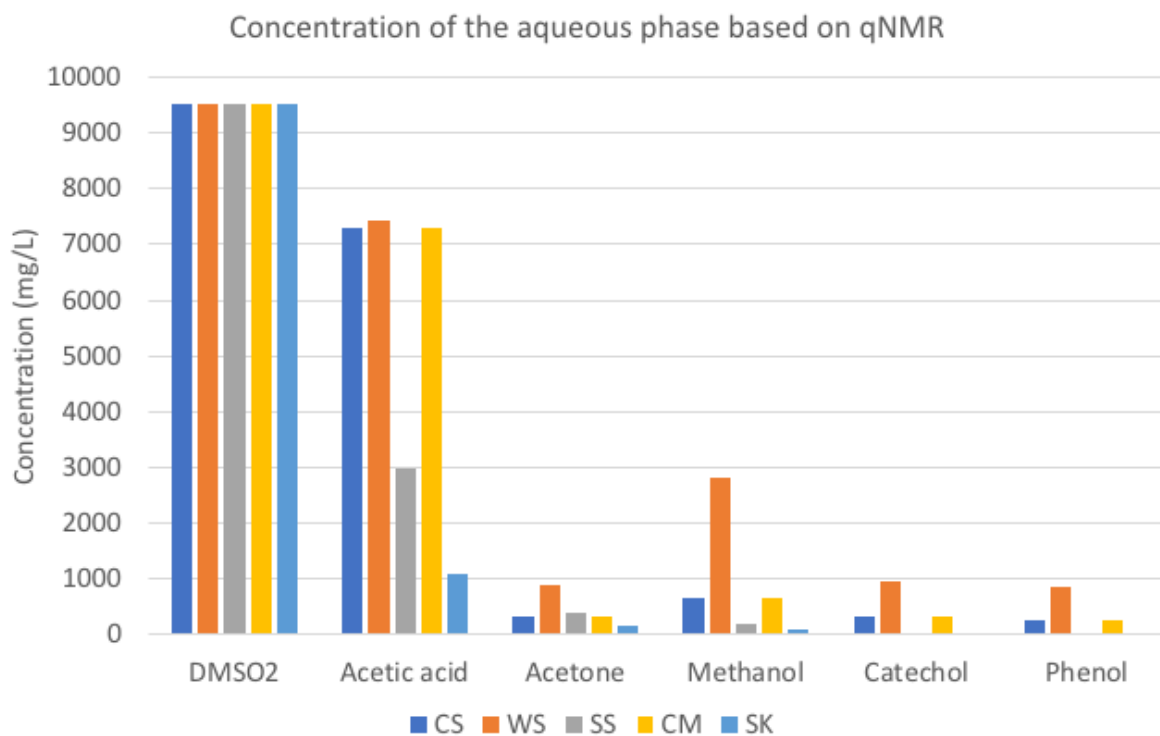


Figure 3.41: The concentration of the compounds identified by qNMR for the aqueous phase from all the experiments, shown in mg/L. The internal standard (DMSO₂) has a constant concentration for all the samples of 9525,96 mg/L. The analyses is from a sample from the middle of the experiment for all the feedstocks.

The aqueous phase from the corn stover experiment contained acetic acid in addition to some amounts of other short chained acids like succinic acid. Cyclopentenones and some monoaromatic compounds in smaller amounts were also detected. Based on the NMR spectra the aqueous phase seems to have very low amounts of catechol and phenols. The less polar compounds were found in the biocrude, where unsubstituted, alkylated phenols together with cyclopentenones as well as *p*-cresol were the dominating compounds. Also, some longer chained fatty acids were detected in this phase.

The aqueous phase from the wheat straw experiment had a concentration of acetic acid similar to the aqueous phase from the corn stover experiment. Compounds such as acetoxy acetic acid,

cyclopentenones, catechol and phenols were also detected in smaller amounts in these samples. The qNMR analyses show that the aqueous phase from the wheat straw experiment has a much higher concentration of methanol than the aqueous phases from all the experiments with other feedstocks. The main products in biocrude phase were methoxyphenols, cyclopentenones, but there were not detected any longer chained fatty acids, unlike for the biocrude from the corn stover experiment.

The aqueous phase from the sewage sludge experiment also had acetic acid as the dominating product, but had a considerably lower concentration of the acid than the aqueous phases from the corn stover and wheat straw experiments. Pyrazines, cyclopentenones and diethylene glycol diacetate are also major compounds in this phase. No phenols or catechol were detected in the aqueous phase in the GC-MS and the NMR analyses. The main products in the biocrude phase were longer chained fatty acids, methoxyphenols and small amounts of cholestene compounds. Cyclopentenones was not found in this phase.

For the aqueous phase from the cattle manure experiment, acetic acid was the dominating product, like all the other feedstocks analyzed. The concentration level of acetic acid in the aqueous phase from the cattle manure experiment was the same as for the corn stover and the wheat straw experiment. In addition acetone and a high concentration of benzoic acid was detected as well as a high number of other acids compared to the aqueous phase from the experiments with the other feedstocks. No phenols or catechol was detected in the aqueous phase in the GC-MS and the NMR analyses. The main products in the biocrude phase were ethyl- and/or methoxy substituted phenols and methoxyphenols and a pyrimidinamine as well as small amounts of other N-compounds. As in the aqueous phase from the sewage sludge experiment, cyclopentenones was not found in this phase.

There seems to be a similarity between the compounds in the corn stover and wheat straw products and the compounds in the sewage sludge and cattle manure products. The lignocellulosic feedstocks have more alcohols in the aqueous phase from the HTL process, while the cattle manure and sewage sludge contain more nitrogen containing compounds in the aqueous phase from the HTL process. This can be explained by the CS and WS feedstocks both being lignocellulosic material, while sewage sludge and cattle manure both comes from feces from different live species, and matches the results from the research done earlier on these types of feedstocks. The alcohols most likely derive from conversion of sugar polymers, while the

nitrogen containing compounds are likely to be products from the decomposition of the proteins in these feedstocks. Sugar kelp also contains some protein, which explains that the aqueous phase from the sugar kelp experiment also contains compounds with nitrogen (Panisko et al., 2015, Maddi et al., 2017, Lu et al., 2018, Seehar et al., 2020).

The GC-MS analyses showed a trend that during the first approximately 40-50 minutes of reaction time, a relative stable composition of compounds was established for all the experiments with different feedstocks. This can imply that the reactor reaches a steady state quite early on in the HTL process, already after about 40-50 minutes after the feedstock is pumped into the reactor system.

3.6.1 Elemental composition and HHV of biocrude

Table 3.20 shows the elemental composition of the biocrude of the corn stover, wheat straw, sewage sludge and cattle manure experiments. The moisture content measured on a Karl Fischer reagent system is also shown in the table, as well as the calculated higher heating value (HHV). The oxygen content is calculated by assuming that the rest of the sample is oxygen after quantifying carbon, hydrogen, nitrogen, sulphur and moisture. As sugar kelp did not produce enough biocrude to do the analysis, there are no results for the elemental analysis of this particular experiment. The biocrude yield of all experiments is also shown in the same table. The biocrude yield from cattle manure is noted to make up 5-50 wt. %, which is not accurate as this particular feedstock produced a biocrude which contained large amounts of sand. Assistant professor Patrick Biller researched the feedstock through batch reactions, which led to 41,7 wt. % biocrude yield.

Table 3.20: Biocrude elemental composition, moisture content, HHV and yields.

	CS	WS	SS	CM	SK*
C (%)	75,10	61,29	71,35	73,27	N/V
H (%)	7,90	6,60	8,46	8,48	N/V
N (%)	2,17	0,91	3,14	3,68	N/V
S (%)	0,17	0,04	0,49	0,86	N/V
O** (%)	14,65	31,16	16,55	13,72	N/V
H ₂ O in oil (%)	0,62	0,80	1,13	0,70	N/V
HHV (MJ/kg)	33,99	25,94	33,16	34,18	N/V
Biocrude yield (wt. %)	37,0	18,4	27,5	5-50***	7,0

*No value as there was not enough biocrude yield to perform the analysis.

**Calculated by difference.

***Inconsistent product recovery, yields range 5-50%. Not accurate. Batch reactions led to 41,7 wt. % biocrude yield.

A column diagram of the elemental composition as well as a plotted graph of the HHV of the last sample taken of the biocrude from the corn stover, wheat straw, sewage sludge and cattle manure experiments is presented in Figure 3.42. The elemental analyses shows the percentage of nitrogen, carbon, hydrogen, sulfur and calculated oxygen in the samples. From the elemental analysis the HHV can be found. These data show that the biocrude from the wheat straw experiment had the highest oxygen content. Thus, the energy content, based on the calculation of the higher heating value was lowest for this feedstock. Corn stover, sewage sludge and cattle manure had an oxygen content in the range 13.7–16.5 %, and had a similarly high calculated HHV in the range 33.1-34.1 MJ/kg, see Table 3.20. The biocrude from the wheat straw experiment also had a very low sulphur content which is beneficial due to low SO₂ emission, and makes it less corrosive to steel in engine injection systems or ovens. The same biocrude also had a very low nitrogen content giving lower NO_x emissions.

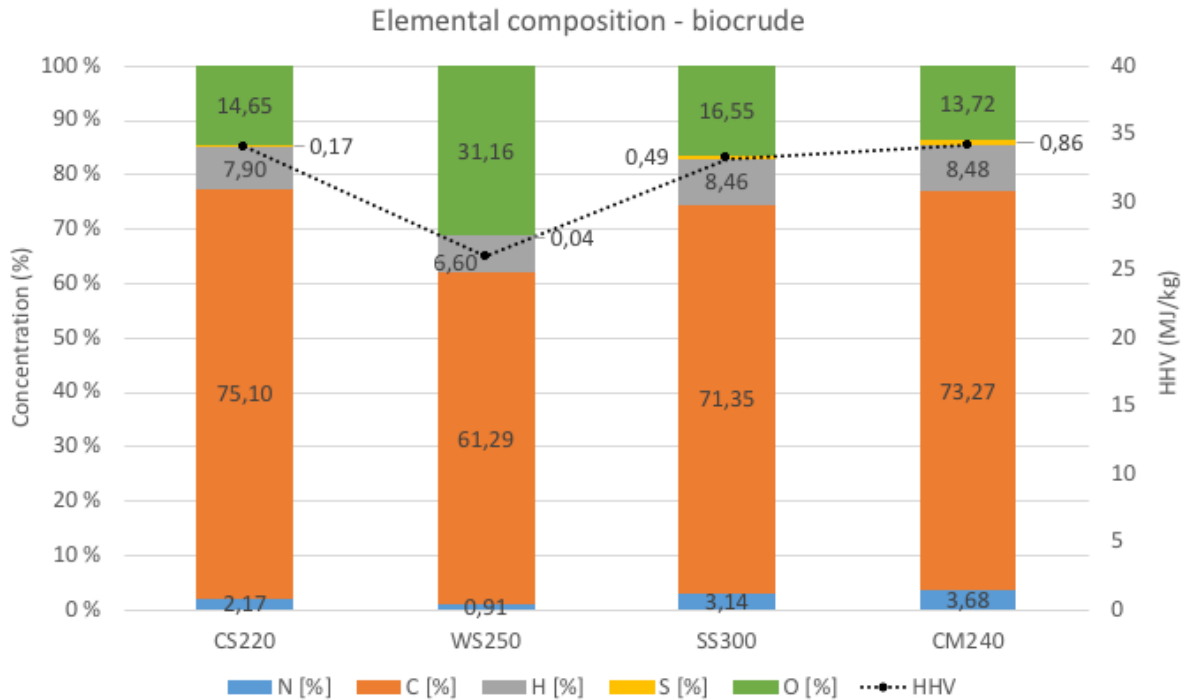


Figure 3.42: The elemental composition with the higher heating value (HHV) of the biocrude from corn stover, wheat straw, sewage sludge and cattle manure.

4 Conclusions

4.1 Conclusions

The problem statement of the thesis was monitoring the aqueous phase chemistry during a HTL run. Both GC-MS and direct NMR profiling were used to identify the organic compounds dissolved in the HTL aqueous phase, and also to determine whether a steady state was reached for a continuous reactor using several different feedstocks. The aqueous phase (AP) and partly the biocrude phase were studied for experiments with corn stover (CS), wheat straw (WS), sewage sludge (SS), cattle manure (CM) and sugar kelp (SK) as feedstock focusing on the GC-MS and NMR analyses.

The HTL process of wet feedstocks sewage sludge (SS) and cattle manure (CM) without pretreatment, and corn stover (CS), wheat straw (WS) and sugar kelp (SK) pretreated through a twin-screw extruder and a grinder followed by addition of carboxymethyl cellulose to obtain sufficiently high viscosity, could be used for decomposing the material into a biocrude phase, an aqueous phase, a gas phase and a solid residue phase. The lignocellulosic feedstocks were

also added KOH as a catalyst during pretreatment. The feedstocks were processed in the HTL reactor at approximately 350 °C and 220 bar for 15-20 minutes during a continuous processing time of up to 250 minutes. Samples were taken during the process for analyses. Figure 3.3 and Figure A1 in Appendix A show results that suggest that the reactor reaches a steady state after approximately 40-50 minutes after the feedstock is pumped into the reactor system.

The composition of the biocrude phase and aqueous phase could be determined by GC-MS with derivatization using MCF, and using 4-bromotoluene as internal standard. The aqueous phase could also be determined with ^1H and ^{13}C -NMR spectroscopy with water signal depression and using DMSO_2 as an internal standard and TSP as reference compound. The proton NMR method could also be used for quantitative analysis.

For all feedstocks acetic acid was the dominating product in the aqueous phase. The aqueous phase from all the feedstocks also included cyclopentanone, acetoxyacetic acid, 2-cyclopenten-1-one, 2-methyl-, diethylene glycol diacetate, and 2-cyclopenten-1-one, 3-methyl-. The aqueous phase from the experiments with the lignocellulosic feedstocks (CS, WS) was similar in the sense that they both contained alcohols, and did not contain N-containing compounds, suggesting that the N-containing compounds derive from proteins. The SS and CM were similar in the sense that they both contained a lot of N-containing compounds, but not alcohols. SK did not contain alcohols either.

The aqueous phase from the CS experiment contained some amounts of short chained acid like succinic acid. Cyclopentenones and some monoaromatic compounds were also detected in smaller amounts. The aqueous phase seems to have very low amounts of catechol and phenols.

The aqueous phase from the WS experiment had a high content of acetic acid compared to aqueous phase of corn stover, and also contained acetoxyacetic acid, cyclopentenones, catechol and phenols in smaller amounts.

The aqueous phase from the SS experiment contained pyrazines, cyclopentenones and diethylene glycol diacetate as major compounds. No phenols or catechol were detected in the aqueous phase.

For the aqueous phase from the CM experiment, acetone and a high concentration of benzoic acid were detected as well as a high number of other acids compared to the aqueous phase from the experiments with the other feedstocks. No phenols or catechol were detected in the aqueous phase.

The aqueous phase from the SK experiment had acetone and methanol in low concentration, and did not contain phenols or catechol.

The biocrude from the WS experiment had the highest oxygen content, and thus the lowest higher heating value. On the other hand the biocrude had a very low sulphur content which is beneficial due to low SO₂ emission, and makes it less corrosive to steel in engine injection systems and ovens. The same biocrude also had a very low nitrogen content giving lower NO_x emissions.

The biocrude from the other three examined feedstock (CS, SS and CM) had oxygen contents in the range 13,7–16,5%, and had similar high calculated energy contents in the range 33,1-34,1 MJ/kg.

4.2 Further work

HTL is a useful process to convert waste material to products in a cost effective way by eliminating the drying process for wet feedstocks. However, there are several challenges, which might be solved by further work. Some of them are listed below.

- The HTL process can still be improved to be a low-cost process, and adapted to be an efficient industrial large-scale process for conversion of waste products.
- Products found in the aqueous phase has a potential to be used as commercial products, and processes might be directed and improved for this purpose (temperature, pressure, redox conditions, recycling etc.)
- The disposal part from the aqueous phase needs to be environmentally friendly, and for the treatment of municipal wastewater, the content of pharmaceutical products or toxic compounds should be removed. In addition, the removal of heavy metals for some waste waters is needed.
- A more thorough characterization of the composition of each biomass input type to develop an understanding of the connection between different biopolymers and their HTL products would be of high value.
- An extended dedicated library for products detected in research may be useful for monitoring the products formed in the process – both for GC-MS, NMR and other analytical methods.
- A large amount of data is collected in the work in this the thesis, which could be examined more in depth with more allocated time. The spectra from GC-MS and the ^1H and ^{13}C NMR spectra could be analyzed more in detail in order to have a wider overview of the numerous compounds found in the aqueous phase, and to be able to quantify them more specifically.
- Also the total organic carbon data was not analyzed from the taken samples due to the situation caused by Covid-19. Such data are recommended to be included in further

research in order to see how much of the carbon content actually is found in the analyses by GC-MS and NMR, and can be quantified.

References

- AKHTAR, J. & AMIN, N. A. S. 2011. A review on process conditions for optimum bio-oil yield in hydrothermal liquefaction of biomass. *Renewable & sustainable energy reviews*, 15, 1615-1624.
- AMIN, N. & CLARIDGE, T. 2017. *Quantitative NMR Spectroscopy* [Online]. Oxford University. Available: <http://nmrweb.chem.ox.ac.uk/Data/Sites/70/userfiles/pdfs/quantitative-nmr.pdf> [Accessed 18 March 2020].
- ANASTASAKIS, K., BILLER, P., MADSEN, R., GLASIUS, M. & JOHANNSEN, I. 2018. Continuous Hydrothermal Liquefaction of Biomass in a Novel Pilot Plant with Heat Recovery and Hydraulic Oscillation. *Energies (Basel)*, 11, 2695.
- ARTURI, K. R., KUCHERYAVSKIY, S. & SØGAARD, E. G. 2016. Performance of hydrothermal liquefaction (HTL) of biomass by multivariate data analysis. *Fuel processing technology*, 150, 94-103.
- BECKER, R., DORGERLOH, U., PAULKE, E., MUMME, J. & NEHLS, I. 2014. Hydrothermal Carbonization of Biomass: Major Organic Components of the Aqueous Phase. *Chemical engineering & technology*, 37, 511-518.
- BILLER, P., ROSS, A. B., SKILL, S. C., LEA-LANGTON, A., BALASUNDARAM, B., HALL, C., RILEY, R. & LLEWELLYN, C. A. 2012. Nutrient recycling of aqueous phase for microalgae cultivation from the hydrothermal liquefaction process. *Algal research (Amsterdam)*, 1, 70-76.
- CHANNIWALA, S. A. & PARIKH, P. P. 2002. A unified correlation for estimating HHV of solid, liquid and gaseous fuels. *Fuel (Guildford)*, 81, 1051-1063.
- DIMITRIADIS, A. & BEZERGIANNI, S. 2017. Hydrothermal liquefaction of various biomass and waste feedstocks for biocrude production: A state of the art review. *Renewable & sustainable energy reviews*, 68, 113-125.
- DONG, K., HOCHMAN, G., ZHANG, Y., SUN, R., LI, H. & LIAO, H. 2018. CO₂ emissions, economic and population growth, and renewable energy: Empirical evidence across regions. *Energy economics*, 75, 180-192.
- DROZD, J. 1981. *Chemical derivatization in gas chromatography*, Amsterdam, Elsevier.
- DUBUIS, A., LE MASLE, A., CHAHEN, L., DESTANDAU, E. & CHARON, N. 2019. Centrifugal partition chromatography as a fractionation tool for the analysis of lignocellulosic biomass products by liquid chromatography coupled to mass spectrometry. *Journal of Chromatography A*, 1597, 159-166.
- ELLIOTT, D. C. 2007. Historical Developments in Hydroprocessing Bio-oils. *Energy Fuels*, 21, 1792-1815.
- ELLIOTT, D. C., BILLER, P., ROSS, A. B., SCHMIDT, A. J. & JONES, S. B. 2015. Hydrothermal liquefaction of biomass: Developments from batch to continuous process. *Bioresour Technol*, 178, 147-156.
- EUROPEAN COMMISSION. *Horizon 2020 | Hydrothermal liquefaction: Enhanced performance and feedstock flexibility for efficient biofuel production* [Online]. Available: <https://cordis.europa.eu/project/id/764734> [Accessed 4 May 2020].
- FIELD, L. D., LI, H. L. & MAGILL, A. M. 2015. *Organic structures from 2D NMR spectra*. Chichester, England ; West Sussex, England: Wiley.
- FLEMING, I. & WILLIAMS, D. 2019. *Spectroscopic Methods in Organic Chemistry*. 7th ed. 2019. ed. Cham: Springer International Publishing : Imprint: Springer.

- GHOREISHI, S., BARTH, T. & DERRIBSA, H. 2019a. Stirred and non-stirred lignin solvolysis with formic acid in aqueous and ethanolic solvent systems at different levels of loading in a 5-L reactor. *Biofuel research journal*, 6, 937-946.
- GHOREISHI, S., BARTH, T. & HERMUNDSGÅRD, D. H. 2019b. Effect of Reaction Conditions on Catalytic and Noncatalytic Lignin Solvolysis in Water Media Investigated for a 5 L Reactor. *ACS Omega*, 4, 19265-19278.
- GOLLAKOTA, A. R. K., KISHORE, N. & GU, S. 2018. A review on hydrothermal liquefaction of biomass. *Renewable & sustainable energy reviews*, 81, 1378-1392.
- GROB, R. L. & BARRY, E. F. 2004. Modern practice of gas chromatography. 4th ed. ed. Hoboken, N.J.: Wiley-Interscience.
- GU, Y., ZHANG, X., DEAL, B., HAN, L., ZHENG, J. & BEN, H. 2019. Advances in energy systems for valorization of aqueous byproducts generated from hydrothermal processing of biomass and systems thinking. *Green chemistry : an international journal and green chemistry resource : GC*, 21, 2518-2543.
- HALLERAKER, H. V. & BARTH, T. 2020. Quantitative NMR analysis of the aqueous phase from hydrothermal liquefaction of lignin. *Journal of analytical and applied pyrolysis*, 151, 104919.
- HE, C., CHEN, C.-L., GIANNIS, A., YANG, Y. & WANG, J.-Y. 2014. Hydrothermal gasification of sewage sludge and model compounds for renewable hydrogen production: A review. *Renewable & sustainable energy reviews*, 39, 1127-1142.
- HUANG, H.-J. & YUAN, X.-Z. 2016. The migration and transformation behaviors of heavy metals during the hydrothermal treatment of sewage sludge. *Bioresour Technol*, 200, 991-998.
- HUANG, H.-J., YUAN, X.-Z., LI, B.-T., XIAO, Y.-D. & ZENG, G.-M. 2014. Thermochemical liquefaction characteristics of sewage sludge in different organic solvents. *Journal of analytical and applied pyrolysis*, 109, 176-184.
- HYFLEXFUEL. *About (The project)* [Online]. Available: <https://www.hyflexfuel.eu/about/> [Accessed 5 May 2020].
- LAZZARI, E., POLIDORO, A. D. S., ONOREVOLI, B., SCHEINA, T., SILVA, A. N., SCAPIN, E., JACQUES, R. A. & CARAMÃO, E. B. 2019. Production of rice husk bio-oil and comprehensive characterization (qualitative and quantitative) by HPLC/PDA and GC × GC/qMS. *Renewable Energy*, 135, 554-565.
- LIU, Z., CIAIS, P., DENG, Z., LEI, R., DAVIS, S. J., FENG, S., ZHENG, B., CUI, D., DOU, X., HE, P., ZHU, B., LU, C., KE, P., SUN, T., WANG, Y., YUE, X., WANG, Y., LEI, Y., ZHOU, H., CAI, Z., WU, Y., GUO, R., HAN, T., XUE, J., BOUCHER, O., BOUCHER, E., CHEVALLIER, F., WEI, Y., ZHONG, H., KANG, C., ZHANG, N., CHEN, B., XI, F., MARIE, F., ZHANG, Q., GUAN, D., GONG, P., KAMMEN, D. M., HE, K. & SCHELLNHUBER, H. J. 2020. COVID-19 causes record decline in global CO2 emissions.
- LIU, Z. & ZHANG, F.-S. 2008. Effects of various solvents on the liquefaction of biomass to produce fuels and chemical feedstocks. *Energy conversion and management*, 49, 3498-3504.
- LØHRE, C., UNDERHAUG, J., BRUSLETTO, R. & BARTH, T. Prepared for submission. Quantitative NMR-analysis of aqueous samples from thermochemical conversion of biomass.
- LU, J., LI, H., ZHANG, Y. & LIU, Z. 2018. Nitrogen Migration and Transformation during Hydrothermal Liquefaction of Livestock Manures. *ACS Sustainable Chem. Eng*, 6, 13570-13578.

- MADDI, B., PANISKO, E., WIETSMA, T., LEMMON, T., SWITA, M., ALBRECHT, K. & HOWE, D. 2017. Quantitative Characterization of Aqueous Byproducts from Hydrothermal Liquefaction of Municipal Wastes, Food Industry Wastes, and Biomass Grown on Waste. *ACS Sustainable Chem. Eng*, 5, 2205-2214.
- MADSEN, R. B., JENSEN, M. M., MORUP, A. J., HOULBERG, K., CHRISTENSEN, P. S., KLEMMER, M., BECKER, J., IVERSEN, B. B. & GLASIUS, M. 2016. Using design of experiments to optimize derivatization with methyl chloroformate for quantitative analysis of the aqueous phase from hydrothermal liquefaction of biomass. *Anal Bioanal Chem*, 408, 2171-83.
- MILLER, J. M. 2004. *Chromatography: Concepts and Contrasts*, Hoboken, Hoboken: John Wiley & Sons, Incorporated.
- MØRUP, A. J., BECKER, J., CHRISTENSEN, P. S., HOULBERG, K., LAPPA, E., KLEMMER, M., MADSEN, R. B., GLASIUS, M. & IVERSEN, B. B. 2015. Construction and Commissioning of a Continuous Reactor for Hydrothermal Liquefaction. *Industrial & engineering chemistry research*, 54, 5935-5947.
- NAZARI, L., YUAN, Z., SOUZANCHI, S., RAY, M. B. & XU, C. 2015. Hydrothermal liquefaction of woody biomass in hot-compressed water: Catalyst screening and comprehensive characterization of bio-crude oils. *Fuel (Guildford)*, 162, 74-83.
- PANISKO, E., WIETSMA, T., LEMMON, T., ALBRECHT, K. & HOWE, D. 2015. Characterization of the aqueous fractions from hydrotreatment and hydrothermal liquefaction of lignocellulosic feedstocks. *Biomass & bioenergy*, 74, 162-171.
- PAVIA, D. L. 2015. *Introduction to spectroscopy*, Stamford, Conn, Cengage Learning.
- QIAN, L., WANG, S., XU, D., GUO, Y., TANG, X. & WANG, L. 2015. Treatment of sewage sludge in supercritical water and evaluation of the combined process of supercritical water gasification and oxidation. *Bioresour Technol*, 176, 218-224.
- QU, Y., WEI, X. & ZHONG, C. 2003. Experimental study on the direct liquefaction of *Cunninghamia lanceolata* in water. *Energy (Oxford)*, 28, 597-606.
- SCHALEGER, L. L., FIGUEROA, C. & DAVIS, H. G. 1982. DIRECT LIQUEFACTION OF BIOMASS: RESULTS FROM OPERATION OF CONTINUOUS BENCH SCALE UNIT IN LIQUEFACTION OF WATER SLURRIES OF DOUGLAS FIR WOOD.
- SCHIENER, P., BLACK, K. D., STANLEY, M. S. & GREEN, D. H. 2014. The seasonal variation in the chemical composition of the kelp species *Laminaria digitata*, *Laminaria hyperborea*, *Saccharina latissima* and *Alaria esculenta*. *Journal of applied phycology*, 27, 363-373.
- SEEHAR, T. H., TOOR, S. S., SHAH, A. A., PEDERSEN, T. H. & ROSENDAHL, L. A. 2020. Biocrude Production from Wheat Straw at Sub and Supercritical Hydrothermal Liquefaction. *Energies (Basel)*, 13, 3114.
- SHAH, A. A., TOOR, S. S., SEEHAR, T. H., NIELSEN, R. S., NIELSEN, A., PEDERSEN, T. H. & ROSENDAHL, L. A. 2020. Bio-Crude Production through Aqueous Phase Recycling of Hydrothermal Liquefaction of Sewage Sludge. *Energies (Basel)*, 13, 493.
- SMART, K. F., AGGIO, R. B. M., VAN HOUTTE, J. R. & VILLAS-BÔAS, S. G. 2010. Analytical platform for metabolome analysis of microbial cells using methyl chloroformate derivatization followed by gas chromatography–mass spectrometry. *Nat Protoc*, 5, 1709-1729.
- SUGANO, M., TAKAGI, H., HIRANO, K. & MASHIMO, K. 2008. Hydrothermal liquefaction of plantation biomass with two kinds of wastewater from paper industry. *Journal of Materials Science*, 43, 2476-2486.

- SUSSMANN, R. & RETTINGER, M. 2020. Can We Measure a COVID-19-Related Slowdown in Atmospheric CO₂ Growth? Sensitivity of Total Carbon Column Observations. *Remote sensing (Basel, Switzerland)*, 12, 2387.
- TENENBAUM, D. J. 2008. Food vs. Fuel: Diversion of Crops Could Cause More Hunger. *Environ Health Perspect*, 116, A254-A257.
- TOMASINI, D. B., CACCIOLA, F., RIGANO, F., SCIARRONE, D., DONATO, P., BECCARIA, M., CARAMÃO, E. B., DUGO, P. & MONDELLO, L. 2014. Complementary Analytical Liquid Chromatography Methods for the Characterization of Aqueous Phase from Pyrolysis of Lignocellulosic Biomasses. *Anal. Chem*, 86, 11255-11262.
- TOMMASO, G., CHEN, W.-T., LI, P., SCHIDEMAN, L. & ZHANG, Y. 2015. Chemical characterization and anaerobic biodegradability of hydrothermal liquefaction aqueous products from mixed-culture wastewater algae. *Bioresour Technol*, 178, 139-146.
- TOOR, S. S., ROSENDAHL, L. & RUDOLF, A. 2011. Hydrothermal liquefaction of biomass: A review of subcritical water technologies. *Energy (Oxford)*, 36, 2328-2342.
- VALDEZ, P. J., NELSON, M. C., WANG, H. Y., LIN, X. N. & SAVAGE, P. E. 2012. Hydrothermal liquefaction of *Nannochloropsis* sp.: Systematic study of process variables and analysis of the product fractions. *Biomass & bioenergy*, 46, 317-331.
- VILLADSEN, S. R., DITHMER, L., FORSBERG, R., BECKER, J., RUDOLF, A., IVERSEN, S. B., IVERSEN, B. B. & GLASIUS, M. 2012. Development and Application of Chemical Analysis Methods for Investigation of Bio-Oils and Aqueous Phase from Hydrothermal Liquefaction of Biomass. *Energy & Fuels*, 26, 6988-6998.
- XU, C. & ETCHEVERRY, T. 2008. Hydro-liquefaction of woody biomass in sub- and super-critical ethanol with iron-based catalysts. *Fuel (Guildford)*, 87, 335-345.
- XU, C. & LANCASTER, J. 2008. Conversion of secondary pulp/paper sludge powder to liquid oil products for energy recovery by direct liquefaction in hot-compressed water. *Water Res*, 42, 1571-1582.
- XU, D., LIN, G., LIU, L., WANG, Y., JING, Z. & WANG, S. 2018. Comprehensive evaluation on product characteristics of fast hydrothermal liquefaction of sewage sludge at different temperatures. *Energy (Oxford)*, 159, 686-695.
- YE, L., ZHANG, J., ZHAO, J. & TU, S. 2014. Liquefaction of bamboo shoot shell for the production of polyols. *Bioresour Technol*, 153, 147-153.
- YIP, J., CHEN, M., SZETO, Y. S. & YAN, S. 2009. Comparative study of liquefaction process and liquefied products from bamboo using different organic solvents. *Bioresour Technol*, 100, 6674-6678.
- ZHANG, B., VON KEITZ, M. & VALENTAS, K. 2009. Thermochemical liquefaction of high-diversity grassland perennials. *Journal of analytical and applied pyrolysis*, 84, 18-24.

Appendix

Appendix A – Corn Stover

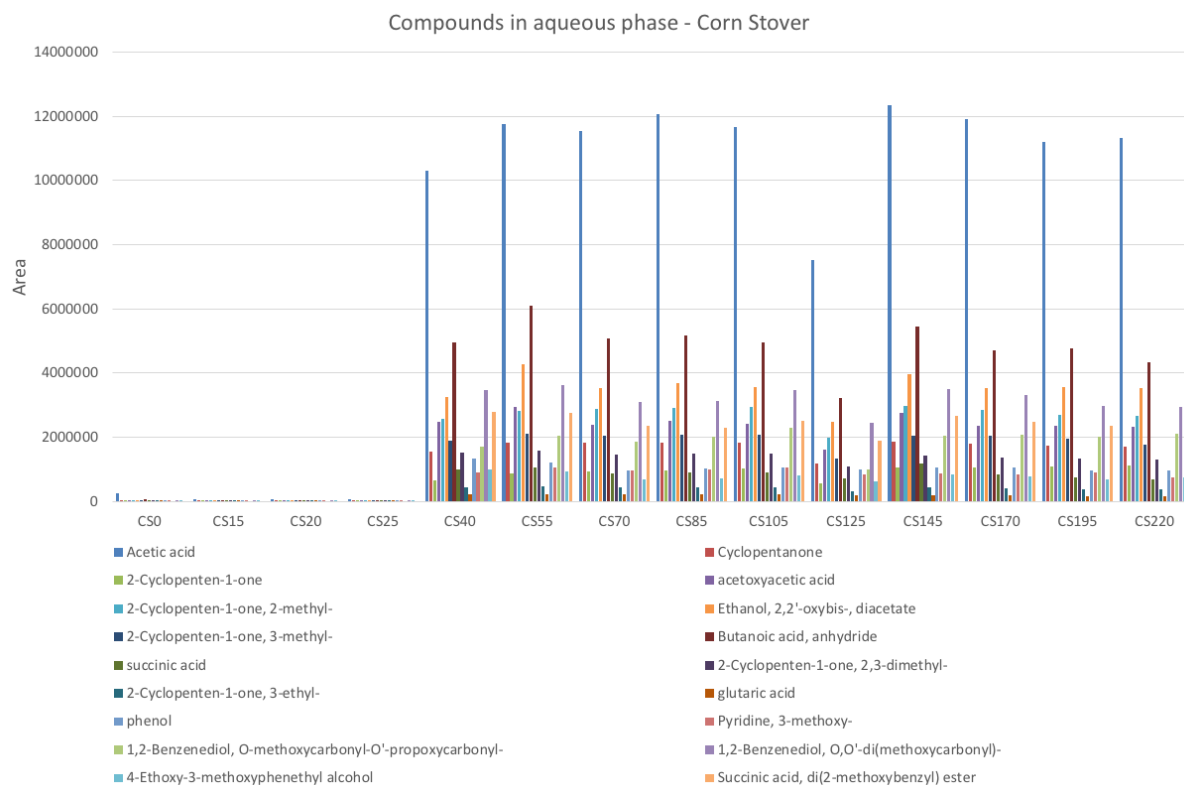


Figure A1: Composition of compounds in the aqueous phase for all samples with corn stover as feedstock based on the GC-MS spectra.

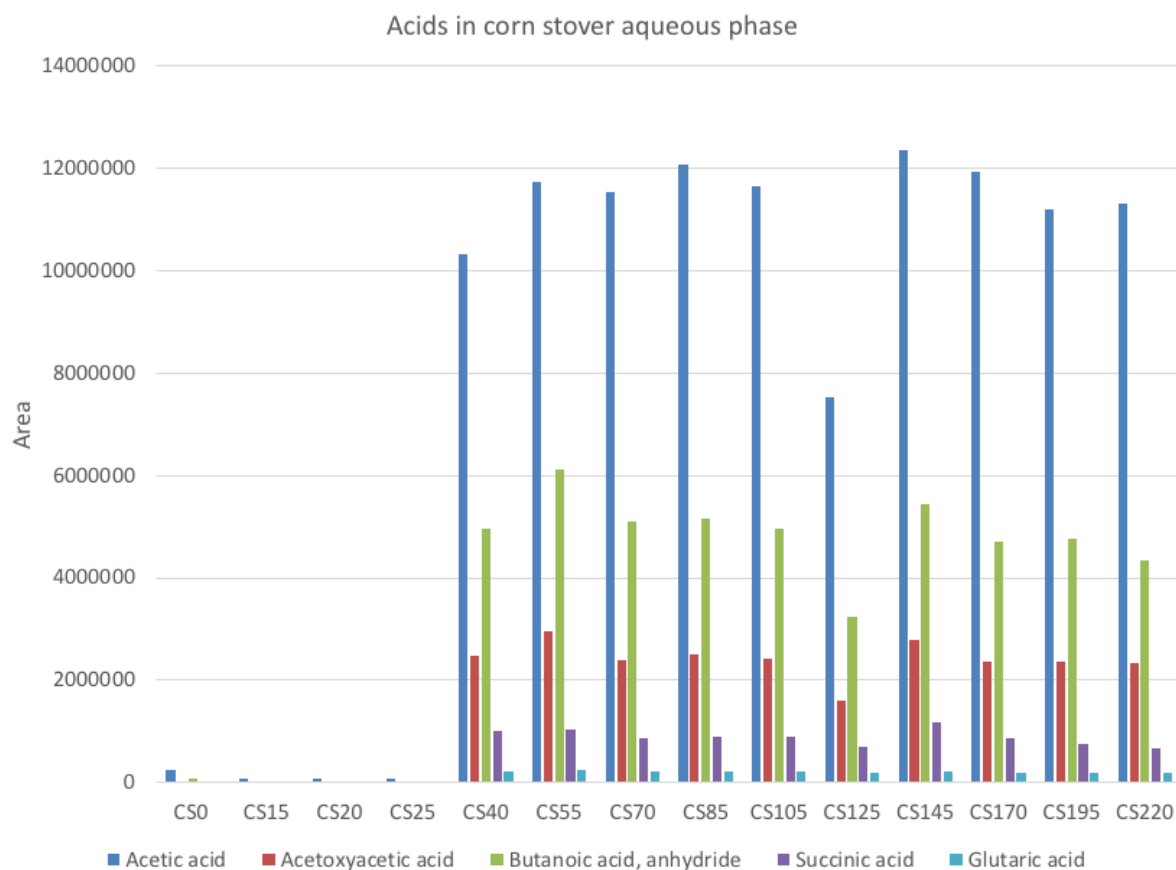


Figure A2: Component composition of the carboxylic acids in the aqueous phase for all samples with corn stover as feedstock obtained from the GC-MS analyses.

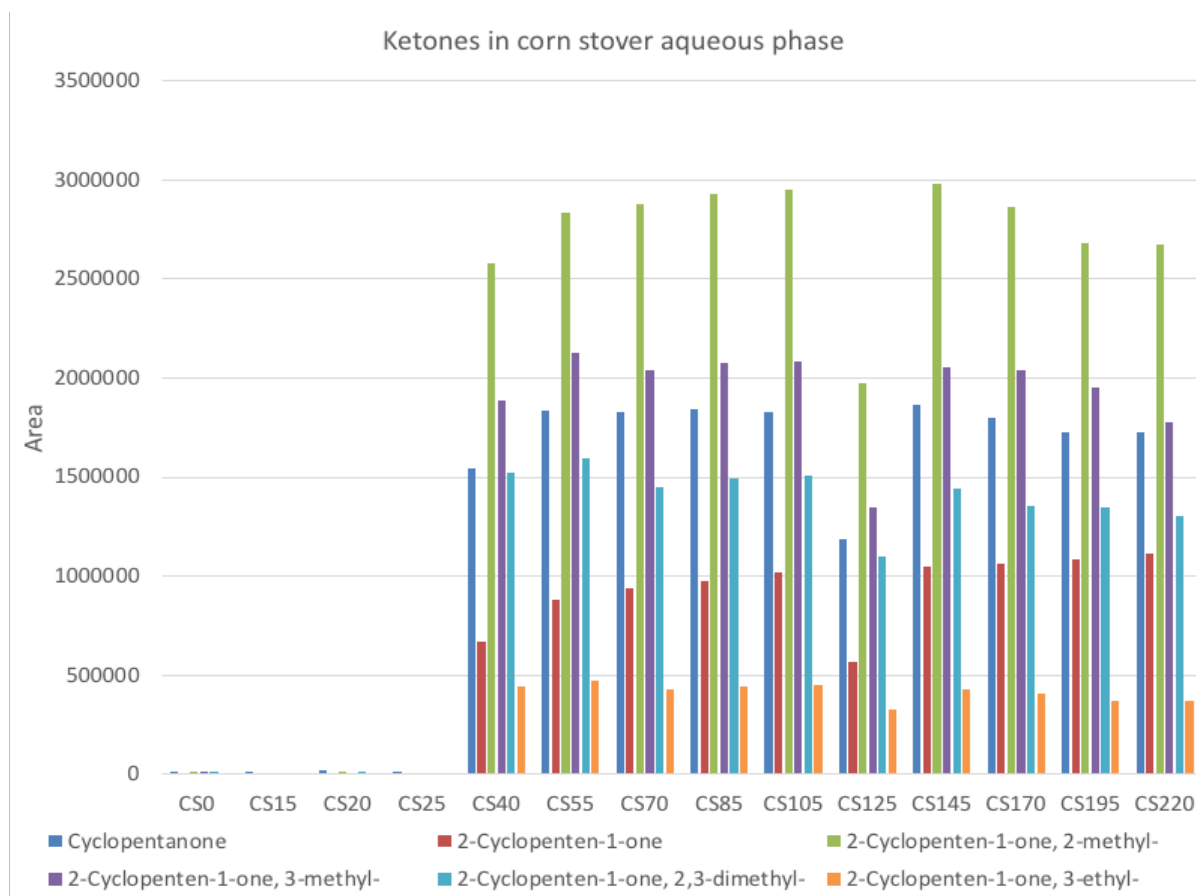


Figure A3: Component composition of the ketones in the aqueous phase for all samples with corn stover as feedstock obtained from the GC-MS analyses.

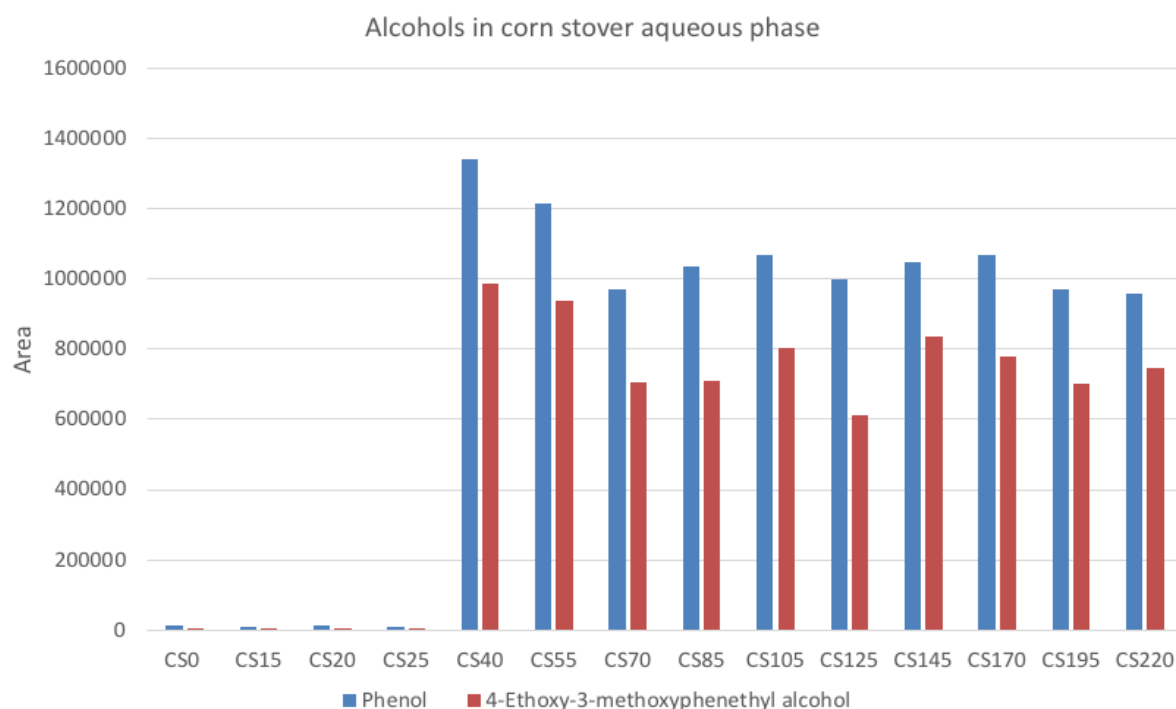


Figure A4: Component composition of the alcohols in the aqueous phase for all samples with corn stover as feedstock obtained from the GC-MS analyses.

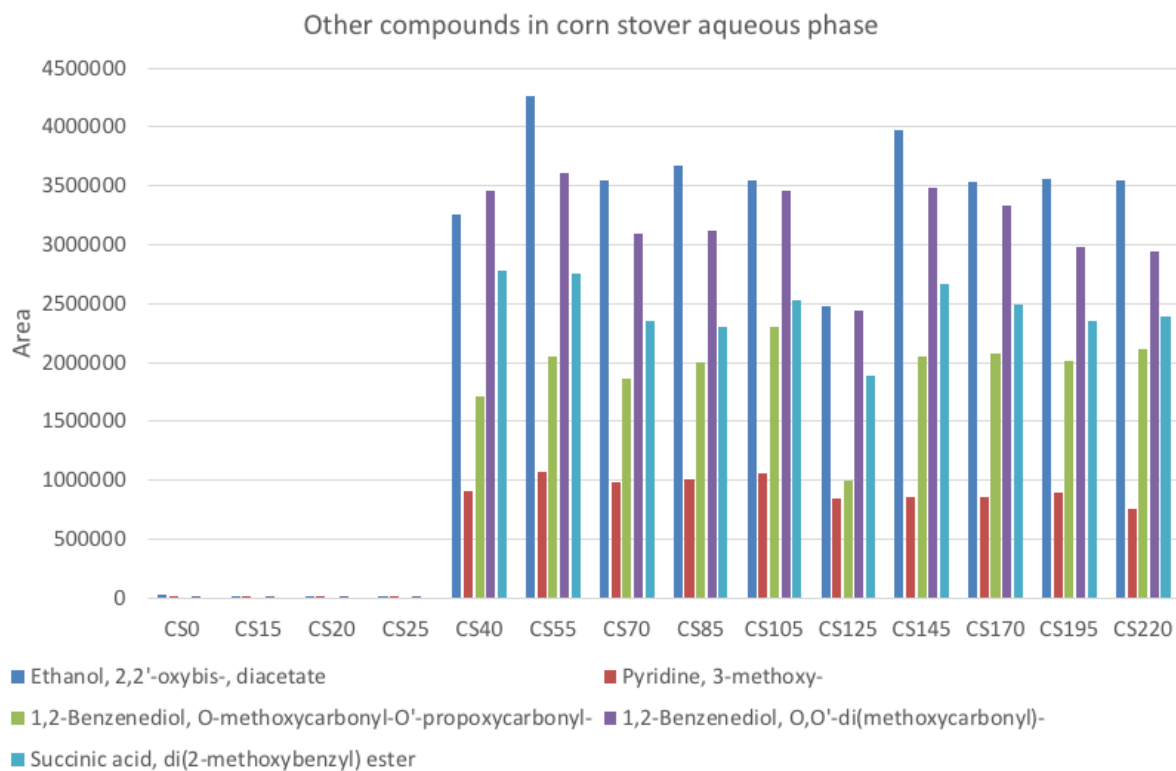


Figure A5: Component composition of other compounds in the aqueous phase for all samples with corn stover as feedstock obtained from the GC-MS analyses.

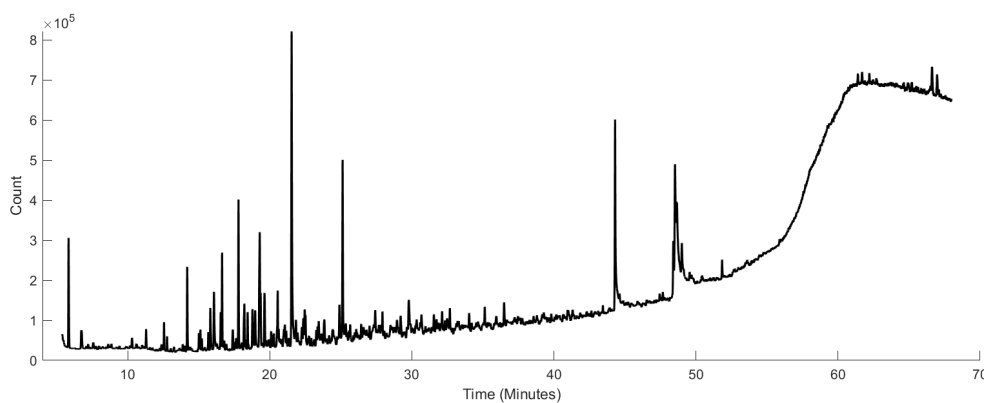


Figure A6: Chromatograms from GC-MS of the biocrude from the corn stover experiment.

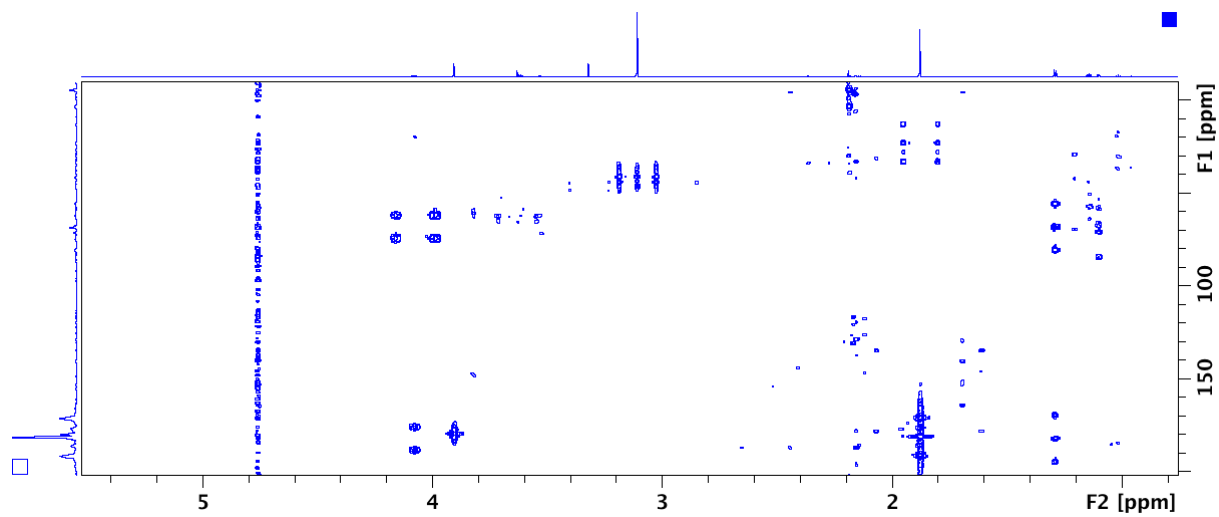


Figure A7: HMBC spectrum of the sample taken after 55 minutes of the aqueous phase from the corn stover experiment.

Appendix B – Wheat straw

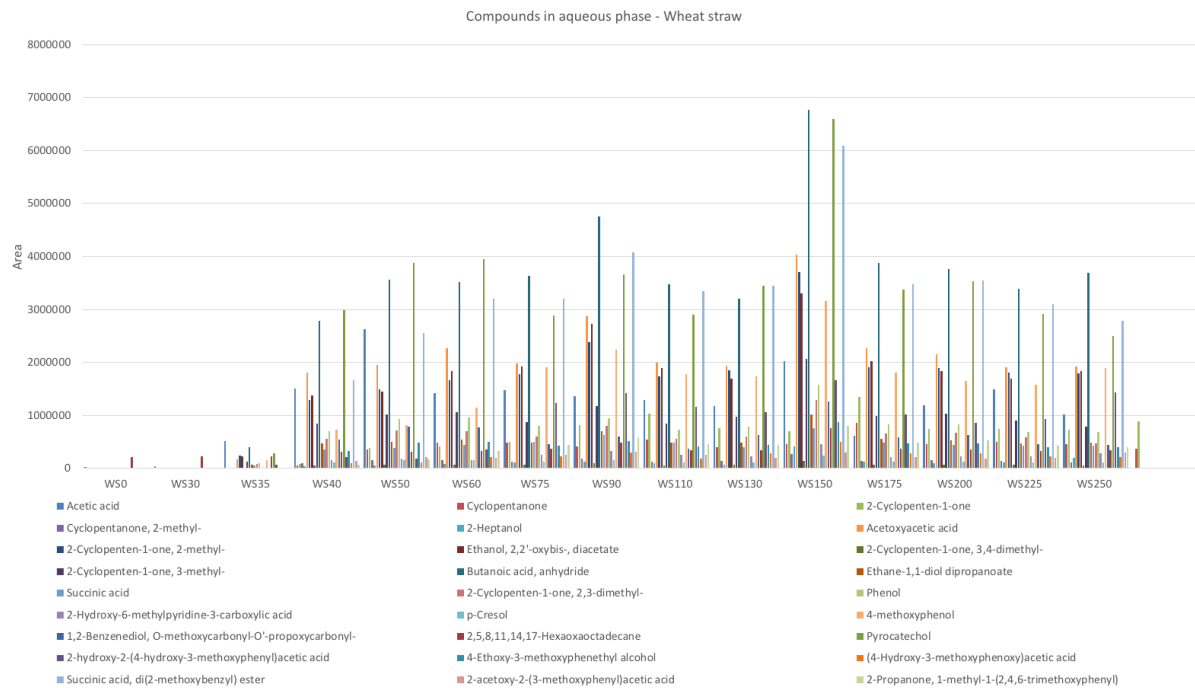


Figure B1: Component composition in the aqueous phase for all samples with wheat straw as feedstock obtained from the GC-MS analyses.

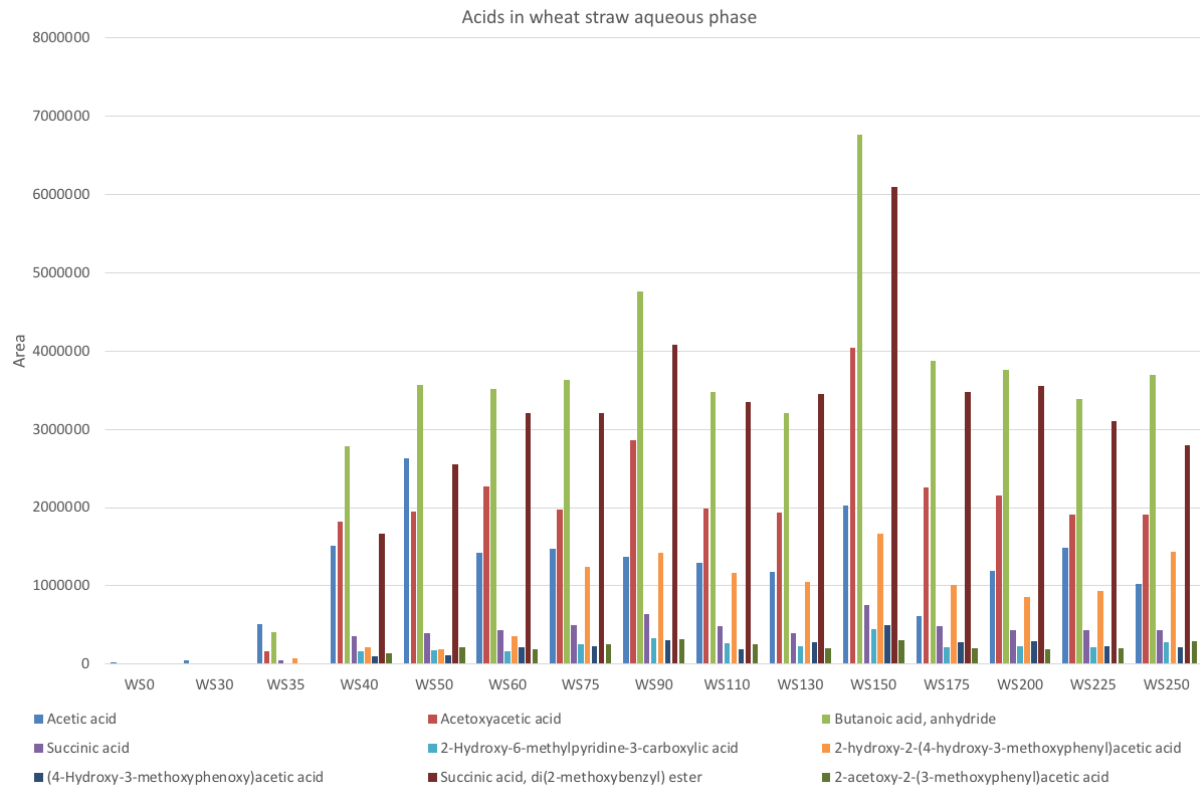


Figure B2: Component composition of the carboxylic acids in the aqueous phase for all samples with wheat straw as feedstock obtained from the GC-MS analyses.

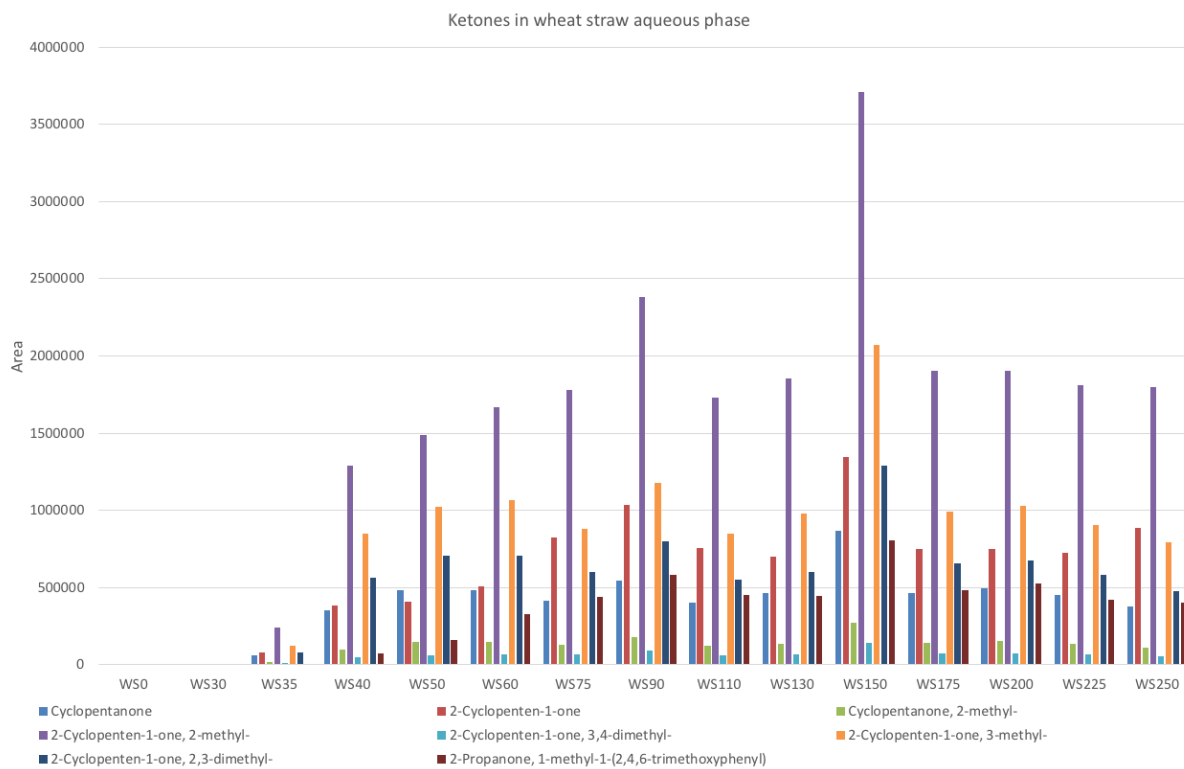


Figure B3: Component composition of the ketones in the aqueous phase for all samples with wheat straw as feedstock obtained from the GC-MS analyses.

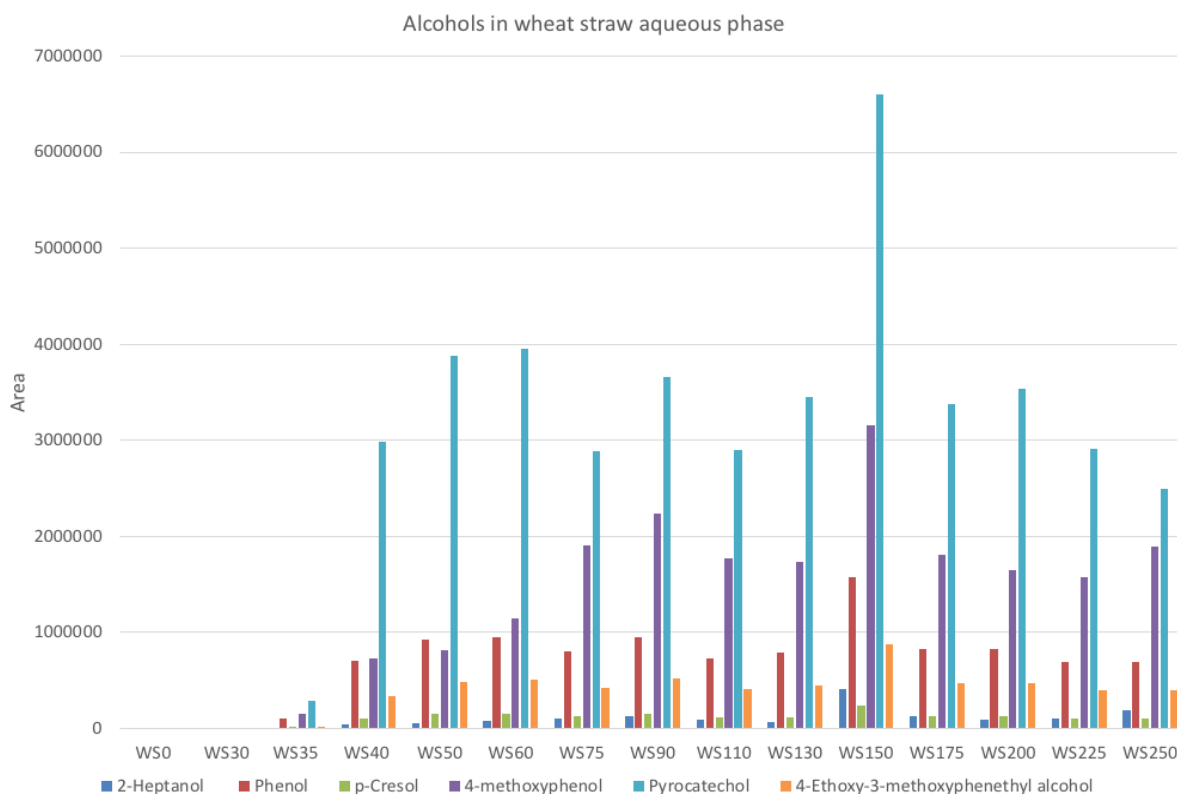


Figure B4: Component composition of the alcohols in the aqueous phase for all samples with wheat straw as feedstock obtained from the GC-MS analyses.

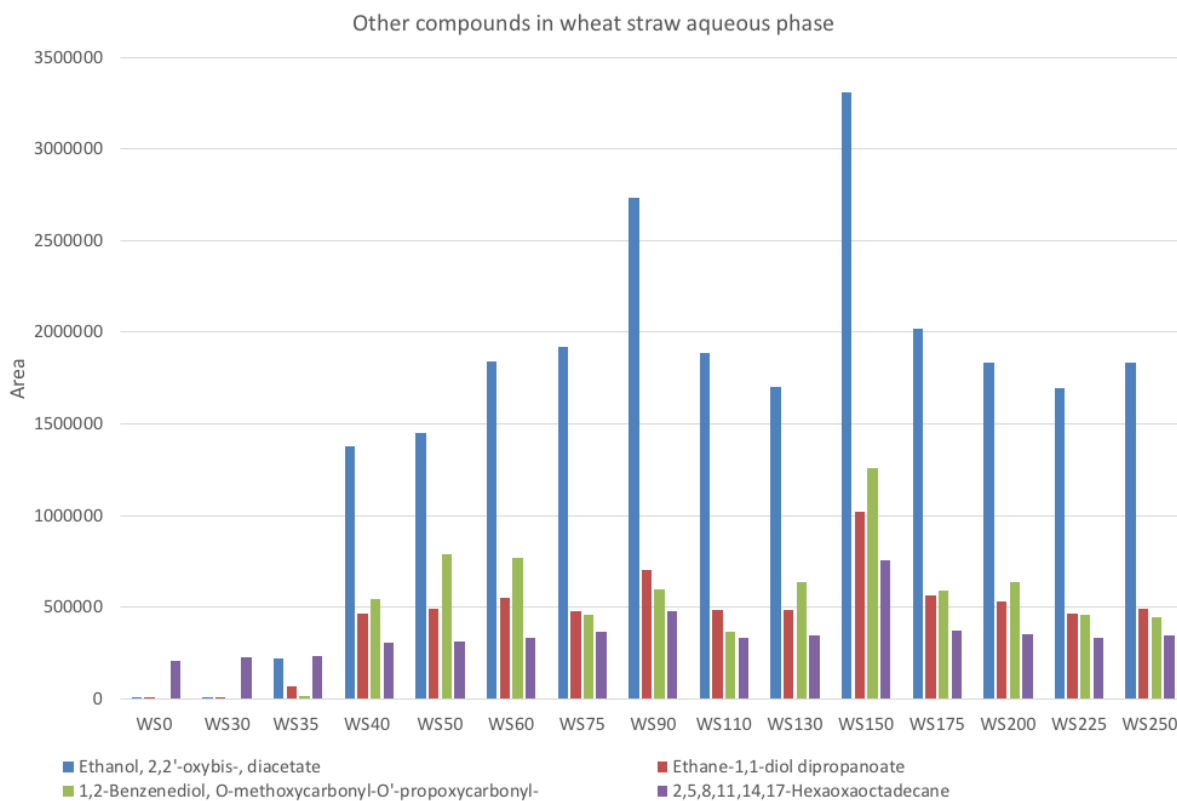


Figure B5: Component composition of the other compounds in the aqueous phase for all samples with wheat straw as feedstock obtained from the GC-MS analyses.

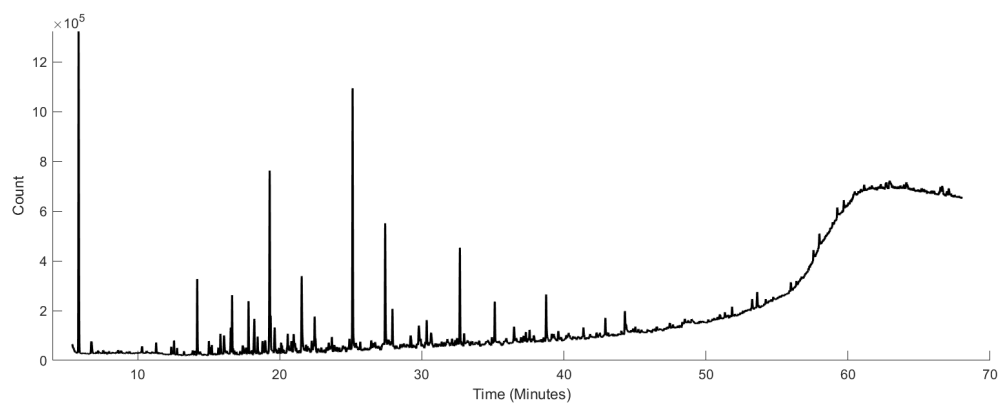


Figure B6: Chromatograms from GC-MS of the biocrude from the wheat straw experiment.

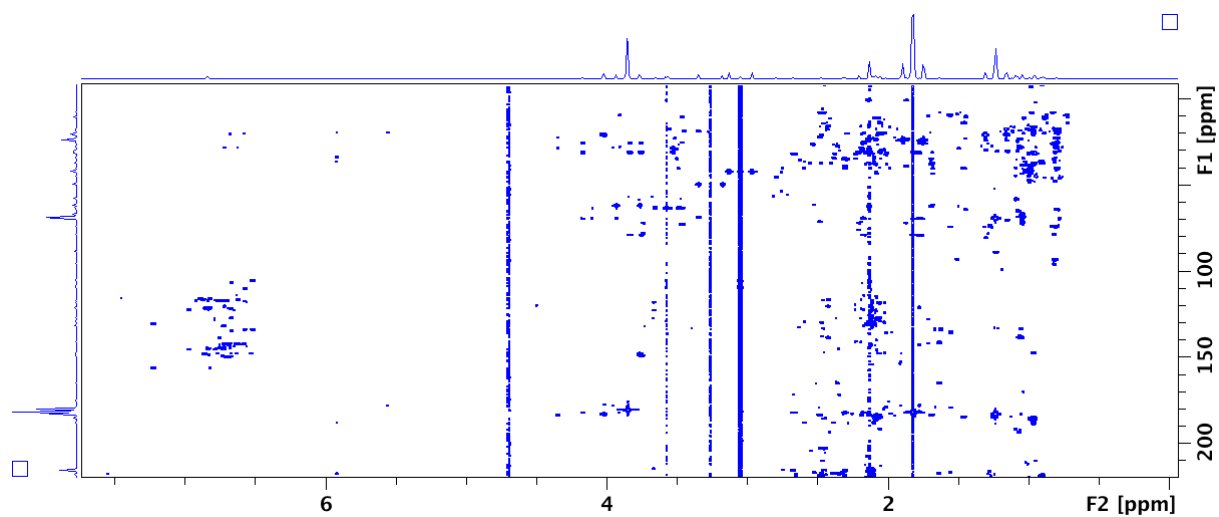


Figure B7: HMBC spectrum of the sample taken after 60 minutes of the aqueous phase from the wheat straw experiment.

Appendix C – Sewage sludge

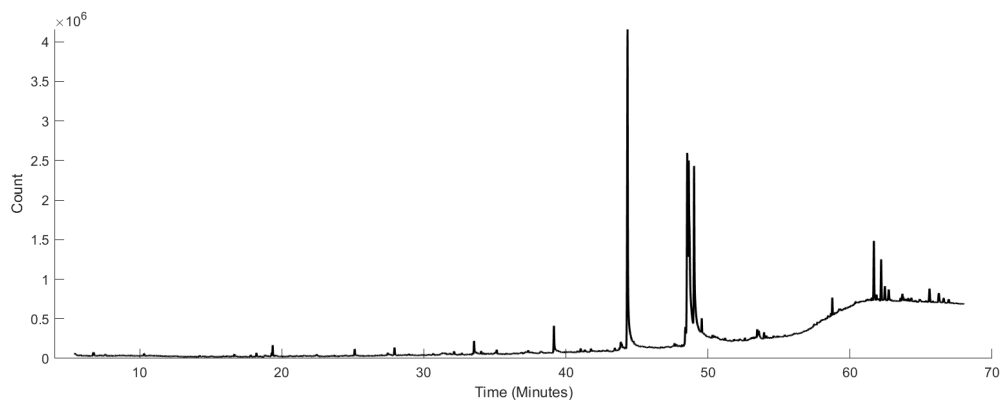


Figure C1: Chromatograms from GC-MS of the biocrude from the sewage sludge experiment.

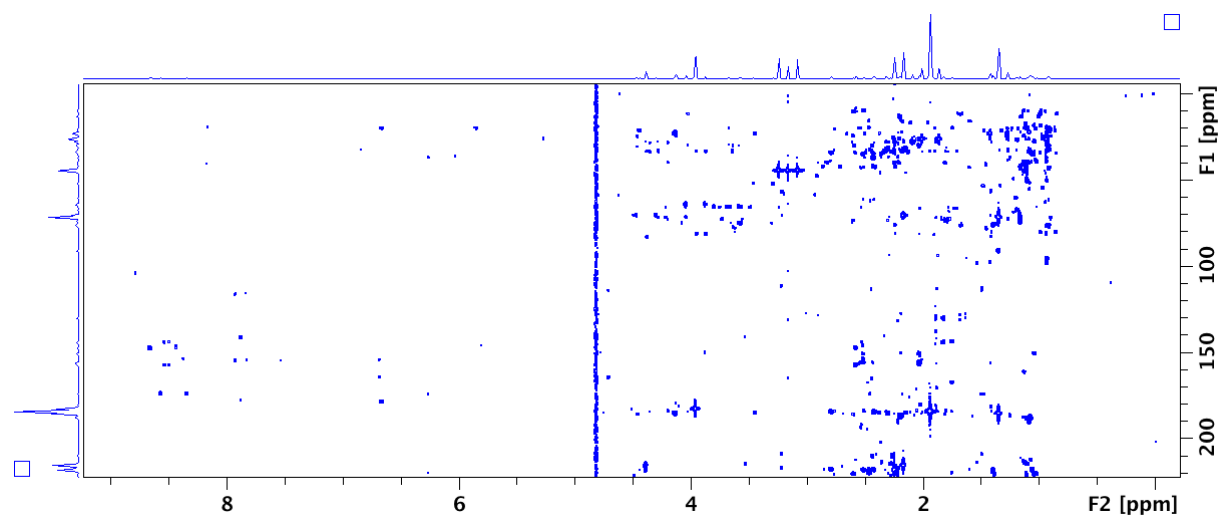


Figure C2: HMBC spectrum of the sample taken after 90 minutes of the aqueous phase from the sewage sludge experiment.

Appendix D – Cattle Manure

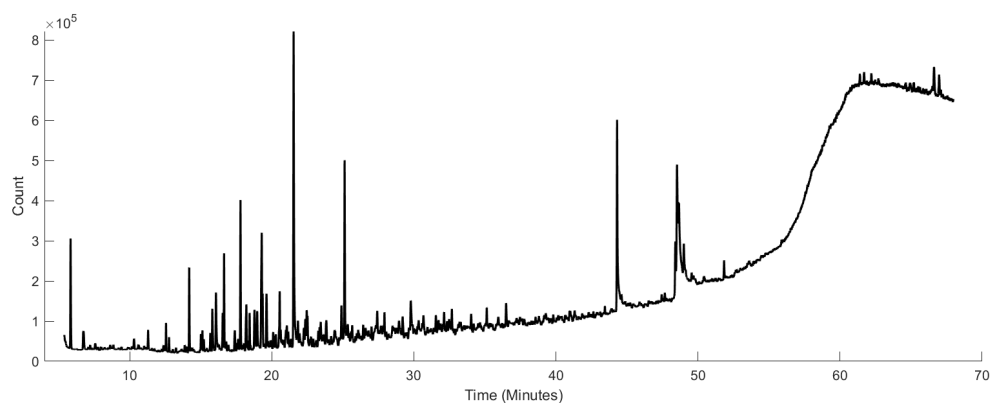


Figure D1: Chromatograms from GC-MS of the biocrude from the cattle manure experiment.

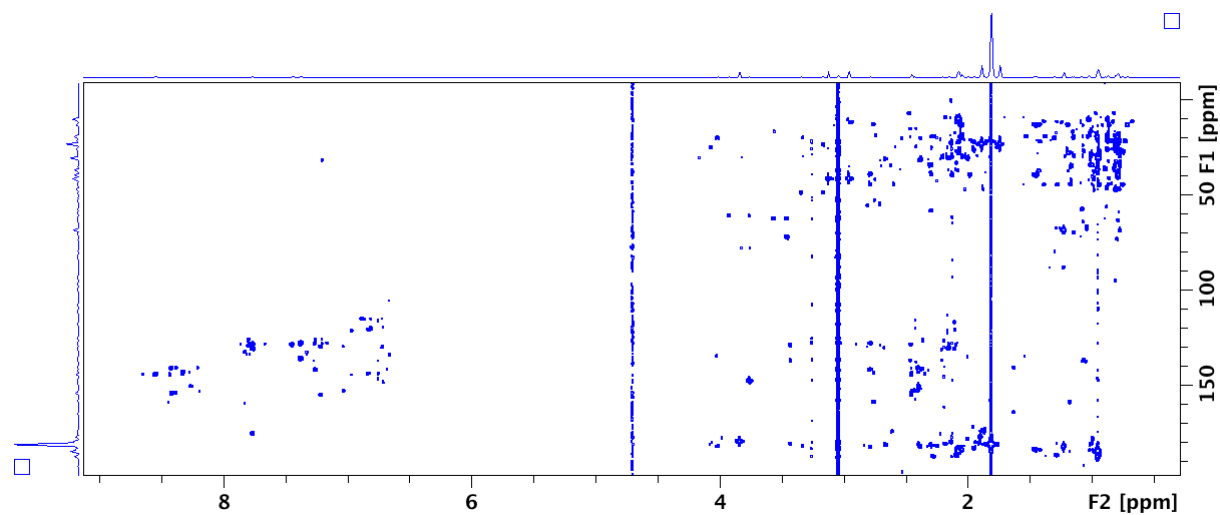


Figure D2: HMBC spectrum of the sample taken after 60 minutes of the aqueous phase from the cattle manure experiment.

Appendix E – Sugar Kelp

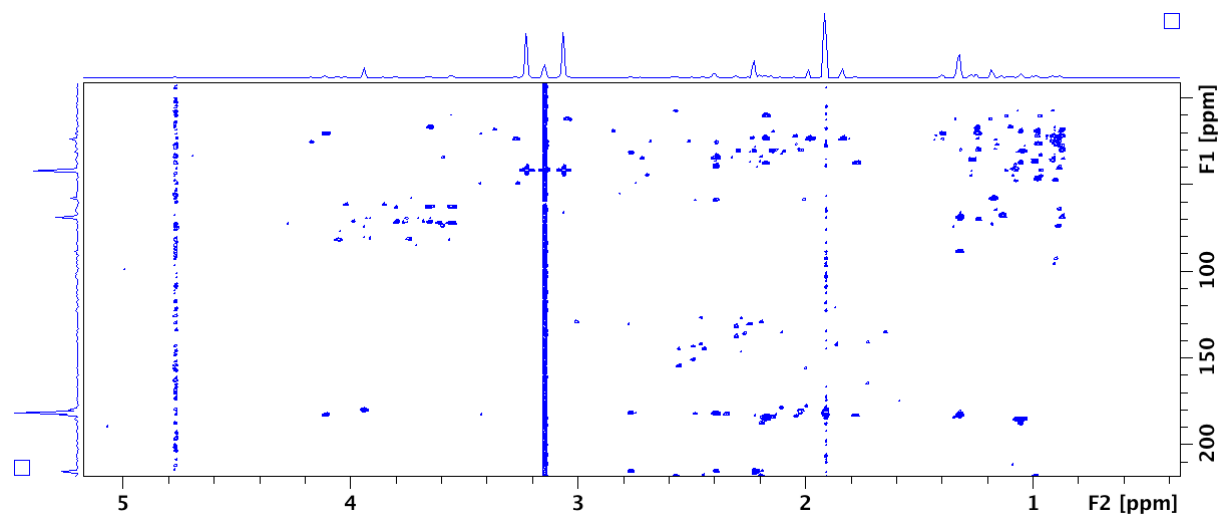


Figure E1: HMBC spectrum of the sample taken after 65 minutes of the aqueous phase from the sugar kelp experiment.

Appendix F – All feedstocks

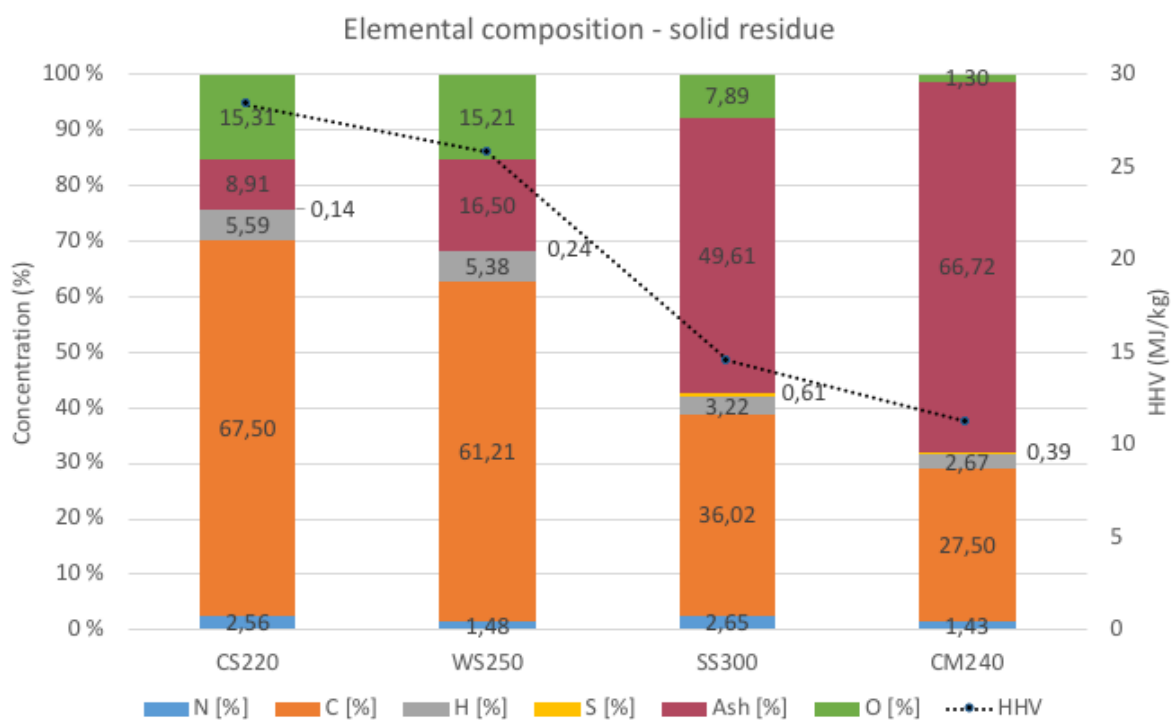


Figure F1: The elemental composition with the calculated higher heating value (HHV) of the solid residue after filtration of biocrude from corn stover, wheat straw, sewage sludge and cattle manure.

Table F1: Solid residue elemental composition, ash content and calculated HHV.

	CS	WS	SS	CM
C (%)	67,50	61,21	36,02	27,50
H (%)	5,59	5,38	3,22	2,67
N (%)	2,56	1,48	2,65	1,43
S (%)	0,14	0,24	0,61	0,39
O** (%)	15,31	15,21	7,89	1,30
Ash in solid residue (%)	8,91	16,50	49,61	66,72
HHV (MJ/kg)	28,35	25,78	14,53	11,21

Table F2: Compounds in the aqueous phase from corn stover, wheat straw, sewage sludge and cattle manure feedstocks based on GC-MS analyses showing their retention times and peak areas.

Name of compound	Rt (min)	CS x10 ⁶	WS x10 ⁶	SS x10 ⁶	CM x10 ⁶
Acetone	5,024				88,6
Acetic acid	5,181	11,31	1,02	1181	568,5
Isobutyric acid	6,407				27,7
Butanoic acid	6,942				135,4
Pyrazine	7,279			35,5	48,4
2-methylbutanoic acid	7,938				60,1
Isovaleric acid	7,938			5,5	
Cyclopentanone	8,415	1,72	0,38	19,5	12,5
Dimethylcarbamic acid	8,785				8,5
Valeric acid	8,975				33,7
Pyrazine, methyl-	9,156			74,9	128,5
2-Cyclopenten-1-one	9,386	1,11	0,89	13,7	
Cyclopentanone, 2-methyl-	9,608		0,11		
Ethylcarbamic acid	9,666			22,6	46,5
2-Heptanol	9,896		0,19		
Isopropylcarbamic acid	10,538				28,8
4-Methylpentanoic acid	10,711				4,8
Acetoxyacetic acid	11,073	2,33	1,92	53,3	
2-Cyclopenten-1-one, 2-methyl-	11,328		1,80	40,7	33,2
Acetoxyacetic acid	11,328				24,8
2-Cyclopenten-1-one, 2-methyl-	11,369	2,67			
Pyrazine, 2,5-dimethyl-	11,509				39,5
Pyrazine, 2,5-dimethyl-	11,509			29,2	
Pyrazine, ethyl-	11,633			13,5	39,3
Ethanol, 2,2'-oxybis-, diacetate	11,921	3,55	1,83	103,5	45,7
2-Cyclopenten-1-one, 3,4-dimethyl-	12,234		0,06		
2-Cyclopenten-1-one, 3-methyl-	13,106	1,78	7,90	24,7	16,2
2-propylpentanoic acid	13,550				2,2
4-oxopentanoic acid	13,559				5,8
2-Ethylbutyric acid, 2-formylphenyl ester	14,209				58,2
Butanoic acid, anhydride (unlikely)	14,209	4,34	3,70		
Pentanoic acid, 2-methyl-2-propyl-	14,209			43,5	
Ethane-1,1-diol dipropanoate	14,563		0,49	32,1	
Succinic acid	14,875		0,43		

2-Oxopentanedioic acid	14,884			19,9	
Succinic acid	14,884	0,68			16,3
2-Cyclopenten-1-one, 2,3-dimethyl-	15,311	1,30	0,48		8,8
Cyclohexanecarboxylic acid	16,093				31
2-Cyclopenten-1-one, 3-ethyl-	16,645	0,37			
Benzoic acid	17,180				196,6
3-Hydroxypyridine monoacetate	17,706				22,7
Glutaric acid	18,225	0,18			
Phenol	18,595	0,96	0,69		
Phenyl hydrogen carbonate	18,595			11,2	46,2
Benzoic acid (not converted from the methyl ester)	19,064				167,2
Phenylacetic acid	19,533				109,8
Pyridine, 3-methoxy-	19,970	0,76			
2-Hydroxy-6-methylpyridine-3-carboxylic acid	20,085			74,9	
Pyridine, 3-methoxy-	20,093				52,3
2-Hydroxy-6-methylpyridine-3-carboxylic acid	20,101		0,28		
<i>p</i> -Cresol	20,595		0,11		
<i>p</i> -tolyl hydrogen carbonate	21,846				30,9
Benzenamine, 4-methoxy-	22,274			22,8	
Phenylpropanoic acid	22,438				90,9
3-Hydroxymandelic acid	24,562				60,6
4-methoxyphenol	24,562		1,90		
7-Oxabicyclo[4.1.0]heptan-2-one, 6-methyl-3-(1-methylethyl)-	25,163			0,5	
1,2-Benzenediol, O-methoxycarbonyl-O'-propoxycarbonyl-	26,841		0,44		
1,2-Benzenediol, O-methoxycarbonyl-O'-propoxycarbonyl-	26,866	2,12			
2,5,8,11,14,17-Hexaoxaoctadecane	28,134		0,35		
1,2-phenylene bis(hydrogen carbonate)	29,014			26,2	20,4
Pyrocatechol	29,047		2,49		
Homoveratric acid	29,319				38,1
1,2-Benzenediol, O,O'-di(methoxycarbonyl)-	29,409	2,95			
2-hydroxy-2-(4-hydroxy-3-methoxyphenyl)acetic acid	29,952		1,44		
Vanillylmandelic acid	29,952				30,3
4-Ethoxy-3-methoxyphenethyl alcohol	30,421	0,75	0,40		
(4-Hydroxy-3-methoxyphenoxy)acetic acid	31,532		0,22		
Succinic acid, di(2-methoxybenzyl) ester	32,084	2,39	2,79		
2-acetoxy-2-(3-methoxyphenyl)acetic acid	33,730		0,30		
2-Propanone, 1-methyl-1-(2,4,6-trimethoxyphenyl)	35,335		0,40		
1-benzylindole	38,684				47,6

Table F3: Compounds in the biocrude phase from corn stover, wheat straw, sewage sludge and cattle manure feedstocks based on GC-MS analyses showing their retention times and peak areas.

Name of compound	Rt (min)	CS x10 ⁶	WS x10 ⁶	SS x10 ⁶	CM x10 ⁶
2,2-Dimethoxybutane	10,308			0,16	
Cyclopentanone	11,288	50,2	0,35		
Cyclopentanone, 2-methyl-	12,333	33,4	0,40		
2-Cyclopenten-1-one, 2-methyl-	14,176		1,74		
1-Cyclohexylethanol	14,193	17,7			
Tetradecanoic acid	15,016	3			
Phenol	16,053		1,55		2,82
Cholest-14-ene, (5.alpha.)-	16,069	10			
Cholest-2-ene	17,798	4,2			
2-Cyclopenten-1-one, 2,3-dimethyl-	17,806		1,45		0,28
p-Cresol	18,752				5,22
Cholest-4-ene	18,777	2,2			
Phenol, 2-methoxy-	19,287		5,88		
Cholest-5-ene	19,295	3,5			
Phenol, 2-methoxy-	19,295				2,38
Undecane	19,361			0,51	
5-Ethyl-2-furaldehyde	20,554		0,54		
2-Cyclopenten-1-one, 2-methyl-	20,563	189,9			
Phenol, 4-ethyl-	21,525		5,45		17,39
Phenol*	21,534	361,2			
2-Methoxy-5-methylphenol	22,447		1,15		0,89
Phenol, 4-propyl-	24,447				1,28
Phenol, 4-ethyl-2-methoxy-	25,122		12,48		13,75
2-Cyclopenten-1-one, 2,3-dimethyl-	25,130	298,9			
Phenol, 4-ethyl-2-methoxy-	25,138			0,78	
Phenol, 2,6-dimethoxy-	27,418		5,05		
Phenol, 2-methoxy-4-propyl-	27,928		2,28	1,08	11,31
1H-Indole, 6-methyl-	28,941				3,52
3,5-Dimethoxy-4-hydroxytoluene	30,340		0,93		
n-Tridecan-1-ol	31,541				0,25
1H-Indole, 2,3-dimethyl-	32,126				0,62
5-tert-Butylpyrogallol	32,677				3,05
Benzene, 1,2,3-trimethoxy-5-methyl-	32,677		2,14		
Dodecanoic acid	34,035			0,02	

4-Pyrimidinamine, 5-fluoro-N-methyl-2-(1-pyrrolidinyl)-	35,129		2,28		8,17
Benzene, 1,1'-propylidenebis-	35,129			0,53	
2-Pentadecanone	37,582				0,70
p-Cresol*	39,154	179,5			
Tetradecanoic acid	39,154			0,38	0,76
2-Heptadecanone	42,915		0,31		0,96
n-Hexadecanoic acid	44,306				1,08
2-Cyclopenten-1-one, 2,3,4-trimethyl-	44,322	266,7			
n-Hexadecanoic acid	44,330		0,19	8,56	
9H-Pyrido[3,4-b]indole, 1-methyl-	45,343				3,42
1-Hexadecanol	47,441				0,17
1,3-Hexadiene, 3-ethyl-2-methyl-, (Z)-	48,528	119,3			
cis-13-Octadecenoic acid	48,536			2,89	
Octadecanoic acid	49,005			1,74	1,02
Phenol, 4-ethyl-	49,021	1539			
Hexadecanamide	49,548			0,87	3,00
N-Methyldodecanamide	50,313				0,66
1-Nonadecene	51,828				0,47
9-Octadecenamamide, (Z)-	53,465				2,37
Octadecanamide	53,943				4,17
Myristamide, N-methyl-	54,618				1,17
Myristamide, N-ethyl-	55,399				0,82
Phenol, 4-ethyl-2-methoxy-	58,765	593,2			
n-Hexadecanoic acid	61,399	170,2			
5-.beta.-cholestan-3.alpha.-ol, butyrate	61,679			0,95	
Cholest-2-ene, (5.alpha.)-	62,189			0,34	0,17
cis-13-Octadecenoic acid	62,197	58,9			
Cholest-4-ene	62,452			0,17	0,20
Octadecanoic acid	62,469	14,8			
Cholest-5-ene	62,724			0,17	0,28
Didecan-2-yl phthalate	62,831	57,4			
Cholest-5-en-3-ol (3.beta.)-, nonanoate	63,687			0,07	
Cyclopropa[7,8]cholestan-3-one, 3',7'-dihydro-, (5.alpha.,7.beta.,8.alpha.)-	65,588			0,28	